REACTOR MATERIALS

ENGINEERING LIBRARY
SERIALS

A Quarterly Technical Progress Review

Prepared for DIVISION OF TECHNICAL INFORMATION, U. S. ATOMIC ENERGY COMMISSION,
by BATTELLE MEMORIAL INSTITUTE

Spring 1968

● VOLUME 11

● NUMBER 1

TECHNICAL PROGRESS REVIEWS

The United States Atomic Energy Commission publishes the Technical Progress Reviews to meet the needs of industry and government for concise summaries of current nuclear developments. Each journal digests and evaluates the latest findings in a specific area of nuclear technology and science. *Nuclear Safety* is a bimonthly journal; the other three are quarterly journals.

Isotopes and Radiation Technology
P. S. Baker, A. F. Rupp, and Associates
Isotopes Information Center, Oak Ridge National Laboratory

Nuclear Safety
Wm. B. Cottrell, W. H. Jordan, J. P. Blakely, and Associates
Nuclear Safety Information Center, Oak Ridge National Laboratory

Reactor and Fuel-Processing Technology
Argonne National Laboratory

Reactor Materials
E. M. Simons and Associates
Battelle Memorial Institute

All are available from the U. S. Government Printing Office. See the back cover for ordering instructions.

The views expressed in this publication do not necessarily represent those of the United States Atomic Energy Commission, its divisions or offices, or of any Commission advisory committee or contractor.

Availability of Reports Cited in This Review

United States Atomic Energy Commission (USAEC) reports are available at USAEC depository libraries and are sold by the Clearinghouse for Federal Scientific and Technical Information (CFSTI), National Bureau of Standards, U. S. Department of Commerce, 5285 Port Royal Road, Springfield, Va. 22151. All reports sold by CFSTI are $3.00 for printed copy and $0.65 for microfiche. Each separately bound part of a report is priced as a separate report. Some reports may not be available because of their preliminary nature; however, the information contained in them will generally be found in later progress or topical reports on the subject.

Other U. S. Government agency reports identified in this journal generally are available from CFSTI.

Private-organization reports should be requested from the originator.

United Kingdom Atomic Energy Authority (UKAEA) and Atomic Energy of Canada Limited (AECL) reports are available at USAEC depository libraries. UKAEA reports are sold by Her Majesty's Stationery Office, London; AECL reports are sold by the Scientific Document Distribution Office, Atomic Energy of Canada Limited, Chalk River, Ontario, Canada. UKAEA and AECL reports issued after March 1, 1967, are sold by CFSTI to purchasers in the United States and its territories.

Contents

Reactor Materials

Vol. 11, No. 1, Spring 1968

Fuel and Fertile Materials (Section I)

Uranium and Uranium Alloys 1
Plutonium 5
Thorium and Its Alloys 7
Coated-Particle Fuels 7
Uranium and Thorium Oxides 8
Carbide and Nitride Fuels 9
Basic Studies of Irradiation Effects in Fuel Materials 11
References 15

Moderator and Control Materials (Section II)

Graphite 18
Beryllium and Beryllium Alloys 19
Beryllium Oxide 24
Solid Hydrides 24
Metallic Poison Materials 25
Dispersion and Nonmetallic Poison Materials 27
References 28

Cladding and Structural Materials (Section III)

Corrosion by Aqueous and Gaseous Media 30
Corrosion by Nonaqueous Liquids . . . 33
Radiation Effects in Structural Materials . . 38
Metallurgy of Refractory Metals . . . 45
Metallurgy of Common Cladding and Structural Materials 52
Diffusion Studies 57
Nonfuel Refractories 59
Concrete 63
Ceramic Technology 63
References 63

Special Fabrication Techniques (Section IV)

Melting, Casting, and Working 68
Powder Metallurgy Materials 71
Pressure Bonding 73
Plating 73
Brazing and Welding 75
Nondestructive Testing 77
References 77

Reactor Materials

is one of a series of technical progress reviews broadly covering the field of nuclear science and technology. Under the auspices of the USAEC Division of Technical Information, *Reactor Materials* is prepared by Battelle personnel from worldwide literature. It covers properties, behavior, and fabrication processes of materials applicable to nuclear reactor components and associated equipment.

The reader will recognize that the scope of this Review is too broad to permit detailed coverage of every topic. Rather, the authors and editors attempt to combine the highlights of significant new developments into an information summary of current research for both management and the technical specialist. As a rule, enough of the results are presented to define the research and summarize the findings. For readers desiring more information on any particular topic, a complete set of references is provided at the end of each section.

Each quarter a number of bibliographies, monographs, and books appear on subjects within the scope of *Reactor Materials*. Although the main purpose of this Review is to call attention to findings that are new and significant, such publications are noted in the text because they often represent excellent compilations of available information on important materials topics.

E. M. SIMONS
S. W. POREMBKA, JR.
D. L. KELLER

Battelle Memorial Institute

Issued quarterly by the U. S. Atomic Energy Commission. Use of funds for printing this publication approved by the Director of the Bureau of the Budget on July 8, 1966.

Section

I

Reactor Materials

Fuel and Fertile Materials

Uranium and Uranium Alloys

Unalloyed Uranium

The hydrogen embrittlement of uranium was studied by the British.[1] Some of their conclusions were:

1. Hydrogen embrittles uranium primarily through the formation of uranium hydride precipitates.
2. The degree of embrittlement can be related to the size of hydride precipitates, and maximum embrittlement can occur at approximately 2.5 ppm hydrogen in thermally charged alloys.
3. The fracture stress of uranium containing 2.5 ppm hydrogen is generally lowered by increasing the strain rate from 1.3×10^{-5}/sec to 2.6×10^{-2}/sec.
4. The formation of uranium hydride precipitates lying on planes perpendicular to the tensile axis produces the maximum embrittlement in cathodically charged specimens.

A Los Alamos[2] investigation has led to the derivation of the heat of vaporization of uranium. The value of 126.6 kcal/mole at 298.15°K was deduced from the behavior of the U–C system.

The British[3] have irradiated 50-μ-thick specimens of uranium of various compositions at 400, 500, 620, and 715°C where induced stresses should be small. The distribution of porosity was studied by means of the electron-microscope transmission technique after irradiation. Results showed that the preexisting precipitates did not affect the scale of bubble distribution, and that swelling due to bubbles within the grains was small. It was therefore concluded that, under stress-free conditions and at burnups of less than 0.2%, no large swelling due to evenly distributed gas bubbles within the grains occurred.

Other papers of interest in the field of unalloyed uranium include: "Grain Size–Fracture Stress Relationships of Uranium,"[7] "Fissiography: Diffusion in Titanium and Iron,"[6] "Activation Energies of Several Deformation Mechanisms from Creep of Uranium Monocrystals and Polycrystals Between 150 and 770°C,"[5] and "Aluminum Coating of Uranium Reactor Parts for Corrosion Protection."[4]

Alpha-Phase Uranium Alloys

National Lead Company of Ohio[8] has conducted elevated-temperature tensile tests on cast binary uranium-base alloys containing small additions of Al, C, Fe, or Si. Figure I-1 presents the yield and ultimate strengths obtained, and Fig. I-2 shows the elongation and reduction-of-area data. The composition of the unalloyed control sample referred to in the plate was 68 ppm C, 62 ppm Fe, 28 ppm Si, and 18 ppm Al.

The comparative 500°C creep rates of adjusted uranium* and uranium containing small additions of various elements were determined by the British.[9] From the sagging-bar tests employed, no significant difference in creep strength was found for adjusted uranium after different heat-treatments to refine the grain size. These treatments consisted of gamma quenching and beta quenching, followed by short- and long-term alpha anneals at 550°C. In tests of 2000 hr or less, no difference was detected between the creep strengths of uranium adjusted to different levels of iron or aluminum. Above 2000 hr, some strengthening appeared to be produced by the highest iron and aluminum level (350 ppm and 900 ppm, respectively).

The beta quenched U–0.125 at.% Mo alloy (iron/aluminum adjusted)† showed no improvement in creep strength over that of the standard adjusted uranium. However, a U–0.375 at.% Mo alloy (iron/aluminum adjusted)‡ alloy exhibited a threefold improvement. The creep strengths of U–0.125 or 0.375 at.% Mo–0.125 or 0.375 at.% Cr alloys (isothermally transformed at 550°C) were all higher than that for adjusted uranium but lower than that for the U–0.375 at.% Mo (iron/aluminum) alloy.

The creep strengths of beta-quenched and alpha-annealed U–0.5 at.% and U–1 at.% V alloys were about the same, and both were improved over that of adjusted uranium by a factor of about 2.5. In contrast, U–2 at.% Zr alloy exhibited a creep strength poorer than that of adjusted uranium.

French investigators[10] found that the addition of small amounts of carbon led to the considerable refinement of the gamma grain size in uranium alloys containing about 1 wt.% molybdenum.

Other publications containing information on alpha-phase uranium alloys include: "Influence of Heat Treatments on the Structure of Uranium Alloys with a Low Niobium Content,"[11] "Hysteresis in the $\alpha-\beta$

*Amounts were 240 ppm iron, 700 ppm aluminum.
†Amounts were 320 ppm iron, 420 ppm aluminum.
‡Amounts were 320 ppm iron, 470 ppm aluminum.

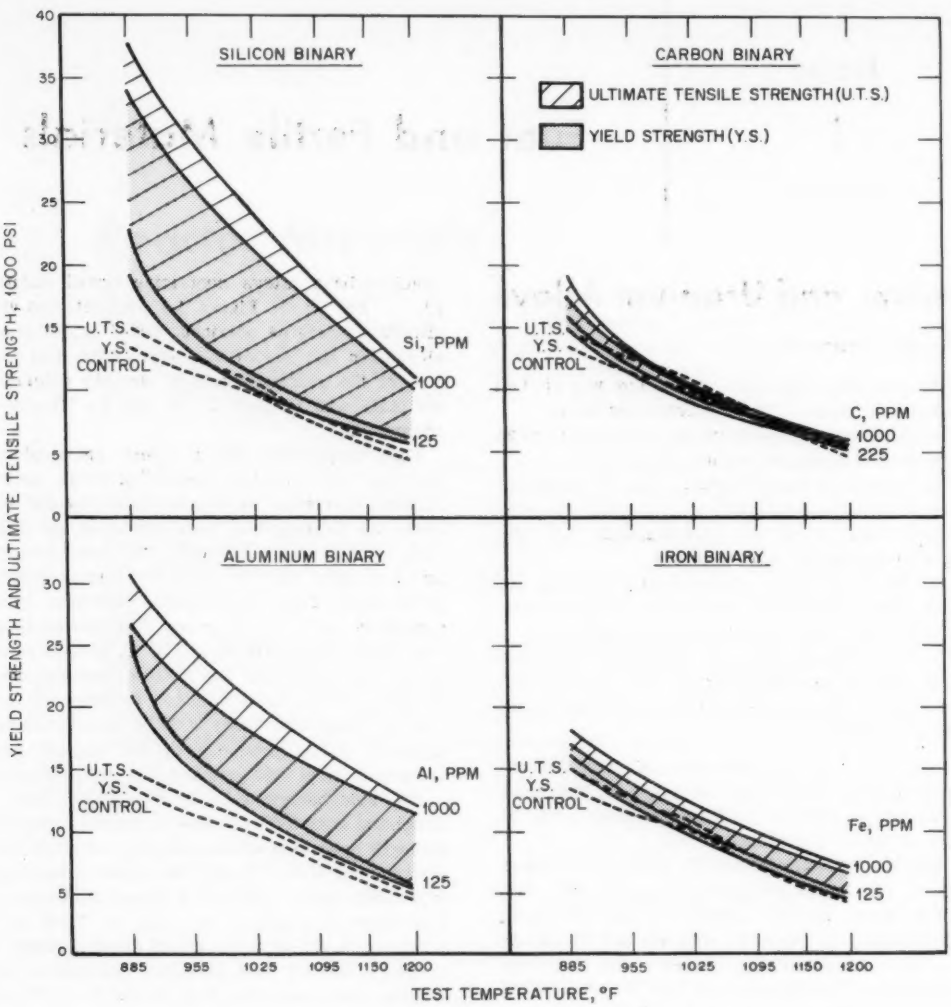

Fig. I-1 Effect of temperature and alloy level on the strength of binary uranium alloys.[8]

Transition of Uranium Saturated with Silicon,"[12] "Influence of the Solubility Limit of Chromium in β-Uranium on the Isothermal Transformations of Uranium–Chromium Alloys Tempered from 720 C,"[13] "The $\beta \rightarrow \alpha$ Phase Change in a Uranium–Platinum–Niobium Alloys,"[14] "Bainitic Reaction in Uranium–Chromium Alloys,"[15] and "Study of the Mechanical Properties and Thermal Properties of Uranium Alloys with Small Additions."[16]

Gamma-Phase Uranium Alloys

The Israelis[17] have determined TTT curves for U–8, 10.8, and 14.3 wt.% Mo alloys. X-ray powder diffraction techniques were used to obtain the $\gamma \rightarrow (\alpha + \gamma)$ and $\gamma \rightarrow (\alpha + \gamma + \gamma')$ transformations. The curves obtained are presented in Fig. I-3. The times required for appearance of the alpha and gamma-prime phases were shorter than those obtained by other investigators. This difference could be due to the use of powder in the present study, which may accelerate the transformation by nucleation on the powder-particle surface.

Investigators at Rocky Flats[18] have determined the tensile properties of arc-cast and hot-rolled U–11, 15, 17, and 19 at.% (4.8, 6.4, 7.4, and 8.4 wt.%) Nb alloys in both the solution-quenched and aged conditions. Typical results obtained in room-temperature tests on as-quenched and aged material are presented in Figs. I-4 and I-5. The results of high-temperature

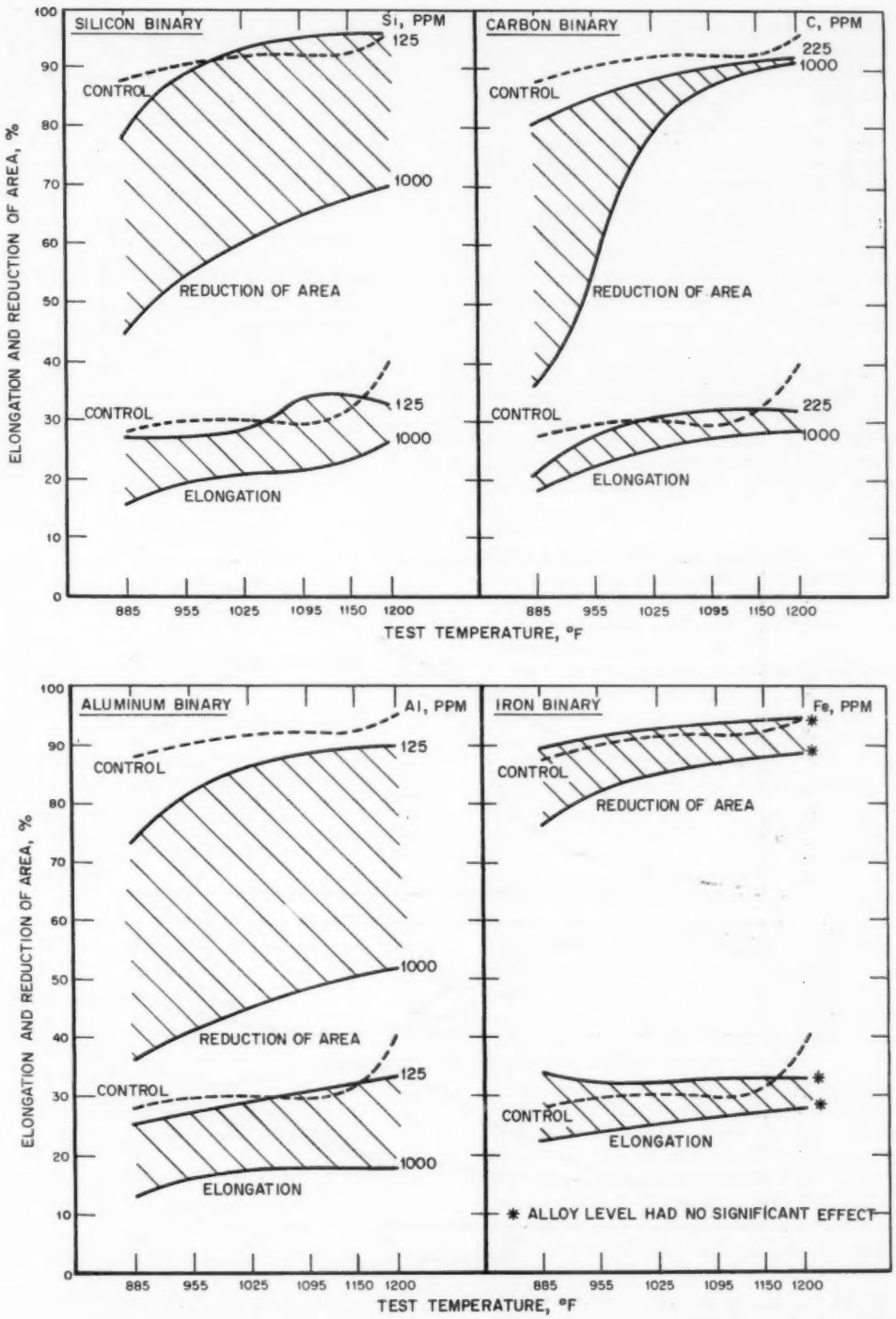

Fig. I-2 Effect of temperature and alloy level on the ductility of binary uranium alloys.[8]

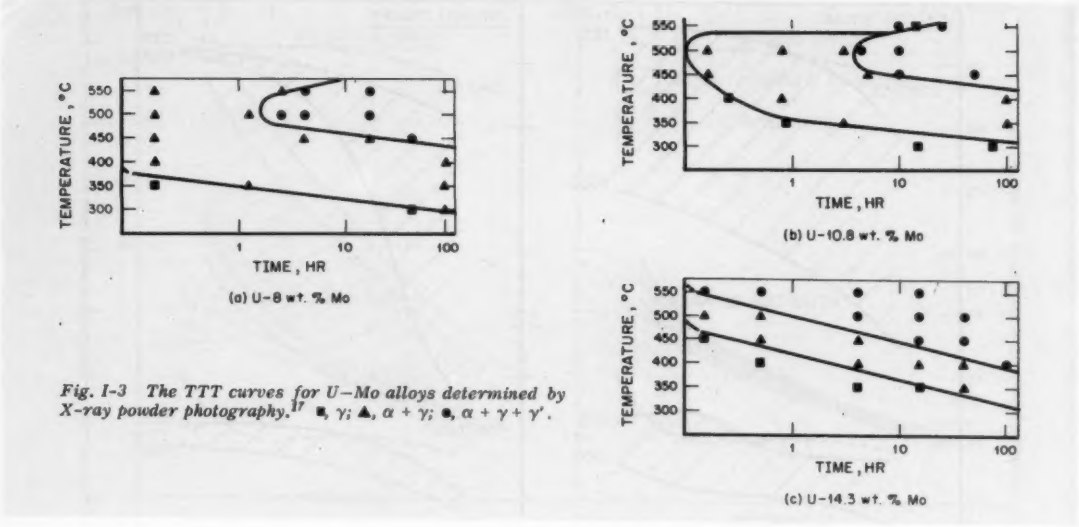

Fig. I-3 The TTT curves for U–Mo alloys determined by X-ray powder photography.[17] ■, γ; ▲, α + γ; ●, α + γ + γ'.

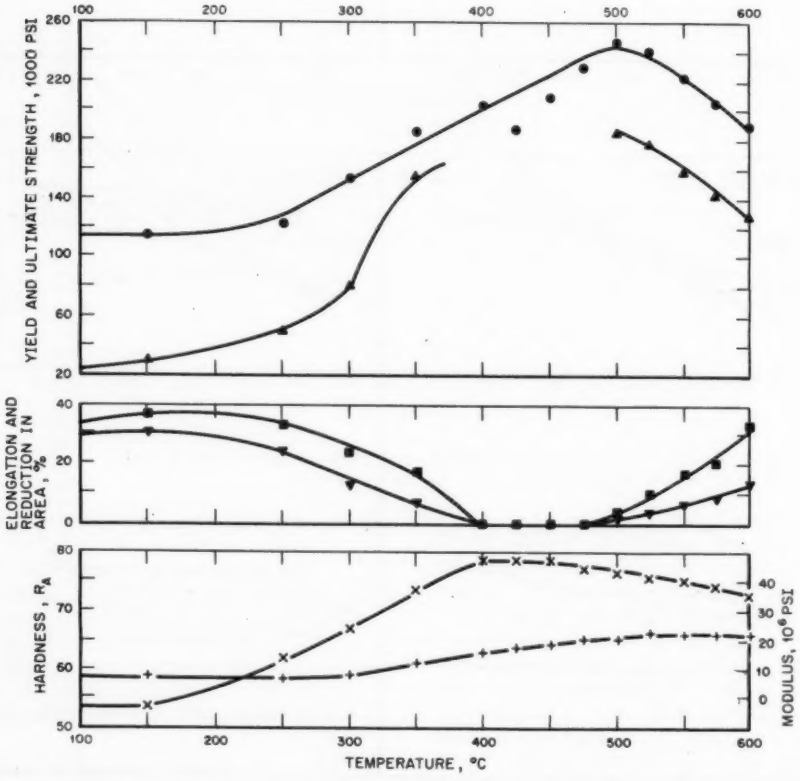

Fig. I-4 Mechanical test data for the U–15 at.% Nb alloy at ambient temperatures.[18] *The samples were aged 1 hr at the indicated temperature and air cooled. All samples were flat bars which were water quenched from 850°C, aged, and then machined.* ●, *ultimate tensile strength;* ▲, *0.2% offset yield strength;* ■, *reduction of area;* ▼, *elongation;* ×, *Rockwell A hardness;* +, *modulus.*

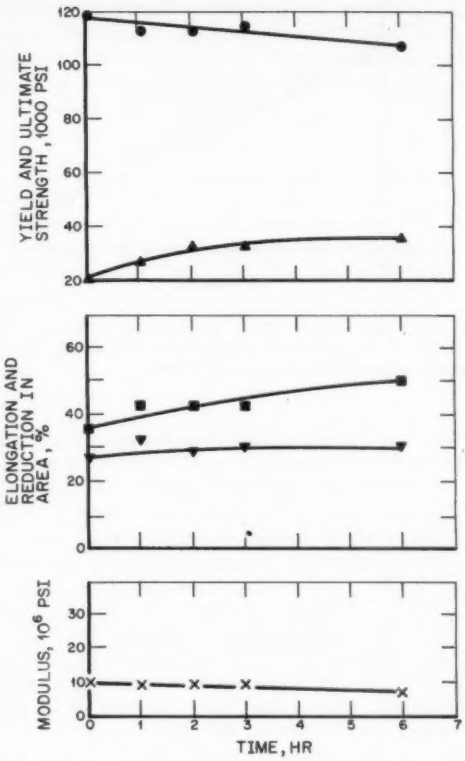

Fig. I-5 Mechanical properties of the U–15 at.% Nb alloy aged at 150°C and tested at ambient temperatures.[18] The samples were aged in oil at 150°C and air cooled. All the samples were flat bars which were water quenched from 850°C, machined, and then aged. ●, ultimate tensile strength; ▲, 0.2% offset yield strength; ■, reduction of area; ▼, elongation; ×, modulus.

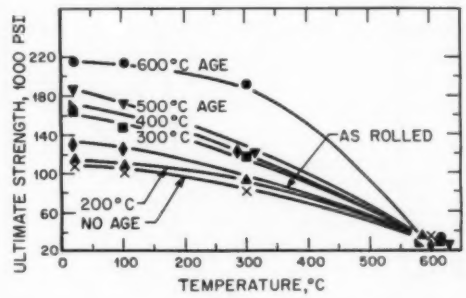

Fig. I-6 Elevated-temperature mechanical test data for the U–15 at.% Nb alloy.[18] The flat bars were machined from hot-rolled sheet, then solution treated 15 min at 850°C and water quenched. The samples were then aged 2 hr at the indicated temperature and air cooled. ♦, as rolled; ×, water quenched at 850°C; ▲, 2 hr at 200°C; ■, 2 hr at 300°C; ◣, 2 hr at 400°C; ▼, 2 hr at 500°C; ●, 2 hr at 600°C.

tensile tests on quenched and aged U–15 at.% Nb are presented in Fig. I-6. The effect of the metastable and stable phases present in these alloys on tensile properties is discussed. (M. S. Farkas)

Plutonium

Plutonium Metal and Alloys

Phase-equilibria studies of the Pu–Fe–Mn system being concluded at Mound Laboratories[19] have been concerned primarily with the Pu–$PuFe_2$–$PuMn_2$ region of the phase diagram. Complete solid solution between $PuMn_2$ and $PuFe_2$ was noted.

Studies at Lawrence Radiation Laboratory[20] on the Pu–Pb system have shown that a miscibility gap exists in the liquidus from approximately 40 to 85 at.% plutonium and that four of the six compounds detected lie under this syntexis. The melting point for the compound $PuPb_3$ was determined as about 1138°C, which disagrees with 845°C as previously reported by the Russians. The $PuPb_2$ compound is formed peritectically at about 1130°C from PuPb and the melt, and a polymorphic transformation at about 1105°C is thought to occur in the $PuPb_2$. All of the compounds except $PuPb_3$ are reported to be pyrophoric and therefore difficult to study.

The kinetics of the alpha ⇌ beta transformation in dilute plutonium alloys containing either neptunium or titanium have been investigated by the British.[21] Time–temperature–transformation curves were derived for the Pu–0.82 and 0.70 at.% Ti alloys and for the Pu–1.3 at.% Np alloy, assuming that the percent transformation was directly proportional to the percent change in electrical resistivity. The results indicate that the greater the driving force for the transformation, the faster is the rate of reaction.

The British[22] have compared the transformation behavior of metastable delta-phase plutonium as a result of thermal cycling to the model suggested by Knapp and Dehlinger for the austenite–martensite transformation in steels. This comparison seems valid since the results of this study suggest that the delta-phase plutonium transforms directly into alpha-phase plutonium.

The results of strain–anneal experiments using Pu–1.22 wt.% Ga alloy have been observed by NUMEC.[23] Grains as large as 5.7 × 3.0 mm were grown in a specimen strained 1.75% at 550 to 600°C, and only minor grain growth was noted in a specimen strained 1.50%. This indicates that the critical strain for this alloy is between 1.50 and 1.75%. A similar alloy containing 1.06 wt.% Ga and 231 ppm metallic impurities has been evaluated at Lawrence[20] at test temperatures of 20 to 576°C using a single torsional strain rate of 4.16%/sec. The data thus obtained have been compared with similar data on a normal-purity Pu–Ga alloy. A ductility transition range between

150 and 250°C which led to "unlimited ductility" between 200 and 400°C for a nominal-purity alloy and 200 to 500°C for the high-purity alloy was noted. The drastic loss in ductility for the normal-purity alloy between 400 and 500°C was attributed to the $Pu-Pu_6Fe$ eutectic. The alloy containing high-purity plutonium was found to be stronger at low and high temperatures (20 to 75°C and 350 to 560°C) but weaker at intermediate temperatures (75 to 350°C) than the normal-purity alloy.

The low-temperature thermal properties of plutonium are being studied by the British.[24] A value for thermal conductivity of 15 mw/(°K)(cm) at 20°K was determined. This value is lower than those for any other metallic element. The specific-heat values between 10 and 90°K agree with data obtained previously.

Los Alamos[25] has examined the corrosion effect of plutonium, Pu–Fe, and Pu–Co–Ce alloys on tantalum and the Ta–5 wt.% W alloy. Carburization greatly improves the corrosion resistance of the materials to the liquid metals when tests are conducted at 900, 1000, and 1100°C. Apparently the plutonium attacks the tantalum at both grain boundaries and along the surface. The effects of annealing the tantalum and Ta–W compatibility cans prior to testing were also evaluated. From these tests, a 1650°C anneal was found to be optimum and the rate of attack increased as the annealing temperature increased. The attack was very rapid at 2050°C.

(N. E. Daniel)

Plutonium Compounds

The solid–liquid phase diagram for the UO_2-PuO_2 system has been experimentally determined by General Electric investigators using a thermal arrest method.[26] Figure I-7 shows a plot of the data points which represent a typical binary pair without maximum or minimum in the liquidus or solidus curves. Observed melting points for UO_2 and PuO_2 were 2840 ± 20°C and 2390 ± 20°C, respectively. Curves computed by ideal solution laws exhibit good agreement with the experimental data.[27]

Investigators[28] at Rocky Flats have studied the effect of maximum exposure temperature and time of exposure on selected properties of PuO_2. The effect of heat-treatments to 900°C for up to 7 hr on the mean crystallite size, specific surface area, lattice constant, particle-size distribution, and rate of dissolution was described. In general, temperatures greater than 500°C resulted in the most significant effect on the properties evaluated.

Los Alamos conducted a literature survey and has compiled the pertinent information published on experimental studies of mixed U–Pu nitrides bonded with sodium. Fifty-three references are cited.[29]

Studies at Battelle–Columbus to evaluate (U,Pu)N as a LMFBR-fuel candidate are continuing.[30a] Properties evaluated include thermal conductivity, thermal stability, plutonium volatilization, and compatibility with various cladding materials. Thermal conductivity, as determined by thermal-diffusivity measurements in vacuum, for PuN ranged from 0.0290 to 0.0353 cal/(sec)(cm)(°C) in the temperature range from 200 to 1000°C, whereas values for $(U_{0.8}Pu_{0.2})N$ ranged from 0.0383 to 0.0483 cal/(sec)(cm)(°C) from 200 to 1175°C. Thermal stability studies of (U,Pu)N indicate that solid-solution $(U_{0.8}Pu_{0.2})N$ can sustain a vacuum exposure (8×10^{-6} torr) for 50 hr at 1300°C with little change in grain size, chemistry, or lattice parameters. Grain size was observed to increase markedly above 1700°C, but (U,Pu)N appears to be more resistant to grain growth than UN (Fig. I-8).

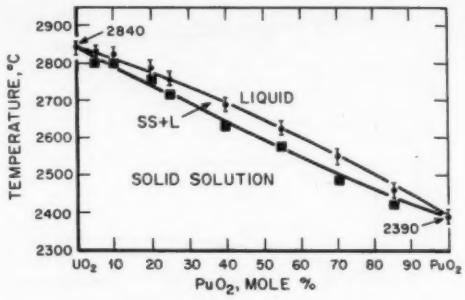

Fig. I-7 Solid–liquid phase diagram for the UO_2-PuO_2 system.[26,27] ◆, observed liquidus; ■, observed solidus. Curves computed by ideal solution laws.

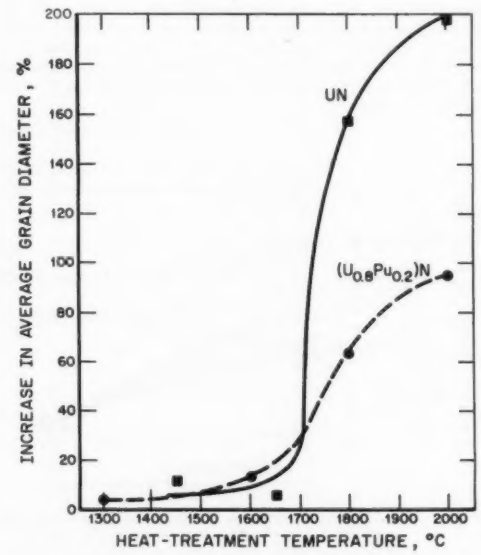

Fig. I-8 Grain growth[30a] as a function of heat-treatment temperature for UN and $(U_{0.8}Pu_{0.2})N$. ■, UN heat-treated for 48 hr; ●, $(U_{0.8}Pu_{0.2})N$ heat-treated for 50 hr.

Volatilization studies revealed that PuN vaporizes congruently under equilibrium conditions at temperatures up to at least 1800°C. The plutonium pressure, as defined by weight-loss experiments, can be represented by the equation

$$\log p = -23{,}300/T + 7.40$$

where p is pressure in atmospheres and T is temperature in degrees Kelvin. Compatibility of (U,Pu)N with 304 stainless steel has been confirmed at 1000°C for times up to 3000 hr. The Nb–1 wt.% Zr and nickel-base alloys are also being evaluated.

The preparation of (U,Pu)N by the carbothermic reduction of mixed oxides with carbon under nitrogen is being investigated at Battelle–Northwest.[31] Several 10-g batches of $(U_{0.8}Pu_{0.2})N$ have been synthesized from ball-milled UO_2–PuO_2–C mixtures in a fluidized-bed reactor by the reaction:

$$(U,Pu)O_2(\text{solid}) + 2C(\text{solid}) + \tfrac{1}{2}N_2(\text{gas}) \rightarrow (U,Pu)N(\text{solid}) + 2CO(\text{gas})$$

Lattice parameters for the major phase varied from 4.892 to 4.906 A, with the higher values being generally associated with the higher residual carbon (observed from 1300 to 7000 ppm). Removal of excess carbon with hydrogen is under study and appears to be practical. (D. F. Askey)

Thorium and Its Alloys

Researchers in the Soviet Union have established phase diagrams for the Th–Pr and Th–Nd systems.[32] The presence of a continuous series of solid solutions between high-temperature modifications of these metals was determined. It was shown that solid-state transitions in reactions $\beta_{Th-Nd} + \alpha_{Th} \rightleftharpoons \alpha_{Nd}$ and $\beta_{Th-Nd} + \alpha_{Th} \rightleftharpoons \alpha_{Nd}$ at 940 and 950°C, respectively, were of a peritectoid type. A wide range of alpha-thorium base solid solutions was found in both systems which extended to 80 at.% praseodymium at 650°C and to 78 at.% neodymium at 750°C. The solubility of thorium in praseodymium and neodymium at these temperatures was found to be below 1 at.%.

High-temperature X-ray diffraction data obtained at the Ames Laboratory[33] on thorium and Th–C alloys containing up to 4.92 wt.% carbon showed a miscibility gap at a critical temperature of 1570 ± 25°C and 2.2 wt.% carbon. At 600°C the gap extends from 0.27 to 3.75 wt.% carbon. The lattice constants for these two solid solutions are 5.135 ± 0.005 and 5.317 ± 0.005 A, respectively. The lattice constant of the fcc solid solution at the critical temperature and composition was 5.301 ± 0.005 A.

Six Th–U and Th–U–Pu fuel alloys jacketed in V–20 wt.% Ti tubing were irradiated in the CP-5 reactor by investigators at Argonne.[34] Objectives of the experiment were to determine the restraint characteristics of the jacket (0.015-in. wall with an outside diameter of 0.198 in.), the relative swelling behavior of the fuels, and the maximum attainable burnup before jacket failure. It was determined by radiography that jacket failure occurred after about 12.1 to 13.5 × 10^{20} fissions/cm^3. The maximum cladding temperature was 590°C during the irradiation, and a power density of 8.7 to 9.2 kw/ft was obtained. Each alloy had an effective density of about 74%.

The diffusion coefficients of carbon, oxygen, and nitrogen in beta thorium from 1400 to 1700°C have been determined at Ames Laboratory.[35a] The measured diffusion coefficients are shown in Table I-1. (R. L. Martin)

Coated-Particle Fuels

Workers at Oak Ridge have confirmed that SiC coatings can be applied to both large-size (420- to 500-μ diameter) and small-size (210- to 250-μ diameter) particles in a 1-in.-diameter fluidized-bed coater without apparent difficulties.[36] The SiC is deposited at temperatures of 1300 to 1800°C at rates of 1.4 to 3.9 μ/min with methyltrichlorosilane as the coating reactant. Deposition of SiC on fuel particles has been demonstrated previously on the Dragon Project[37] and by workers at Battelle–Columbus.[38] Other work at Oak Ridge includes the develop-

Table I-1 INTERSTITIAL DIFFUSION IN BETA THORIUM[35a]

Carbon diffusion		Nitrogen diffusion		Oxygen diffusion	
Temp., °C	Diffusion coefficient, 10^{-6} cm^2/sec	Temp., °C	Diffusion coefficient, 10^{-6} cm^2/sec	Temp., °C	Diffusion coefficient, 10^{-6} cm^2/sec
1495	1.1	1450	2.2	1440	5.8
1555	1.2	1500	2.7	1470	4.6
1600	1.3	1560	2.8	1505	6.0
1640	1.6	1595	4.2	1540	4.9
1680	2.5	1665	3.3	1575	8.0
		1715	5.0	1615	8.2
				1650	6.5
				1700	7.5
Q = 27 kcal/mole		Q = 17 kcal/mole		Q = 11 kcal/mole	
D_0 = 0.02 cm^2/sec		D_0 = 0.003 cm^2/sec		D_0 = 0.001 cm^2/sec	

ment of a 5-in.-diameter coating unit, to be operated by remote control,[39,40] for application of pyrolytic carbon coatings on nuclear fuel particles. The coating unit is under construction and about 80% complete. A computer program has been written for detailed tabulation of the experimental data from coated-particle production. The program also yields calculated coating thickness, coating density, diameter of coated particles, initial flux, final flux, and deposition efficiency.[41]

General Atomic is studying the properties of both SiC and ZrC for use as barrier coatings.[42] An etchant reported to be effective for metallographic examination of the structure of the SiC is a eutectic mixture of K_2CO_3 and NaF heated at 600°C.[43] Methods for evaluation of the ZrC are being considered.[42]

In other work at Battelle–Columbus, a feasibility study of coating fuel particles with graphite by precipitation from liquid-metal solutions has been completed.[30b] The graphite was precipitated from a carbon-saturated liquid-nickel bath containing the fuel particles. It was concluded that the preparation of graphite-coated particles by this technique should be feasible since (1) the particles survive the required exposure, (2) graphite can be controllably precipitated from the melt, and (3) graphite does form on the particles. The major obstacle to be overcome is incomplete coverage due to insufficient wetting of the particle surface by the bath. (N. D. Veigel)

Uranium and Thorium Oxides

Properties and Behavior

The migration of fission-gas bubbles in irradiated UO_2 was studied at 1400, 1450, and 1500°C by Gulden[44] using electron microscopy. The bubble-migration distance of bubbles with radii greater than 37 A was dependent on the bubble radius, a characteristic of a migration mechanism controlled by volume diffusion. Migration rates were very much smaller than would be predicted from a surface-diffusion-controlled mechanism, and the activation energy for bubble migration was found to be 130,000 cal/mole. Smaller bubbles migrated at a slower rate than would be predicted on the basis of a volume-diffusion-controlled mechanism.

The release of the nongaseous species bromine, rubidium, and cesium from sintered UO_2 and ThO_2 after ion bombardment was studied by Matzke.[45] Two different concentrations of these species were obtained by varying the ion dose. In most experiments, several mass-transport processes appeared to contribute to the release. Release compatible with a volume-diffusion mechanism was observed for rubidium and cesium in ThO_2 at the lower dose of 3×10^{13} ions/cm^2. The release occurred at temperatures similar to those for fission-gas diffusion and indicated an activation enthalpy of about 100 ± 7 kcal/gram mole, which is similar to those observed for fission-gas diffusion or uranium self-diffusion. All other releases studied were found to follow complex patterns. In contrast to gas release, no trapping was found at the high bombardment dose of 1.5 to 2×10^{16} ions/cm^2. Release of bromine was not affected, and release of rubidium and cesium occurred at lower temperatures than in samples given the lower dose. If most of the bromine or rubidium was near the surface of the ThO_2, an enhanced release at low temperatures was observed. Release of bromine from ThO_2 was faster when the samples were annealed in hydrogen than when they were annealed in air.

Investigators in the United Kingdom[46] have studied the kinetics of the oxidation of UO_2 spheres in dry air at temperatures between 320 and 380°C. Oxidation was found to be best described as a first-order reaction occurring in two steps, with the rate constant being higher for the second step. The rate curves did not fit those predicted by any single model for the oxidation mechanism, possibly because of the complicating effects of grain boundaries. Neutron irradiation up to 9% burnup of all the uranium atoms did not alter the oxidation mechanism fundamentally but produced a general decrease in the reaction rates. The Arrhenius activation energy for the second oxidation step increased from about 15 kcal/gram mole for unirradiated UO_2 to about 25 kcal/gram mole for UO_2 irradiated to 8.5% burnup.

At General Electric[47] the vapor pressure of hypostoichiometric UO_2 was measured as a function of temperature for a series of compositions. The following relations for the vapor pressure were obtained:

$$\ln P\,(\text{atm}) = 15.2 \pm 0.4 - (59{,}100 \pm 1000/T) \text{ for } UO_{1.88}$$

$$\ln P\,(\text{atm}) = 14.6 \pm 0.6 - (59{,}200 \pm 1700/T) \text{ for } UO_{1.92}$$

$$\ln P\,(\text{atm}) = 15.1 \pm 1.5 - (61{,}000 \pm 1500/T) \text{ for } UO_{1.94}$$

(R. H. Barnes)

Fabrication

German investigators[48] have investigated the precipitation of ammonium uranyl carbonate by the reaction of slightly enriched UF_6 with gaseous NH_3 and CO_2 in water. A UO_2 powder demonstrating good pressing and sintering characteristics was obtained following reduction in a fluidized-bed furnace without intermediate drying steps.

A process involving the flame spraying of UO_2 (both depleted and enriched) coatings on stainless steel has been developed at Los Alamos Scientific Laboratory.[49] The UO_2 powders employed in the process were −325 mesh with an average particle size of 12 to 15 μ. Coarser powders were not readily

adaptable to the process; however, it was postulated that finer sizes could be employed as long as feed rates were not impaired. Suitable masking or blanketing of the substrate with argon was necessary to retard oxidation of the UO_2 and thus the resulting loss of adherence. The optimized process resulted in a coating that demonstrated good adherence and chemical characteristics similar to those of the starting material. After spraying the coating, the workers were able to treat it at 1000°C in hydrogen to achieve complete chemical stoichiometry with no sacrifice in adherence.

Studies at Harwell[24] involved the preparation of 95%-dense spheres of UO_2 and ThO_2-UO_2 in the 500-μ size range. Sintered pellets were first prepared and then spheroidized in an abrasive-lined drum using a jet of argon to propel the pellet. Rounded particles were finally lapped with 600-grit SiC in aluminum tracks to achieve accurate sphericity. Low-density (80% of the theoretical density) spheres were also prepared by the addition of a burnout material to the powder prior to pressing and by spheroidizing pellets of a coarse UO_2 powder prepared by controlled oxidation and reduction of previously sintered pellets.

Fabrication trials were conducted on the preparation of $ThO_2-Y_2O_3$ tubes by slip casting. Blends for fabrication were prepared by ball-milling mixtures of reactor-grade ThO_2 and Y_2O_3. Although there was some doubt concerning the efficiency of this technique in achieving a uniform solid solution, this characteristic was not considered critical for the application. Fabrication indicated that material having a surface area of 12 m^2/g can be slip cast with little or no difficulty. A second material was prepared by mixing nitrate sols of the two oxides, gelling the mixture, and decomposing the nitrate. Mixing occurred at the 100-A particle-size level and was expected to provide a uniform solid solution.

Thoria microspheres with porosities of from 25 to 70% were obtained from sol–gel-prepared microspheres containing C : ThO_2 ratios of 1 to 6 by burnout of the carbon in oxygen.[40] The carbon was added to the sol prior to gelatin. The firing cycle by which the carbon was removed involved a "densification" of the ThO_2 matrix at 1400°C prior to carbon removal at 800°C. Subsequent refiring to 1400°C completely destroyed this porosity by closing the pores, which were originally 120 to 250 A in diameter. At lower temperatures, sintering still occurred, although at 1200°C it was much less severe.

Investigations were conducted to determine the variation of the specific surface of ThO_2 gel upon thermal treatment in air at 35 to 1000°C.[50] The specific surface areas and pore volumes of the parent gel and its various hydration products were calculated from the adsorption of nitrogen at the temperature of liquid nitrogen. The X-ray and thermogravimetric analyses revealed structural changes after thermal treatment. The gel was amorphous at temperatures up to 300°C where it transformed to cubic ThO_2. Below 300°C the surface area decreased continuously, probably by a mechanism of diffusion and material transport from wide pores to fill the fine pores (surface annealing). This was followed at higher temperatures by a crystallization (activation) stage, and finally, by a sintering and crystal-growth stage.

(T. R. Wright)

Carbide and Nitride Fuels

Properties and Behavior

Evstyukhin et al.[51] have investigated the phase diagram of the W–UC system. The solidus on a tie from UC to metallic tungsten was observed at 2180°C. An unusually high solubility (8 wt.%) was noted for tungsten in UC at the solidus. The solubility of UC in tungsten was very small; but between 1500 and 2100°C, the diffusion rate of uranium into tungsten was given by the expression: $D = 0.11 \exp(-91{,}700/RT)$ cm^2/sec.

Much of the mystery surrounding the nature of the U–C–O system has been eliminated by the appearance of papers by Henry et al.[52] and by Dutta and White.[53] At all temperatures in the solid-state regions, quasi-binary ties exist between UO_2 and graphite, between UO_2 and UC_2, and between UO_2 and UC or U(C,O). The UO_2 forms a tie with U_2C_3 at low temperatures and up to some temperature near 1600°C. This tie is displaced between 1600 and 1800°C as shown in Fig. I-9 (Ref. 52) by a tie between U(C,O) and UC_2. Above 1800°C, U_2C_3 disappears from the system entirely. Carbon monoxide pressures that must exist at equilibrium with all the ternary alloys in this system were also determined.

In studies of the systems involving UC and the constituents of stainless steel, Dutta and White[53] found that $UNiC_2$ apparently decomposes between 1400 and 1450°C, and that quasi-binary ties exist in the U–Ni–C system from UC to UNi_2, UNi_3, and $UNiC_2$ and from $UNiC_2$ to UNi_3, UNi_5, and graphite.

Workers at Iowa State[33,35b,54] have obtained electrical-resistivity data and high-temperature X-ray data confirming the major features of the Th–C phase diagram proposed by Wilhelm and Chiotti in 1950 (Ref. 55). This diagram features complete solid solution between thorium metal, ThC, and ThC_2 at temperatures just below the solidus. This solid solution separates on cooling into the three phases found at room temperature, beginning at 2100°C.

Bowman et al.[56] have obtained high-temperature neutron-diffraction data which show that, at high temperatures, $UC_{1.85}$ ("UC_2") has the face-centered cubic NaCl structure in which paired carbon atoms possessing a spherical symmetry are located at the anion

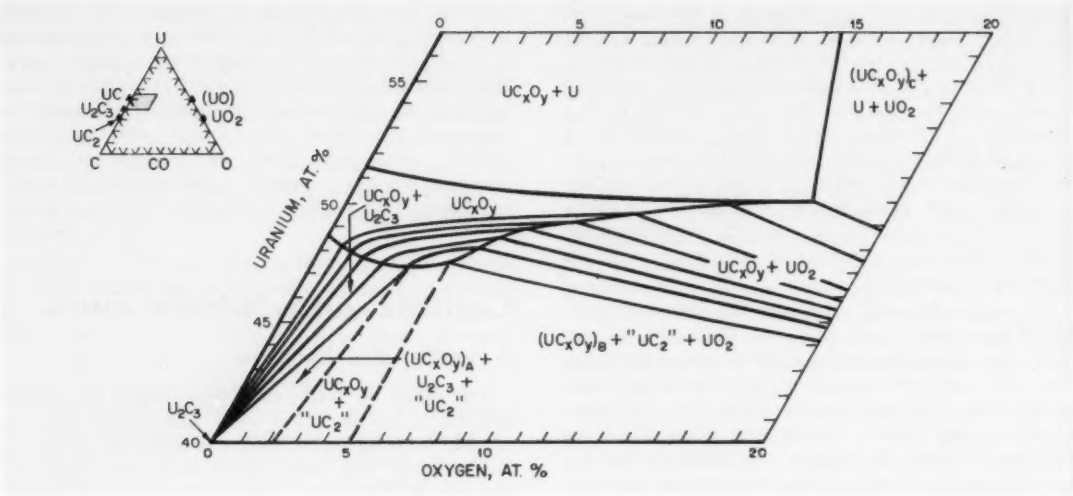

Fig. I-9 The U–C–O system at 1700°C (Ref. 52).

positions. The concept of "covalent" bonding of these carbon pairs must be altered slightly to include the resonating motion of the carbon atoms in their realm of spherical symmetry.

Eremeev et al.[57] have studied the layers formed at 1000°C between UC and molybdenum and tungsten. After 2500 hr, a layer 17 μ thick formed on molybdenum in contact with UC that originally contained 5.0 to 5.2 wt.% carbon. Under the same conditions the layer formed on tungsten was only 1 to 2 μ thick. An explanatory review of the application of the chemical technique known as "buffering" to prevent carburization of stainless steel and other cladding materials by UC has been prepared by Chubb.[58]

Storms and Huber[59] have measured the heat of combustion of UC and calculated the heat of formation to be approximately −23,000 cal/mole at 298°K. Comparison of these data with work reported previously fixed the heat of vaporization of uranium near 126.5 kcal/mole at 298°K.

Extensive studies of the self-diffusion of carbon and uranium in UC are summarized in Fig. I-10 (Ref. 60*a*). These results, obtained at Atomics International, are in good agreement with results obtained by Lee in Great Britain and by Chubb et al. at Battelle [*Reactor Materials*, 9(4) and 8(4)].

(W. Chubb)

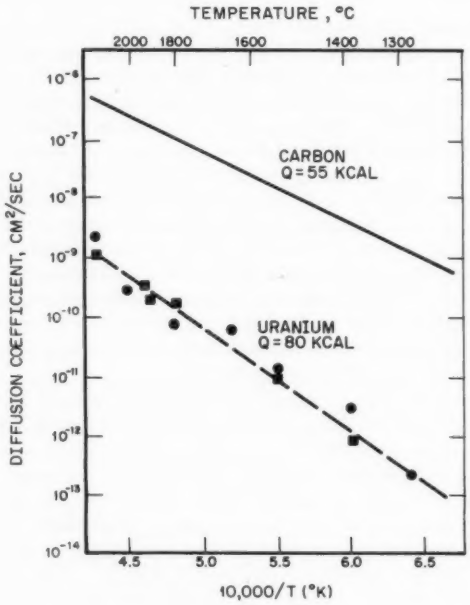

Fig. I-10 Self-diffusion of uranium and carbon in hyperstoichiometric UC (4.9 wt.% carbon).[60a] ●, *zone melted;* ■, *arc cast.*

Preparation and Fabrication

Continuing efforts at Atomics International have led to some improvements in the surface quality of cast UC slugs required for the HWOCR (Heavy Water Organic Cooled Reactor) program.[61] However, centerless grinding remains a necessity to meet the arbitrary specifications of surface finish, dimensions, roundness, and straightness. Significant improvements in surface finish were achieved by outgassing and preheating the molds and by increasing the fluidity of the melt. By pouring with little or no

header, bowing of the cast UC slugs was considerably reduced. The feed stock for these castings was prepared by the carbothermic reduction of UO_2.

A concurrent program[62] involved the economics of preparing enriched UC from uranium compounds intermediate in the processing of the ore to the dioxide.

Among several thermodynamically possible reactions for the conversion of uranium chloride to UC, feasibility was established[63] for the reaction of UCl_4, aluminum, and graphite. Although magnesium and calcium are stronger reducing agents, the metal chloride formed by aluminum has a higher vapor pressure and offers the potential of higher product purity. The process reacts a loose mixture of the constituents under a flow of argon sufficient to sweep the volatilized $AlCl_3$ from the chamber. Purity and conversion efficiency were highest at 900°C when using high-purity UCl_4 and argon. Losses of uranium due to the sweeping of UCl_4 vapor resulted in the incomplete conversion of the initial charge. Detailed analyses of the product for impurities are being performed; however, X-ray diffraction of UC prepared from distilled UCl_4 indicates a single-phase material.

(J. T. Lowder)

Basic Studies of Irradiation Effects in Fuel Materials

Metals

Results of studies of the irradiation behavior of uranium at cryogenic temperatures were presented[64] at the 10th Metallurgical Colloquium on Fragility and Effects of Irradiation. Zone-refined uranium was irradiated with neutrons at 4.5°K and measurements were made of the electrical-resistivity change, $\Delta\rho$. After the initial variation, which depended upon the texture and previous "history" of the sample, $\Delta\rho$ definitely tended toward a saturation value. Post-irradiation annealing confirmed the existence of a defect already mobile at 5°K and seems to show that vacancies migrate in alpha uranium at temperatures lower than 100°K. Such experiments are useful for understanding the mechanism for damage created by fission products in a metal; they also permit observation of defects in a material as anisotropic as uranium.

A study of gas-atom configurations in alpha uranium is being conducted at Atomics International.[60b] This study utilized an unpublished potential for uranium developed by Abrahamson of the City University of New York, based on the Thomas–Fermi–Dirac statistical model of the atom. A Rimmer–Cottrell potential for the Xe–U interaction was developed and is shown in Fig. I-11, along with the Xe–Cu potential for comparison.

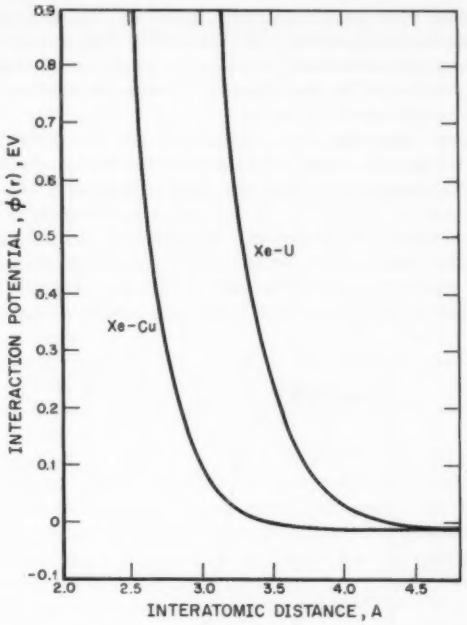

Fig. I-11 Rimmer–Cottrell-type heteronuclear potentials, for Xe–Cu and Xe–U (Ref. 60b).

Castleman and Tang[65] have investigated the behavior of fission products released from metallic uranium and a U–Mo alloy into helium and air. A thermochromatographic technique for investigating the nature of low-concentration gas species was applied to the release of Ba, La, Ce, and Mo from irradiated fuels. Barium, lanthanum, and cerium, which deposited at high temperature in helium, were not significantly released into air because of the low volatility of their respective oxides. Molybdenum, which was nonvolatile in helium, was released as MoO_3 in air.

Studies of the interrelation between linear thermal expansion and irradiation growth rate in uranium have been conducted by Kunchenko and Roenko.[66] It was noted that some correspondence between changes in the average thermal-expansion factor and the growth rate existed, as observed in the case of similar uniaxial textures. This type of texture forms in low-temperature deformation of uranium rods.

Plutonium metal undergoes continual self-irradiation due to its own natural radioactivity, and, when stored at low temperatures, substantial numbers of lattice defects are accumulated. Miner and Elliott[67] examined the annealing behavior of self-irradiation-induced defects in alpha plutonium stored at 87°K. After the defects were annealed at given temperatures, resistivity measurements were made at a 5°K reference temperature. The results are illus-

trated and compared with those of Wigley[68] for plutonium stored at 5°K (Fig. I-12). The four data points lying above the curve in the temperature range of 75 to 100°K resulted from overnight storage in liquid nitrogen at 77°K.

The Russians have calculated the temperature drops in the walls of cassette-type fuel elements under neutron fluences with radial gradients.[69] The thermal deformations of the walls were measured in the working range of these temperature drops. One of the conclusions reached was that deformation of the fuel elements due to temperature gradients will be the factor limiting the power of a reactor.

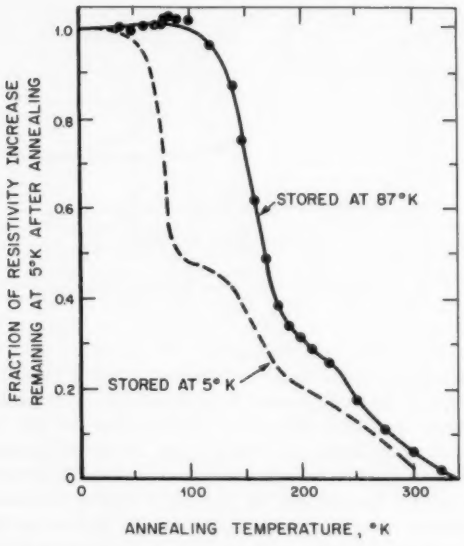

Fig. I-12 Isochronal annealing behavior of alpha plutonium. The fraction of the resistivity increase retained at 5°K after the stored specimen had been heated to each annealing temperature is plotted as a function of annealing temperature. The dashed line represents Wigley's data[68] for plutonium stored at 5°K; the solid line shows results for plutonium stored at 87°K (Ref. 67).

Studies of the behavior of inert gases in various nonfissionable metals represent valuable assets to analogous studies of inert-gas fission products in nuclear fuels. Kawasaki[70] has used a novel method to study the diffusion of xenon in copper in the temperature range 900 to 1000°C. In this experiment the diffusion coefficient of xenon (introduced into copper specimens as a recoil fission product) was obtained from measurements of the xenon distributions in annealed specimens. The results, illustrated in Fig. I-13, were less influenced by any "initial burst" than were results obtained by gas-release methods.

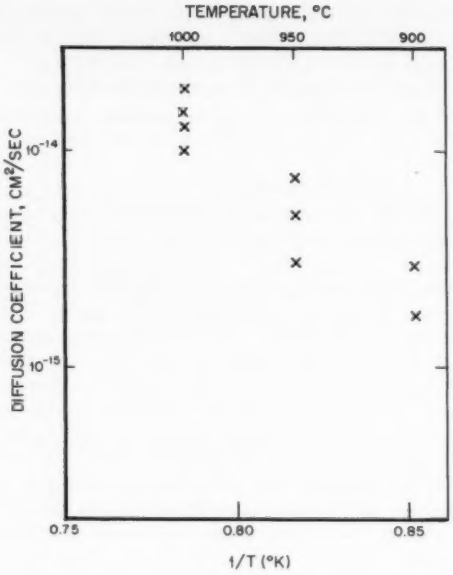

Fig. I-13 Plot of the temperature dependence of the diffusion coefficient of xenon in copper.[70]

Hastings and Russell[71] have investigated helium precipitation in irradiated Cu–B alloys. It was found that the fractional change in lattice parameter of copper was proportional to the concentration of dissolved interstitial helium up to approximately 0.03 at.%. When the concentration of helium was increased to within 0.08 to 0.1 at.%, the gas precipitated to form bubbles during irradiation at temperatures in the range 75 to 100°C. During annealing at 500°C, the lattice parameter contracted owing to the formation of helium-vacancy complexes at a rate proportional to the helium concentration. Subsequent expansion of the lattice, which also occurred at a rate proportional to helium concentration, was caused by the precipitation of these complexes to form bubbles. The time required for complete precipitation of the gas was inversely proportional to the helium content since the scale of gas-bubble nucleation became increasingly fine as the helium concentration increased. The behavior of the fractional change in lattice parameter, $\Delta a/a$, during the 500°C anneal is illustrated in Fig. I-14.

Speight[72] and Rosolowski[73] have commented on a paper by Russell and Vela[74] dealing with a theory of grain-boundary degeneration in materials containing an inert gas. This theory considered the lenticular growth of grain-boundary bubbles and the resultant force generated across the boundary of the gas within them in order to explain spontaneous cracking at high temperatures. Russell[75,76] subsequently stated that the theory should be regarded as phenomenologi-

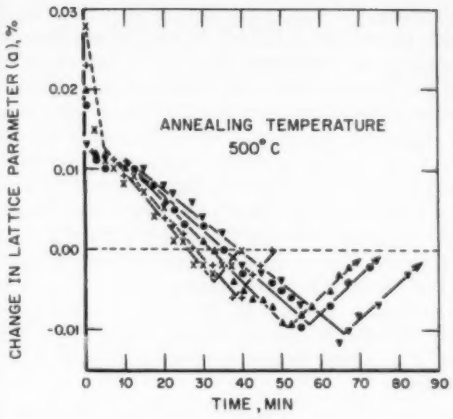

Fig. I-14 The effect of annealing time upon change in lattice parameter for a range of helium concentrations in irradiated Cu–B alloys.[71] ×, 0.028 at.% helium; +, 0.023 at.% helium; ▲, 0.020 at.% helium; ●, 0.018 at.% helium; ▼, 0.013 at.% helium.

cal in that it accounts formally for both the stress-rupture behavior of Cu–He alloys above 700°C and the existence of a temperature above which spontaneous growth begins. It also offers an explanation of the observed bubble distribution and shape. A much more detailed knowledge of the conditions for spontaneous bubble growth would be required for a more elaborate fundamental theory.

A theoretical study of radiation damage in crystals, using computer techniques, has been conducted at Atomics International.[77] The materials examined were copper, aluminum, and gold. Two major areas of investigation were pursued: (1) the various static configurations of lattice defects in copper and aluminum, and (2) the threshold displacement energies in gold. The major focus of all the work done was the effect of the choice of interatomic potential on the results calculated.

Ceramics

The effect of a thermal gradient on a pore in a solid has been analyzed from first principles by Nichols[78] under the assumption that evaporation and condensation constitute the dominant mechanisms of material transport. It was found that very small, initially spherical pores will migrate, with little distortion, up the thermal gradient and that somewhat larger ones (with smaller surface-tension effects) are unstable and will migrate as pores elongated along the temperature gradient. Still larger pores (with still smaller surface-tension effects) are completely unstable and will extend along the gradient, forming a cylindrical pore that, in turn, breaks up into a series of smaller pores aligned along the gradient. The application of these results to fabricated voids and fission-gas bubbles in fuel rods has provided an explanation for some of the experimental observations of pore shapes, sizes, and distribution in irradiated rods. It was suggested that lenticular voids felt to be necessary for the formation of relatively wide columnar grains may require some sort of nucleation and that the stress field and crack pattern may be intimately involved.

The shape of voids migrating in solids has been treated graphically by de Halas[79] by considering a perturbation applied to the shape of a void in a thermal gradient. Assuming vapor pressure to be proportional to temperature, evaporation and condensation vectors were drawn at selected points around the surface with their "lengths" proportional to the distance of the point from the thermal midplane of the void. The envelope of the vectors defined the new shape of the void. This treatment showed a sphere-like shape to be stable. Lenticular voids were also stable against most types of perturbations (although the trailing surface should be round) unless they ran into a small cavity, in which case the leading surface also tended to become rounded. If, however, vapor pressure increased exponentially with temperature, a spherical cavity would tend to become elongated in the direction of motion as it migrated up the thermal gradient. A possible mode of formation of lenticular voids was postulated and is illustrated in Fig. I-15.

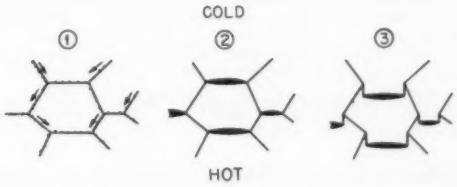

Fig. I-15 Possible mode of lenticular void formation.[79]

The lattice diffusion coefficient of ^{133}Xe in cast UC has been measured by Shaked, Olander, and Pigford[80] by postirradiation anneal experiments in the temperature range 1000 to 2000°C. The diffusion coefficient of specimens with large grains (700 to 1000 μ) at these temperatures was found to be best approximated by:

$$D = (1.17 \times 0.16) \times 10^{-6} \exp\left(-\frac{54{,}900 \pm 1200}{RT}\right) \text{ cm}^2/\text{sec}$$

Specimens with smaller grains (20 to 150 μ) exhibited the same diffusion coefficient as the large-grain samples above 1500°C. However, below 1500°C, diffusivities in small-grained specimens varied widely, indicating a dependence on grain size and, conse-

quently, the existence of appreciable grain-boundary diffusion. The results are illustrated in Fig. I-16.

Measurements of the rate of uranium-atom emission from a fissioning surface have been made by Peterson and Thorpe[81] using uranium and UO_2 sources.

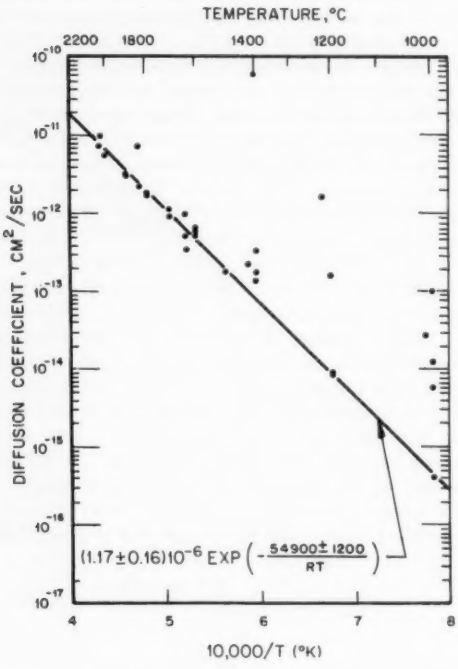

Fig. I-16 Diffusion coefficient of ^{133}Xe in UC (Ref. 80).

A technique was employed in which the source could be maintained in vacuo at all times during the experiments. It was found that at the start of an experiment the rate of emission was high but declined with increasing reactor exposure to a low constant value of about 6 uranium atoms ejected per fission fragment penetrating the surface for the metal and about 38 atoms for the oxide. Exposure of a uranium-metal source to moist helium, after a constant emission rate was achieved, led to a rapidly increased rate that approximated the pretreatment value.

Radial and axial distributions of ^{137}Cs, ^{144}Cs, and plutonium were determined in three UO_2 fuel rods by General Electric.[82] The rods represented three different levels of fuel thermal performance: incipient center melting, moderate center melting, and gross center melting. Gross radial migration of ^{137}Cs was observed in all three rods, and axial migration was noted in the two higher rated rods. Grain growth was a necessary condition for radial migration, whereas center melting was required for axial migration. Direct evidence was obtained for convective mixing in the molten UO_2. Burnup in the molten zone was independent of axial location and did not reflect the axial flux profile. Significant segregation of ^{144}Cs and plutonium was superimposed on the convective mixing. Such segregation appeared to result from recrystallization of the molten fuel. In addition, separative effects were observed in UO_2 vapor deposited near the top of a central void. The U–Pu separative effects in mixed-oxide, fast reactor fuel are important in reactor control. The prompt negative power coefficient provided by fission recoil heating of the ^{238}U depends upon intimate mixing of the ^{238}U and plutonium. Separative effects, similar to those observed in high-rated UO_2, could reduce this coefficient in mixed-oxide fuel.

Released fission products may, in principle, be characterized according to their volatility by observing the temperature at which they deposit when passed through a tube along which the temperature is uniformly reduced. Studies of this technique have been conducted in the United Kingdom,[83] including the development of a mathematical model to describe the process. The model correctly predicts the shape of the deposit and relates the temperature at which deposition begins to the vapor-pressure curve of the associated compound. Adaptation of the technique as a sampling method for general use in fission-product transport experiments has been studied using CsI as a typical fission-product compound. It was found that behavior under carefully controlled conditions followed that predicted by the mathematical model but was susceptible to factors such as the low mass levels of CsI. Application to the study of fission products released from irradiated UO_2 in laboratory experiments gave results impossible to interpret because of the low mass levels concerned. It was concluded that, for application to many conditions of interest, further development is required.

A literature survey of fission-product behavior was conducted by Phillips Petroleum.[84] The survey was restricted to the literature concerning fission-product release, transport, and deposition, with parameters representative of water-cooled and -moderated power reactors. The types of fuel considered for survey were limited to low-enriched UO_2, with special emphasis given to zirconium-clad fuel.

Baskin[85] has studied the effect of irradiation on the lattice structure of stoichiometric UP at a temperature estimated to be less than 100°C. The results of X-ray diffraction experiments (given in Table I-2) show the dependence of lattice parameters on irradiation. The lattice parameter initially increased with increased irradiation and reached a maximum at about 10^{17} fissions/cm^3. This effect is consistent with the behavior of UC and UN noted by Adam and Rogers[86] and presumably resulted from the presence of displaced atoms in interstitial positions. The lattice

Table I-2 EFFECT OF IRRADIATION DOSE ON UP LATTICE CONSTANT[85]

Specimen	Time in reactor, hr	Irradiation, fissions/cm³	Lattice constant,* A
Untreated			5.589
A	1.0	1.22×10^{16}	5.590
B	10.2	1.25×10^{17}	5.592
C	106.5	1.30×10^{18}	5.589
D	1054.5	1.29×10^{19}	5.590

*The lattice constants were accurate to ±0.001 A, with the exception of that for specimen C, which was accurate to ±0.003 A.

parameter then fell sharply to essentially its original value at 10^{18} fissions/cm³ and subsequently increased slowly with further irradiation. After 10^{18} fissions/cm³, the X-ray reflections became very broad and diffuse in the high-angle region, indicating lattice strain, but became sharp again with the higher levels of irradiation. Similar behavior was observed (and a tentative interpretation given) by Wait et al.,[87] with UO_2 irradiated at 400°C under similar conditions. Annealing of the irradiated UP powders in vacuum at 1200°C invariably produced a contraction in the lattice parameter and sharpening of the diffraction pattern. The lattice parameters of all irradiated powders were lower after annealing than those of the original materials. A possible explanation might be loss of interstitial phosphorus during annealing, leaving a slight nonmental-atom deficiency. This hypothesis could not be tested because the specimens were too small for chemical analysis.

(A. J. Markworth)

References

1. C. J. Beevers and G. T. Newman, Hydrogen Embrittlement in Uranium, *J. Nucl. Mater.*, 23(1): 10-18 (July 1967).
2. E. Storms, An Evaluation of the Heat of Vaporization of Uranium from the Behavior of the U–C System, USAEC Report LA-DC-8790, Los Alamos Scientific Laboratory, June 1967.
3. B. Hudson, The Distribution of the Swelling Produced by Fission Gas Bubbles in α and β Uranium Irradiated Under Low Stress, *J. Nucl. Mater.*, 22(2): 121-136 (May 1967).
4. D. M. Mattox and R. D. Bland, Aluminum Coating of Uranium Reactor Parts for Corrosion Protection, *J. Nucl. Mater.*, 21: 349-352 (March 1967).
5. P. Grenier and P. Lacombe, Activation Energies of Several Deformation Mechanisms from Creep of Uranium Monocrystals and Polycrystals Between 150 and 770°C (in French), *J. Nucl. Mater.*, 22(3): 241-256 (June 1967).
6. F. de Keroulas, J. Mory, and Y. Quere, Fissiography: Diffusion of Uranium in Almost Infinite Dilution in Titanium and Iron (in French), *J. Nucl. Mater.*, 22(3): 276-284 (June 1967).
7. G. T. Newman and C. J. Beevers, Grain Size–Fracture Stress Relationship of Uranium, *J. Nucl. Mater.*, 23(1): 95-97 (July 1967).
8. R. Burgett (Ed.), Summary Technical Report [on Feed Material Production] for the Period April 1–June 30, 1967, USAEC Report NLCO-1001, pp. 5.1-5.9, National Lead Company of Ohio, August 1967.
9. G. F. Slattery and W. N. Miller, The Creep Strength of Uranium Containing Small Alloying Additions, *J. Nucl. Mater.*, 22(3): 320-331 (June 1967).
10. M. Colombie and J. Decours, Influence of Carbon on the Primary Crystallization of Low-Concentration U–Mo Alloys, USAEC Report ORNL-tr-1668 (from French Report CEA-R-3093), February 1967.
11. C. Fizzotti and A. Masperoni, Influence of Heat Treatments on the Structure of Uranium Alloys with a Low Niobium Content, USAEC Report ORNL-tr-1695 [from Italian Report RT/MET-(66)-1, 1966].
12. R. Benz and M. C. Tinkle, Hysteresis in the α–β Transition of Uranium Saturated with Silicon, *J. Nucl. Mater.*, 22(2): 228-231 (May 1967).
13. M. Violle and M. Degois, Influence of the Solubility Limit of Chromium in β-Uranium on the Isothermal Transformations of Uranium–Chromium Alloys Tempered from 720°C (in French), *Compt. Rend., Ser. C*, 264: 1629-1632 (May 17, 1967).
14. W. J. Kitchingham and K. M. Pickwick, The $\beta \rightarrow \alpha$ Phase Change in a Uranium–Platinum–Niobium Alloy, *J. Inst. Metals*, 95: 61-63 (February 1967).
15. I. Amity, A. Rosen, and A. Bar-Or, Bainitic Reaction in Uranium–Chromium Alloys, *J. Inst. Metals*, 95: 48-52 (February 1967).
16. C. Collet, J. P. Lauque, and M. Columbie, Study of the Mechanical Properties and Thermal Properties of Uranium Alloys with Small Additions (in French), *Mem. Sci. Rev. Met.*, 64: 393-402 (April 1967).
17. Y. Goldstein and A. Bar-Or, Decomposition of Gamma Phase in Uranium Alloys Containing 8, 10.8, and 14.3 Wt.% Molybdenum, *J. Inst. Metals*, 95: 17-21 (January 1967).
18. R. J. Jackson, R. P. Brugger, and D. V. Miley, Tensile Properties of Gamma Quenched and Aged Uranium-Rich Niobium Alloys, USAEC Report RFP-933, Dow Chemical Co., Rocky Flats Division, June 2, 1967.
19. Mound Laboratory, Reactor Fuels and Materials Development Plutonium Research, April–September 1966, USAEC Report MLM-1347, p. 11-18, July 28, 1967.
20. University of California, Lawrence Radiation Laboratory, Contributions to the 1967 US/UK Plutonium Newsletter, USAEC Report UCID-15141, May 15, 1967.
21. L. G. T. Davy, M. E. Faiers, and J. S. White, The Kinetics of the $\alpha \rightleftharpoons \beta$ Transformations in Some Dilute Plutonium Alloys, *J. Nucl. Mater.*, 22(2): 197-204 (May 1967).
22. B. R. Spicer and J. S. White, The Effect of Thermal Cycling upon the Transformation of Metastable Delta-Phase Plutonium, *J. Nucl. Mater.*, 22(3): 269-275 (June 1967).
23. Nuclear Materials and Equipment Corp., Growth of Single Crystals of Plutonium, Progress Report April 1, 1967–June 30, 1967, USAEC Report NUMEC-3428-35, August 1967.
24. U. K. Atomic Energy Authority, Atomic Energy Research Establishment Ceramics Division, unpublished.
25. R. L. Andelin, L. D. Kirkbride, and R. H. Perkins, High-Temperature Environmental Testing of Liquid Plutonium Fuels, USAEC Report LA-3631, Los Alamos Scientific Laboratory, Jan. 17, 1967.
26. W. L. Lyon and W. E. Baily, The Solid–Liquid Phase Diagram for the UO_2–PuO_2 System, *J. Nucl. Mater.*, 22(3): 332-339 (June 1967).
27. L. F. Epstein, Ideal Solution Behavior and Heats of Fusion from the UO_2–PuO_2 Phase Diagram, *J. Nucl. Mater.*, 22(3): 340-349 (June 1967).
28. G. F. Molen and R. D. White, Properties of Plutonium Dioxide, Part II, USAEC Report RFP-927, Dow Chemical Co., Rocky Flats Division, July 12, 1967.
29. B. J. Thamer, The Use of (U,Pu)N Fuel with a Sodium Bond: A Summary of Existing Data, USAEC Report LA-3646, Los Alamos Scientific Laboratory, Jan. 6, 1967.

30. D. L. Keller, Progress Relating to Civilian Applications, During July 1966–June 1967, Annual Report, USAEC Report BMI-1809, (*a*) pp. A20-56, (*b*) pp. C30-44, Battelle Memorial Institute, July 1, 1967.
31. W. O. Greenhalgh and E. T. Weber, Carbothermic Synthesis of (U,Pu)N from $(U,Pu)O_2$–Carbon Mixtures, presented at U. S.–Japan Information Exchange Meeting on Ceramic Nuclear Fuels, Richland, Wash., Sept. 25–29, 1967.
32. T. A. Badacua and R. I. Kuznetsova, Phase Diagrams of the Th–Pr and Th–Nd Systems, *Izv. Akad. Nauk SSSR, Metal.*, No. 1: 175-181 (January–February 1967).
33. P. Chiotti and R. W. White, Miscibility Gap in the Th–ThC System from High Temperature X-Ray Data, *J. Nucl. Mater.*, 23(1): 37-44 (July 1967).
34. Argonne National Laboratory, Reactor Development Program Progress Report, June 1967, USAEC Report ANL-7349, p. 95, July 31, 1967.
35. Ames Laboratory, Annual Summary Research Report, Ceramic and Mechanical Engineering, Chemical Engineering, Chemistry, Mathematics and Computer Science, Metallurgy, Physics, and Reactor Divisions, July 1, 1966–June 30, 1967, USAEC Report IS-1600, (*a*) pp. M7-8, (*b*) p. M30.
36. Oak Ridge National Laboratory, Gas-Cooled Reactor Program Semiannual Progress Report for Period Ending March 13, 1967, USAEC Report ORNL-4133, pp. 10-16, August 1967.
37. H. J. Nordwall and J. B. Sayers, The Value of a Silicon Carbide Barrier in HTR Fuels, paper presented at AIME Nuclear Metallurgy Symposium, Delavan, Wis., October 3–5, 1966.
38. H. S. Rosenburg, D. L. Morrison, C. W. Townley, and D. N. Sunderman, Postirradiation Fission-Product Release from Coated Fuel Particles, USAEC Report BMI-1734, Battelle Memorial Institute, July 7, 1965.
39. Oak Ridge National Laboratory, unpublished, June 6, 1967.
40. Oak Ridge National Laboratory, unpublished, July 7, 1967.
41. M. Feliciano, Jr. (Comp. and Ed.), Mathematics Division Annual Progress Report for Period Ending December 31, 1966, USAEC Report ORNL-4083, pp. 29-30, April 1967.
42. General Atomic Division, General Dynamics Corp., HTGR Base Program Quarterly Progress Report for the Period Ending May 31, 1967, USAEC Report GA-7981, Sept. 29, 1967.
43. T. D. Gulden, Deposition and Microstructure of Vapor-Deposited Silicon Carbide, Gulf General Atomic Incorporated, submitted for publication to *J. Amer. Ceram. Soc.* (GA-8275, Dec. 1, 1967).
44. M. E. Gulden, Migration of Gas Bubbles in Irradiated Uranium Dioxide, *J. Nucl. Mater.*, 23(1): 30 (July 1967).
45. Hj. Matzke, The Release of Some Non-Gaseous Fission Products from CaF_2, UO_2, and ThO_2, *J. Nucl. Mater.*, 23(2): 209 (August 1967).
46. K. T. Harrison, C. Padgett, and K. T. Scott, The Kinetics of the Oxidation of Irradiated Uranium Dioxide Spheres in Dry Air, *J Nucl. Mater.*, 23(2): 121 (August 1967).
47. R. Szwarc and R. E. Latta, Vapor Pressure of Hypostoichiometric Urania as a Function of Composition, USAEC Report GEMP-528, General Electric Company, Nuclear Materials and Propulsion Operation, June 19, 1967.
48. K. G. Hackstein and H. Pirk, Production of Sinterable, Slightly Enriched UO_2 in Fluidized Bed Furnaces (in German), *Kerntechnik*, 9: 261-263 (June 1967).
49. J. J. Rosenthal and M. C. Tinkle, Flame Spraying Uranium Oxide, USAEC Report LA-3677, Los Alamos Scientific Laboratory, February 1967.
50. R. Sh. Mikhail and R. B. Fahim, Thermal Treatment of Thorium Oxide Gel at Low Temperatures, *J. Appl. Chem. (London)*, 17: 147-150 (May 1967).
51. A. I. Evstyukhin, G. B. Fedorov, G. I. Solov'ev, E. A. Smirnov, F. I. Zhomov, and A. G. Zaluzhnyi, Phase Diagram of the U–W System and Diffusion of Uranium from UC into Tungsten, in *High Purity Metals and Alloys*, pp. 79-83, Consultants Bureau, New York, 1967.
52. J. L. Henry, D. L. Paulson, R. Blickensderfer, and H. J. Kelly, Phase Relations in the UC Region of the U–C–O System at 1700°C, *U. S. Bureau of Mines Report of Investigations*, No. 6968, July 1967.
53. S. K. Dutta and J. White, Compatibility of UC with Alloys of Iron, Nickel, and Chromium, *Proc. Brit. Ceram. Soc.*, No. 7: 177-203 (February 1967).
54. P. Chiotti, F. W. Korbitz, and G. J. Dooley, Electrical Resistivity and Phase Relations for the Thorium–Carbon System, *J. Nucl Mater.*, 23(1): 55-67 (July 1967).
55. H. A. Wilhelm and P. Chiotti, Thorium–Carbon System, *Trans. Amer. Soc. Metals*, 42: 1295-1310 (1950).
56. A. L. Bowman, C. P. Arnold, W. G. Witteman, T. C. Wallace, and N. G. Nereson, Crystal Structures of UC_2, *Acta Crystallogr.*, 21: 670-671 (November 1966); also LA-DC-7759.
57. V. S. Eremeev, A. S. Panov, B. F. Ushakov, and E. V. Fiveiskii, Diffusion of Carbon from UC into Molybdenum and Tungsten, in *Thermodynamics*, Symposium Proceedings, Vienna, 1965, Vol. II, pp. 161-172, International Atomic Energy Agency, Vienna, 1966 (STI/PUB/109); also LA-TR-67-31.
58. W. Chubb, Buffering of UC to Control Carbon Activity, *Nucl. Sci. Eng.*, 29: 176-179 (1967).
59. E. K. Storms and E. J. Huber, Jr., The Heat of Formation of UC, *J. Nucl. Mater.*, 23(1): 19-24 (July 1967); also LA-DC-8790.
60. Atomics International, AEC Unclassified Programs Quarterly Technical Progress Report, January–March 1967, USAEC Report NAA-SR-12395, (*a*) pp. 150-152, (*b*) pp. 91-93, May 31, 1967.
61. S. Strausberg, N. H. Katz, and H. J. Wolfe, Heavy Water Organic Cooled Reactor. Surface Finish Improvement in Cast UC Slugs, USAEC Report AI-CE-48, Atomics International and Combustion Engineering, Inc., Aug. 15, 1967.
62. L. A. Hanson, Heavy Water Organic Cooled Reactor. The Preparation of Uranium Carbide from Economical Uranium Compounds, USAEC Report AI-CE-73, Atomics International and Combustion Engineering, Inc., Aug. 15, 1967.
63. T. Mukuibo, M. Kanno, T. Mitamura, and K. Yoshihara, Preparation of Uranium Carbide from Uranium Chloride, *J. Nucl. Sci. Technol. (Tokyo)*, 3(9): 388-392 (September 1966).
64. G. Burger, K. Isebeck, H. Wenzl, J. C. Jousset, and Y. Quere, Irradiation of Uranium with Neutrons at 4.5°K, USAEC Report ANL-Trans-432 (from CONF-660656-1), February 1967.
65. A. W. Castleman, Jr., and I. N. Tang, Vaporization of Fission Products from Irradiated Fuels—1. Experimental Method and General Fission-Product Behavior, *Nucl. Sci. Eng.*, 29(2): 159-164 (August 1967).
66. V. V. Kunchenko and N. M. Roenko, Interrelation Between Linear Thermal Expansion and Irradiation Growth Rate, *At. Energ. (USSR)*, 20(2): 169-170 (February 1966).
67. W. N. Miner and R. O. Elliott, Annealing of Self-Irradiation Induced Defects in Alpha Plutonium Stored at 87°K, *J. Nucl. Mater.*, 23(1): 115-117 (July 1967).
68. D. A. Wigley, Ph. D. Thesis, University of Oxford, 1963.
69. E. Ya. Safronov, B. A. Briskman, V. D. Bondarev, and V. S. Shishov, Thermal Deformation of Fuel Elements, *At. Energ. (USSR)*, 21(1): 22-26 (July 1966).
70. S. Kawasaki, Diffusion of Xenon in Copper, *J. Nucl. Mater.*, 22(2): 192-196 (May 1967).
71. I. J. Hastings and B. Russell, The Effect of Concentration upon Helium Precipitation in Irradiated Copper Boron Alloys, *J. Nucl. Mater.*, 23(1): 1-9 (July 1967).
72. M. V. Speight, Growth of Grain-Boundary Bubbles in

Materials Containing Inert Gases (A Comment on the Paper of Russell and Vela), *J. Nucl. Mater.*, 22(2): 234-235 (May 1967).
73. J. H. Rosolowski, A Theory of Grain Boundary Degeneration in Materials Which Contain an Inert Gas (Comments on the Paper by B. Russell and P. Vela), *J. Nucl. Mater.*, 22(2): 237-238 (May 1967).
74. B. Russell and P. Vela, A Theory of Grain Boundary Degeneration in Materials Which Contain an Inert Gas, *J. Nucl. Mater.*, 21(1): 32-37 (January 1967).
75. B. Russell, Spontaneous Growth of Grain Boundary Bubbles in Materials Which Contain Inert Gas, *J. Nucl. Mater.*, 22(2): 236 (May 1967).
76. B. Russell, Comments on a Theory of Spontaneous Grain Boundary Degeneration, *J. Nucl. Mater.*, 22(2): 239-240 (May 1967).
77. A. Anderman, Computer Investigation of Radiation Damage in Crystals, Report AFCRL-66-688 (AI-66-252), Atomics International, September 1966.
78. F. A. Nichols, Theory of Columnar Grain Growth and Central Void Formation in Oxide Fuel Rods, *J. Nucl. Mater.*, 22(2): 214-222 (May 1967).
79. D. R. de Halas, The Shape of Migrating Voids, *J. Nucl. Mater.*, 23(1): 118-120 (July 1967).
80. H. Shaked, D. R. Olander, and T. H. Pigford, Diffusion of Xenon in Uranium Monocarbide, *Nucl. Sci. Eng.*, 29(1): 122-130 (July 1967).
81. P. J. Peterson and M. M. Thorpe, Comparative Measurements of Uranium Atom Emission from Fissioning Surfaces, *Nucl. Sci. Eng.*, 29(3): 425-431 (September 1967).
82. J. H. Davies, R. F. Boyle, and J. F. Hanus, Fission Product and Plutonium Redistribution in High Performance UO_2 Fuel Rods, USAEC Report GEAP-5100-4, General Electric Company, Atomic Power Equipment Department, January 1966.
83. D. A. Collins, R. D. Collins, R. Taylor, A. E. McIntosh, and W. B. Roys, The Temperature-Gradient Tube Technique for Characterization of Released Fission Products, British Report TRG-Report-1332 (W), Jan. 20, 1967.
84. E. G. Good, Fission Product Behavior Literature Review, USAEC Report IDO-17237, Phillips Petroleum Company, February 1967.
85. Y. Baskin, Properties of Uranium Monophosphide, *J. Amer. Ceram. Soc.*, 49(10): 541-546 (October 1966).
86. J. Adam and M. D. Rogers, X-Ray Diffraction Studies of Fission Fragment Damage in Uranium Carbide and Nitride, *J. Nucl. Energy*, 14(1): 51-53 (1961).
87. E. Wait, M. J. Duck, A. C. Fox, E. E. Jackson, and A. R. Junkison, A Single Crystal X-Ray Diffraction Technique for the Study of Radiation Damage, in *Radiation Damage in Solids*, Symposium Proceedings, Venice, 1962, Vol. II, pp. 231-238, International Atomic Energy Agency, Vienna, 1962 (STI/PUB/56).

Section II

Reactor Materials

Moderator and Control Materials

Graphite

Dynamic Young's modulus values have been measured over the temperature range −196 to 1000°C for nuclear-grade carbon heat-treated at temperatures[1] between 1200 and 3000°C. The results were discussed in terms of the uniform-stress model for graphite, whereby the elastic modulus depends essentially on the effective C_{44} shear stiffness of the single crystal, on the orientation of crystallites, and on the artifact porosity. Dislocations lying in the basal plane reduced the effective C_{44} to values below that expected for the lattice alone. This effect was dependent on temperature because of the thermal unpinning of dislocations, and on crystallite size. It was deduced that the lattice value of C_{44} was 4.5 times higher for material treated at 3000°C than for that treated at only 1200°C. The increase in modulus with temperature, occurring above 300°C, was attributed to a process of void filling determined by the difference between the volume thermal-expansion coefficients of artifact and constituent crystallites. The effect of these voids was to reduce the modulus measured at room temperature by a factor of about 5 for material treated at 3000°C.

A British investigator has conducted a microscopic study on the formation and growth of cracks in polycrystalline graphite.[2] The need for improved understanding of the strength-limiting factors for polycrystalline graphite makes this study of special importance. The experimental technique permitted control of tensile strains to about 1% of the breaking strain of the graphite. Thus it was possible to propagate a crack slowly and in a controlled manner. Three types of graphite were studied: coarse grained (nuclear grade), medium grained (Morgan EY 9), and fine grained (POCO AXF).

The major summary observations from this investigation are as follows. First, for the anisotropic graphite stressed parallel to the extrusion direction, propagating cracks tended to be diverted around filler particles and thus proceeded by a more tortuous route than when stress was applied perpendicular to extrusion. The difference in crack path was reflected in the higher stress to fracture for parallel vs. perpendicular directions. Second, the effect of pores on fracture appeared to be important mainly in the coarse-grained material. The rate of propagation of a crack was reduced when entering a large pore, owing to stress relief at the crack tip. This stress relief in conjunction with the stress field behind the tip tended to produce further secondary cracks. In the medium-grained material, isolated pores appeared to have no effect on the crack propagation, but areas of higher porosity in the specimen tended to resist passage of cracks and to produce secondary cracking. In fine-grained graphite the fracture path appeared to be unaffected by porosity. Third, weaknesses in both coarse- and medium-grained graphite appeared to be associated with the larger filler grains. With fine-grained graphite it was not easy to attribute a weakness to any particular part of the structure, but it was evident that fracture proceeded by a similar path, suggesting that the weak features observed in the coarse- and medium-grained materials were also operative in the case of fine-grained graphite.

The same investigators analyzed published graphite data and arrived at the following empirical relation of strength to grain size and porosity:

$$S = 1.2 \times 10^8 \exp(-6.8\,\epsilon)\, d^{-1/2}$$

where S is the average bend strength and is $\frac{1}{3}$ (parallel strength plus two times the perpendicular strength) in dynes per square centimeter, ϵ is the fractional porosity, and d is the maximum grain size in centimeters.

The effect of irradiation at 300 to 1500°C on the thermal conductivity and electrical resistivity of anisotropic and isotropic graphites was examined by General Atomic.[3] The postirradiation thermal conductivities of all the graphites at room temperature were found to be lower than the preirradiation conductivities. For specimens irradiated at 300°C, the fractional reduction in conductivity, $1 - (k/k_0)$ (where k_0 and k are pre- and postirradiation values, respectively), was about 0.85. For specimens irradiated at 1250 to 1500°C, the fractional reduction was about 0.35. When postirradiation measurements were made at the specimen irradiation temperatures, the fractional reduction in conductivity ranged from about 0.80 at 300°C to zero at 1250 to 1500°C.

Irradiation defects in an anisotropic CHN graphite started to anneal at 1200°C, and a fractional change

in conductivity of only 0.03 remained after heating to 1500°C. In contrast, a fractional change of 0.15 remained in the isotropic graphite (H-315-A) after heating to 2000°C, and all defects were not removed until annealing temperatures were increased to 2300 to 2600°C.

The radiation-induced fractional increase in electrical resistivity, $(\rho/\rho_0) - 1$ (where ρ and ρ_0 are the post- and preirradiation resistivities), ranged from 1.5 for 300°C irradiation temperatures to 0.5 for 1250°C irradiation. The radiation-induced changes in room-temperature thermal conductivity and electrical resistivity were attributed to vacancies retained in the graphite-layer planes after high-temperature irradiation.

An extensive summary of radiation-induced dimensional change in several graphites has been compiled by General Atomic.[4] The anisotropic, needle-coke graphite grades, NC7, NC8, and TS-688, have been most extensively evaluated and thus represent most of the data. However, data are also summarized for grades 9567, H-327, H-328, and RC-4/SX4.

The effect of irradiation on the hardness of a near-isotropic reactor graphite was investigated by Brown.[5] The Vickers hardness increased by a factor of 7 on irradiation at 150°C to a maximum fluence of 11.5×10^{20} neutrons/cm^2 and showed no signs of saturation. At low fluences this hardening was attributed to radiation-induced pinning of basal-plane dislocations. At higher fluences it was attributed to pore closure brought about by a c-axis growth of the crystallites. On thermal annealing the hardness eventually returned to the unirradiated value in stages, owing to a decrease in pinning points and the annealing of large interstitial clusters by vacancy diffusion.

The effect of crystallite orientation and of impregnation on the radiation-induced contraction of graphite has been studied at Battelle–Northwest.[6] Maximum fluences of 1.3×10^{21} neutrons/cm^2 ($E >$ 0.18 Mev) in a temperature range of 500 to 700°C were used in these experiments. For a series of graphites, identical except in the relative orientation of the crystallites, it was found that contraction rates can be predicted for the different orientations on the basis of contraction-rate data for any one orientation. Thus the single-phase model may be used effectively to predict contraction rates of very similar nuclear graphites at fluences below "turnaround," providing radiation data on one graphite are available. The contraction behavior of impregnated graphites was found to be more complex. At the higher impregnant levels (approximately 16% for the graphite in this study), the contraction rate increased with impregnant level. The suggested explanation was that, as open pores were filled and the impregnant assumed part of the supporting structure, increased contraction occurred because the binder contracted at a more rapid rate than did the filler. Thus these results support a two-phase model of graphite contraction under irradiation.

The bond mechanism in brazing graphite has been the subject of studies by Los Alamos.[7] It was found that the strength of the braze joint varies directly with the brazing temperature, although previous data indicated that too high a brazing temperature for a specific material can result in a weak joint. X-ray diffraction studies of samples brazed with molybdenum revealed that the 0 0 2 reflection is about five times greater in specimens brazed above 2660°C than in those brazed at 2450°C and below. Metallographic analysis of the samples brazed at the higher temperatures revealed precipitated graphite across the joint interface. Table II-1 summarizes low and high average room-temperature flexural strength for braze materials studied.

Table II-1 ROOM-TEMPERATURE FLEXURE STRENGTH OF BRAZED UNLOADED GRAPHITE[7]

Braze alloy	Corrected braze temperature and time	Modulus of rupture, psi
0.0006 in. Mo	2150°C for 15 min	2850^{+510}_{-280}
	2660°C for 3 min	4430^{+30}_{-40}
0.0005 in. W	2650°C for 3 min	3760^{+420}_{-645}
	2850°C for 3 min	4420^{+450}_{-880}
0.0005 in. Ta	2400°C for 3 min	1920^{+30}_{-30}
	3000°C for 3 min	3490^{+130}_{-360}
0.0005 in. Fe	1100°C for 3 min	1380^{+30}_{-20}
	2500°C for 3 min	3325^{+65}_{-20}
0.0005 in. Zr	1750°C for 3 min	3580^{+100}_{-150}
	1890°C for 3 min and 2900°C for 3 min	1880^{+200}_{-240}
	2850°C for 3 min	6350^{+260}_{-160}
0.0005 in. Nb	2280°C for 3 min	2700^{+530}_{-330}
	2500°C for 3 min and 2850°C for 3 min	4730^{+110}_{-130}

(M. C. Brockway)

Beryllium and Beryllium Alloys

Physical Metallurgy

LOW-OXIDE, FINE-GRAINED, WROUGHT BERYLLIUM AND Be–Cu ALLOY

Lympany, Theodore, and Beaver are investigating the effect of high purity on the mechanical behavior of fine-grained beryllium sheet.[8] A process has been devised for producing subsieve powder and subsequent hot pressings with a minimum of contamination. Emphasis was placed on procedures for achieving a final microstructure and preferred orientation typical of commercial sheet. The grain sizes of pressings

prepared from unscreened powder containing 52 to 64% of −20-μ fines are only slightly larger than those of a pressing obtained with screened powder containing 100% −20-μ particles. These results indicate that factors other than powder size alone are contributing to the final grain size. Tensile-strength and elongation values greater than those for S-200 sheet were obtained on the first sheet prepared from the subsieve pressings. However, the corresponding bend ductility (third-dimensional ductility) was apparently unaffected by the decreased grain size. The second sheet showed very poor elongation and low ultimate strength, which were attributed to contamination by Fe, Ni, Cu, and Ag during powdering.

Kaufmann has continued studies of the production of beryllium powder by splat cooling for consolidation into a low-oxide fine-grained material with a desirable combination of strength and ductility.[9] SR-grade beryllium and SR Be−4 wt.% Cu were splat cooled using a rotating electrode to supply drops of liquid metal and a moving sheet for the quenching of the molten drops. The resulting splat materials were consolidated either by extrusion to bar stock or by hot pressing and rolling to sheet. Oxygen contents of 2500 to 3000 ppm were about one-tenth that of powder-metallurgy beryllium having similar grain size, i.e., 5 to 20 μ.

The major conclusion of this investigation was that, in bend tests, unusually high values for strain were achieved in the thickness direction of the sheet, accompanied by high levels of strength. Tensile tests did not reveal so much improvement, but the data appeared comparable to those for commercial sheet that had been given higher levels of reduction. Typical values for bend-test elongation of commercially rolled beryllium sheet are about 0.6 to 1.2% at yield strengths of about 80,000 psi, whereas the best values obtained in this investigation on the unalloyed SR were 3 to 5% elongation at yield strengths of 70,000 to 90,000 psi. It was apparent that the relatively high properties in the longitudinal direction were not obtained at the expense of those in the transverse direction, and splat cooling therefore may be a promising way to achieve improved third-dimensional ductility in beryllium sheet.

The addition of 4% copper to SR beryllium did not remarkably improve properties; however, higher transverse ductilities were obtained with the copper alloy. This may mean that alloying increased the critical resolved shear stress (CRSS) on the basal planes enough to force some slip on the prism planes during transverse testing, thus leading to a small increase in third-dimensional ductility. The copper-alloy sheet had a relatively weak texture that could be due to the CRSS on the basal and prism planes being more nearly equal than in unalloyed beryllium.

The poor elongation of the extruded SR splat appears anomalous, especially since the same material in the form of sheet exhibited improved third-dimensional ductility. Likewise, the copper alloy as bar stock had better ductility than did the unalloyed SR beryllium but was inferior to the latter as sheet.

BERYLLIUM–HYDROGEN

The Be–H system was examined using tritium instead of hydrogen since small quantities can be measured easily with ion chambers. The tritium release at any temperature followed the type of logarithmic equation expected for a diffusion-controlled process.[10] However, when the temperature was increased further, gas was evolved to a new limiting value. This behavior was repeated at a series of temperatures. It was postulated that the tritium became trapped, possibly in molecular form, at sites with a range of energies such that only a fraction of the gas was available at any temperature. Diffusion and solubility constants were calculated to be as follows:

$$\log D(\text{cm}^2/\text{sec}) = (6.53 \pm 0.15) - (965 \pm 106)/T(^\circ\text{K})$$

$$\log S(\text{std ml/gram atom}^{1/2}) = -(2.12 \pm 0.27) + (0.095 \pm 0.211)/T(^\circ\text{K})$$

BERYLLIUM–HELIUM

Satisfactory agreement has been obtained for calculated and measured values for the quantity of helium formed in beryllium samples irradiated in a fast fluence.[11] Helium is formed by the following three reactions:

1. ${}^9_4\text{Be} + n \rightarrow {}^8_4\text{Be} + 2n$
2. ${}^9_4\text{Be} + n \rightarrow {}^6_2\text{He} + {}^4_2\text{He}$
3. ${}^6_2\text{He} \xrightarrow{\beta} {}^6_3\text{Li}$

   ${}^6_3\text{Li} + n \text{ (thermal)} \rightarrow {}^4_2\text{He} + {}^3_1\text{H}$

The quantity of helium formed for each reaction is directly proportional to the average nuclear cross section for each reaction. The total average cross section for helium formation is the sum of the average nuclear cross sections for each reaction. Helium analysis was performed by chromatography on the gas evolved during dissolution of the beryllium in sulfuric acid. A comparison of the measured and calculated values is presented in Table II-2. This ability to perform helium analysis in irradiated beryllium permits the calculation of a mean effective cross section for a given neutron spectrum if the fluence is known or the determination of the fluence if the mean effective cross section in the relevant neutron spectrum is known.

Deformation Modes

The deformation modes of beryllium have been studied by Poirier, Antolin, and Dupouy.[12] They have

Table II-2 COMPARISON OF CALCULATED AND EXPERIMENTAL RESULTS FOR HELIUM QUANTITIES AND NUCLEAR CROSS SECTION[11]

Fluence, 10^{19} neutrons/cm^2	Helium, cm^3/g		Cross section, mb	
	Calculated	Measured	Calculated	Measured
0.61	9.85	9.1		609
0.83	13.4	12.7	649	624
0.83	13.4	12.4		590
0.63	9.2	9.2		595
0.75	11	11.6	588.5	632
1.3	19	17.8		560
1.3	17.2	17		532
2.2	29.15	26.4	532.2	490
2.7	35.8	34		510
2.11	27	27		512
2.84	36.2	34.1	512.1	480
3.35	42.7	41.3		500

observed diverse types of dislocations, which supports the theory of twinning by dislocations. Numerous stacking faults were found in twins and were related to the condensation of vacancies created during twinning. In order to explain beryllium ductility above 400°C, the existence of a slippage of the dislocations $\bar{c} + \bar{a}$ was investigated. Pyramidal slippage in a direction outside the base plane was not demonstrated, but a deformation that can be ascribed to the climb of $\bar{c}$ dislocation loops, possibly created by Bardeen–Herring source, was shown.

Anisotropy

The effect of orientation on the hardness of beryllium single crystals at room temperature to 400°C has been studied by Tsuya using Knoop and Vickers indenters.[13] The variation of Knoop hardness with the inclination of basal plane was not affected by the change in testing temperature. Since beryllium has two slip systems at room temperature, the Knoop hardness–ϕ (angle between the long axis of the indenter and projection of the c-axis on the surface) curve for larger θ values (c-axis inclination) has two maxima over 180°, which is in contrast to other hexagonal metals. The directionality of Knoop hardness varies with testing temperature. This can be explained by the decrease in critical resolved shear stress for $(10\bar{1}0)$ slip with increasing temperature. The ratio of the lengths of the two diagonals of Vickers impressions in the $(10\bar{1}0)$ or the $(11\bar{2}0)$ plane changes with temperature, which reflects the alteration of predominant slip systems with temperature. Calculated orientation factors seemed adequate to account for the observed deformation markings around Vickers impressions.

The anisotropic elastic behavior of rolled beryllium sheet has been measured by Moment, using a pulse-echo technique, and these data were compared with X-ray diffraction data.[14] Calculated values for elastic stiffness constants compared favorably with published values for beryllium single crystals; this was attributed to the strong (0002) rolling-plane texture. Variation of Young's modulus in the rolling plane was associated with the relative distribution of (0002) planes out of their ideal position in the rolling plane. The texture was found to be (0002) in the rolling plane with $(10\bar{1}0)$ normal to the rolling direction. This $(10\bar{1}0)$ texture was strongest in the predominant rolling direction. The spread of (0002) planes about the normal to the rolling plane was greatest in the cross direction, but the range of tilt for the highest intensity of diffracted X rays was greater in the rolling direction.

The elastic stiffness constants showed fairly good correlation with the single-crystal values as illustrated in Table II-3 and Fig. II-1. Variations were

Table II-3 ELASTIC PROPERTIES OF ROLLED BERYLLIUM[14]

Direction	Young's modulus, 10^{11} dynes/cm^2		
	Rolled sheet	Single crystal	Difference, %
In the rolling direction	29.85	29.07	+3.3
In the cross direction	30.67		
In the [0001] direction (normal to rolling plane)	34.25	33.67	+2.0

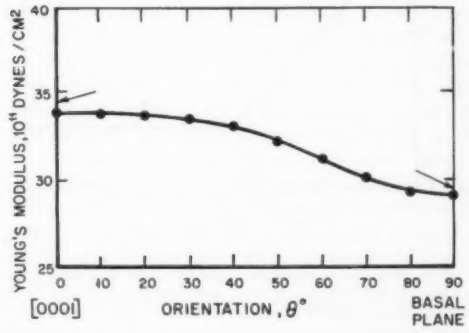

Fig. II-1 Young's modulus of a single crystal of beryllium as a function of orientation.[14] The angle θ varies between the c and a axes of the hexagonal unit cell. The arrows indicate measured values for rolled beryllium.

explained by the relative tilting of the (0002) planes as observed by means of X rays. As a result, the elasticity results proved to be a sensitive indicator of the rolling texture.

Fracture Toughness

Lawrence Radiation Laboratory has performed measurements on the fracture toughness of beryllium.[15] The materials tested were N50A, which is of relatively high purity (0.8% BeO), and S-200, a com-

mercial alloy (2% BeO). Values of K_c (plane-stress fracture toughness) for equivalent thicknesses of these two grades of beryllium were about the same. The lower purity S-200 tended to show the higher toughness. However, the agreement in the fracture-toughness measurements of the N50A material from batch to batch was appreciably better than that of the S-200 material. Data obtained are summarized in Fig. II-2. Sources of the materials tested were as follows:

Grade	Batch	Supplier
N50A	I	Brush
N50A	II	General Astrometals
N50A	III	General Astrometals
S-200	I	General Astrometals
S-200	II	Lawrence Radiation Laboratory

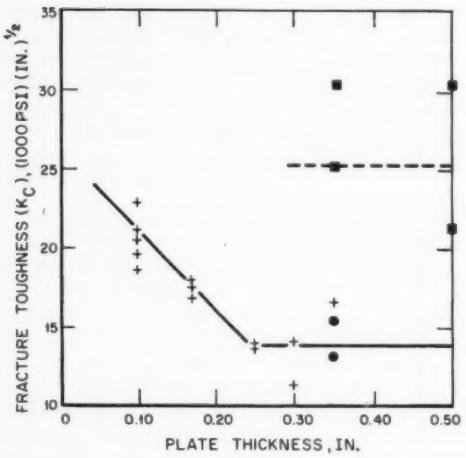

Fig. II-2 Fracture-toughness measurements on batches of N50A and S-200 beryllium.[15] +, N50A batches II and III; ●, S-200 batch I; ■, S-200 batch II.

Very few fracture-toughness measurements have been made on beryllium owing to difficulties encountered in producing controlled cracks in test specimens. A new method of precracking the specimens was devised to overcome this difficulty. As shown in Fig. II-3, a compression zone was produced on the side of the specimen just below the machined-notch root. This zone was achieved by mounting a No. 8 nut on each face of a vise, placing the specimen in the vise, and forcing the nuts against the side of the specimen. A wedging force, which tended to open the machined notch, was then applied by pounding a chisel into the notch. A crack in this sample would run from the root of the machined notch and be arrested in the zone of compression.

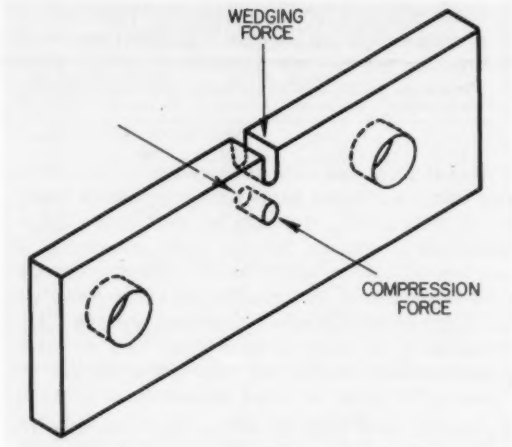

Fig. II-3 Precracked fracture-toughness specimen.[15]

Properties

General. The available technical data on beryllium metal have been compiled in *The Beryllium Metal Handbook* which contains 67 tables and graphs.[16] Structural properties of beryllium under ambient and cryogenic conditions are covered. Thermodynamic data; the effect of structure on mechanical properties; and data on soldering, brazing, and welding of beryllium are presented. Data on purity of various types of beryllium metal and detailed specifications for beryllium powder and hot-pressed products are also given.

Welding

A technique was developed by Westland and Lohmann for vapor-plating aluminum on beryllium and welding the surfaces with an electron-beam-welding unit.[17] The following three methods of adding aluminum to the joint were investigated:

1. Placing a sheet of aluminum in the joint before welding. This was unsuccessful because the weld metal baffled and made the beam erratic.
2. Precoating the surface with aluminum wire using a gas tungsten arc under pressure. This method was successful.
3. Precoating the surface by vacuum evaporation of aluminum. This method was also successful.

Full-penetration welds in hot-pressed S-200 beryllium were stronger than the parent material. The quantity of aluminum in the joint was much less in braze welds with a gas tungsten arc under pressure.

Corrosion

Tests to determine the corrosion and compatibility of reactor materials in the Argonne Advanced Re-

search Reactor (AARR) vessel were conducted in deionized H_2O with a specific resistivity of 10^6 ohm-cm or greater.[18] The test revealed that the corrosion rate of beryllium is linear with time and dependent upon the ratio of exposed surface area to water volume. On the basis of these data, the corrosion rate of beryllium in the AARR is expected to range from 1.1 to 2.8 mils/year, which is an acceptable rate.

Metallography

A method was developed by Danforth and Krashes for polishing beryllium by vibration.[19] Grinding with light pressures followed by vibratory polishing with a heavy slurry of chromic oxides produced good metallographic specimens of both beryllium alloys and wrought beryllium. Improved inclusion retention and grain-boundary definition under polarized light were the advantages of the method.

Metallographic techniques for vacuum-cast and rolled ingot beryllium sheet have been developed by Calabra and Jackson.[20] Both methods yielded metallographically prepared surfaces considered to be of the highest quality. The first method, involving mechanical and vibratory polishing and swab etching, retained inclusions and required polarized illumination for structural delineation. The second method was an electrolytic swab-etch technique which yielded bright-field delineation of the microstructure; however, inclusions were not retained. The effects that improper preparation can have on the resulting microstructure were emphasized.

Chemical Analysis

Blosser and Henry have investigated the development of analytical techniques for the determination of minute quantities of selected elements in beryllium.[21] High-purity beryllium became a reality during the period that this program was under way. Beryllium available at the outset of their research was, at best, in the 99.99% purity range; however, research quantities are now in the 99.999% range, with individual impurity-element levels demanding refined analytical instrumentation for determination. The techniques discussed satisfy the requirements for determination of 1-ppm quantities of selected elements in beryllium, although not all of these elements (H, C, N, O, Na, Al, S, K, Ti, V, Cr, Mn, Fe, Co, Ni, and Cu) have been lowered to this level in any beryllium analyzed at Battelle–Columbus. Certain elements have a greater degree of uncertainty in their determination than others but, in general, the cross-check data indicated that errors greater than a factor of 2 are infrequent and that ±20% accuracy is attained in some instances. Uncertainties of this magnitude in the 1-ppm concentration range have, for the most part, been compatible with the analytical requirements of high-purity beryllium-purification programs.

This research has shown that impurities in the ultrahigh-purity beryllium can be determined with reasonable accuracy and good detectability if several techniques are employed. The mass spectrograph is the most useful single tool presently available for low and sub parts-per-million analyses. It is capable of complete elemental coverage, of accuracy generally compatible with materials requirements, and of parts-per-billion detectability for most elements. Carefully controlled sample preparation and vacuum environment are prerequisites for obtaining analyses for the interstitial elements. Further improvements in mass-spectrographic analysis will depend on minimizing the influence of inhomogeneity of the samples, on controlling the variables inherent in the technique, and on additional availability of low and sub parts-per-million standards.

Gamma- and neutron-activation techniques are of great value for specific elements if an adequate amount of sample is available. In this program, gamma-activation analyses performed by Lawrence Radiation Laboratory were used to provide reference values for carbon, oxygen, and manganese in many samples. Chemical and thermal techniques have applications in less pure materials, but appear to offer only a slight hope of practical success as sub parts-per-million levels are encountered. Furthermore, these techniques usually are specific for only one or two elements, making complete impurity analyses almost prohibitive because they are extremely time-consuming and require large samples. Emission-spectrographic techniques are valuable for the analysis of moderate-purity beryllium and offer an accurate and relatively fast means of determining many elements at the few parts-per-million level. The choice of the most suitable technique depends on accuracy and detectability of the technique and on the time required.

Analytical techniques for the determination of trace-metal impurities in beryllium have been described by Kallmann and Collier.[22] Chemical as well as spectrographic procedures were employed. Spectrographic techniques were developed for the determination of a number of impurity elements in beryllium metal involving a maximum of 50 mg of sample. For spectrographic methods the beryllium samples were analyzed using either the original metal or the oxide after conversion from the metal. The metal form was not suited for the determination of most impurity elements in the less-than-10-ppm range because of comparatively low spectral sensitivity. The spectral characteristics of BeO in the arc were such that most elements showed a greater sensitivity than when the metal was used. Reliable analytical-chemical procedures were available for the determination of most impurity elements in beryllium. These procedures were summarized for the determination of

elements such as Fe, Ni, Cr, Mn, Si, Cu, Ti, Mo, B, and Al and several combinations of elements.

Texas Nuclear Corp. has described the development of a neutron-activation technique for determining small amounts of C, O, and N in Be, Mo, and W.[23] The equipment was developed for determinations in the parts-per-million range. No determination of the accuracy of beryllium analyses was made, but a series of determinations on the same spot in high-purity beryllium indicated a standard deviation of 2.5% for oxygen, 15.9% for nitrogen, and <1% for carbon. The technique offers certain advantages in that all three elements can be determined with a single activation in a total time of less than 30 min. The technique is nondestructive, and selected areas less than 0.1 in. in diameter can be analyzed.

Since only surface concentrations can be determined by this method, matrix impurity content cannot be determined unless one assumes that the impurities are homogeneous. In the case of beryllium, it is doubtful that the surface oxygen content is typical of the bulk material. It also is doubtful that the etching methods employed will produce surfaces that are free of adsorbed oxygen.

(H. D. Hanes and F. T. Zurey)

Beryllium Oxide

British investigators have studied the effects of SiC and MgO additions on the grain size and strength of BeO after thermal anneals up to 1000 hr at temperatures[24] of 1400, 1550, and 1750°C. This information supplements previous data by several investigators concerning grain-growth inhibition in BeO by SiC–MgO additions. In this study the doped BeO demonstrated a reduced range of grain sizes and a more pronounced variation of strength with grain size compared with the undoped oxide. The data are summarized in Table II-4. (M. C. Brockway)

Solid Hydrides

Zirconium Hydrides

The diffusion of zirconium in ZrH_2 has been studied at Atomics International by depositing radioactive ^{95}Zr on the hydride surface.[25] The diffusion coefficients as a function of temperature for two hydride compositions are shown in Fig. II-4. It was concluded that the diffusion of zirconium in the hydride can be attributed not only to volume diffusion but also to "short circuit" paths such as grain boundaries and dislocations.

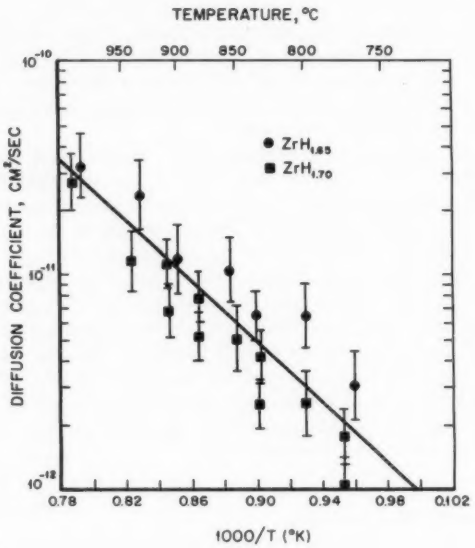

Fig. II-4 Diffusion coefficients[25] of zirconium in $ZrH_{1.65}$ and $ZrH_{1.70}$.

Table II-4 EFFECT OF ANNEALING ON STRENGTH AND GRAIN GROWTH[24]

		BeO			BeO + 1 wt.% MgO + 8 wt.% SiC		
Temperature, °C	Time, hr	Density, g/cm³	Mean transverse rupture strength, psi	Mean grain diameter, μm	Density, g/cm³	Mean transverse rupture strength, psi	Mean grain diameter, μm
As sintered		2.8–2.85	44,550	65	2.95	53,280	9.3*
1400	30	2.861	33,500	36	2.934	52,850	10.1
	100	2.815	44,890	36	2.941	56,830	9.6
	300	2.940	40,160	19	2.930	54,450	11.9
1550	30	2.833	36,950	13	2.944	56,115	9.3
	100	2.924	24,290	61	2.947	54,150	10.5
	300	2.946	22,620	74	2.936	50,900	11.8
	1000	2.965	21,390	56	2.915	40,000	14.2
	1300			68			16.8
1750	10	2.968	21,240	74.0	2.941	52,940	17.2
	30	2.972	19,250	64	2.928	46,270	13.7
	100	2.967	19,190	75	2.946	42,050	16.8
	300	2.925	9,840	84	2.944	34,180	18.4

*Microns.

The rate of initial hydriding of Zircaloy-2 with various surface coatings has been determined by Combustion Engineering and Atomics International.[26] The experiments were carried out at 750°F (400°C) and at a hydrogen pressure of 600 torrs. The time required for absorption of 500 ppm of hydrogen by Zircaloy-2 with different surface conditions and by a 3Z1 alloy was measured, and the results are as follows:

Material	Time, hr
Zircaloy-2, pickled	0.15
Zircaloy-2, aluminum coated by plasma spray	0.1
Zircaloy-2, oxidized at 500°C	12.0
Zircaloy-2, aluminum coated by diffusion	16.0
3Z1 alloy, pickled	0.5

A British patent for the production of ultrafine ZrH_2 powder has been issued.[27] The preparation consisted of heating zirconium powder in hydrogen at low pressure and then cooling. The resultant hydride was pulverized and degassed.

Hydrided Zr–U Alloys

In connection with the nuclear safety program, information on the effect of large-transient, power-excursion conditions on a hydrided Zr–U alloy was obtained by Phillips Petroleum.[28] The specific heat of Zr–10 wt.% ^{235}U hydrided to H/Zr = 1.8 was measured in-pile and the data correlated with out-of-pile data of other investigators. The results are presented in Fig. II-5.

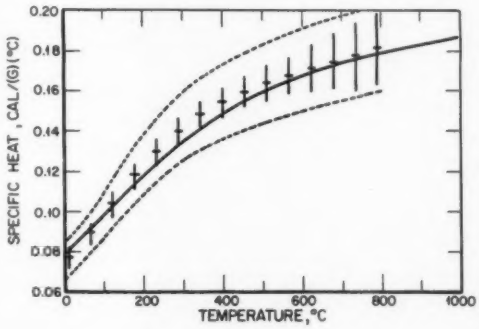

---, *±12% uncertainty*
†††, *individual uncertainty in temperature dependence*

—, $C_p = 5.96 \left[1 + \left(\frac{1625}{T + 273}\right)^2 \frac{(e^{1625/(T+273)})}{(e^{1625/(T+273)} - 1)^2}\right] + 2.67 \times 10^{-3}(T + 273)$

Fig. II-5 Specific heat of SNAPTRAN fuel[28] (10.0 wt.% ^{235}U in $ZrH_{1.8}$).

Lithium Hydride

Large LiH crystals, about 1.5 in. in diameter and 4 in. long, have been made at Lawrence[29] by the following procedure: (1) purifying lithium metal by distillation, (2) sealing the purified lithium metal in a pure iron crucible by welding, (3) hydriding the lithium by diffusing hydrogen through the walls of the crucible, (4) growing the lithium hydride crystal by the Störber process, which involves slow cooling with a vertical gradient, and (5) annealing the crystal while it is sealed in the crucible. It was expected that this procedure would yield single crystals, but to date, only large bicrystals have been obtained.

Titanium Hydride

The reaction of hydrogen with titanium 50A and with Ti–6 wt.% Al–4 wt.% V at low temperatures has been studied at Battelle–Columbus.[30] Specimens stressed by bending in 1 atm of hydrogen did not react unless they had previously been vacuum annealed to clean the surface. The titanium 50A reacted with hydrogen over the entire pressure range studied (1 to 69.5 atm) if it had been abraded. Acicular titanium 50A was more reactive than cold-rolled or equiaxed material. No effect of static stress near the yield stress was found at 22.2 atm hydrogen pressure. Hydriding of aircraft tubing occurred at 99°F (38°C) and 22.4 atm hydrogen but could be prevented by etching with HNO_3–HF–H_2O. Abrasion of the surface of the aircraft tubing increased the hydrogen absorption.

Thorium Hydride

The activation energies for the diffusion of hydrogen in several compositions of the Th–H system have been determined at Ames using nuclear-magnetic-resonance techniques.[31] Activation energies ranged from 11.2 ± 3 to 17.7 ± 2 kcal/mole. Similar values were found for both low and high hydrogen concentrations, suggesting that no change occurs in the diffusion mechanism at the ThH_2 stoichiometry. A previous study of ThH_2 at Ames gave an activation energy of 12.3 kcal/mole on the basis of reaction-rate constants and pressure–temperature–composition variation of the ThH_2 phase. Measurements on Th_4H_{15} gave values in the range 6.2 ± 0.5 to 8.1 ± 0.7 kcal/mole for the activation energy of hydrogen diffusion. (H. H. Krause)

Metallic Poison Materials

Cyclic strain fatigue tests have been conducted on irradiated hafnium specimens[32] at 600°F (316°C). Specimens irradiated at 500°F (260°C) to fast fluences of up to 6.3×10^{21} neutrons/cm^2 yielded the

test results shown in Fig. II-6. The ordinate of the fatigue curve is given in terms of $S_a = \frac{1}{2}E\epsilon_t$, where E is the elastic modulus and ϵ_t is the total strain. It was found that irradiation reduces the fatigue life at large total strains and increases the fatigue life at low total strains.

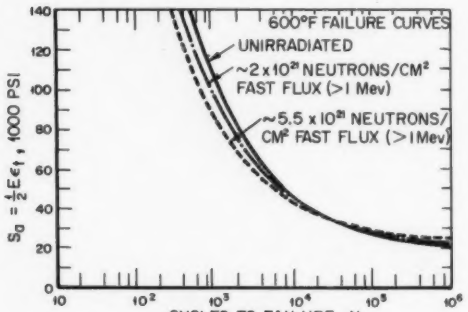
600°F FAILURE CURVES
UNIRRADIATED
~2 x 10²¹ NEUTRONS/CM² FAST FLUX (>1 Mev)
~5.5 x 10²¹ NEUTRONS/CM² FAST FLUX (>1 Mev)
$S_a = \frac{1}{2}E\epsilon_t$, 1000 PSI
CYCLES TO FAILURE, N

Fig. II-6 Effect of fast fluence on fatigue of hafnium.[32]

Stainless-steel specimens containing 2 wt.% natural boron exhibited drastic embrittlement as a result of irradiation in the Elk River reactor.[33] The Charpy V-notch specimens were embrittled to such an extent after irradiation to a thermal fluence of 8.6×10^{20} neutrons/cm² that they broke on removal from specimen holders. Results of the mechanical tests after irradiation to the higher thermal fluence level and a previously reported lower level of 1.4×10^{20} neutrons/cm² are reported in Table II-5. Examination of the 13 stainless-steel–boron control rods in the Elk River reactor indicated that 2 of them had sufficiently large cracks to warrant their removal from the reactor.

A British patent has been issued for a material that consists of additions of Gd, Eu, Sm, and Dy to austenitic stainless steel.[34] These rare-earth additions increase the absorption cross section of the alloy sufficiently so that it can be used as a control-rod material. Maintenance of ferrite content at 5 to 25% allows good hot-workability. Other alloying conditions like Cu, Sn, Mn, S, and P may be used to obtain good machinability or corrosion resistance.

The Russians[35] are studying the preparation and structure of various europium alloys. A series of Ni–Eu alloys containing 0.77 to 37.47 wt.% europium were melted from electrolytic nickel and 99.77% pure metallic europium. The alloys were melted in a helium atmosphere at a pressure of 0.5 atm, forged, and vacuum annealed at 1100°C for 50 hr, or annealed at 1100°C and quenched. All alloys were found to have a two-phase structure. Small individual inclusions of the second phase precipitated within grains of the alloys containing up to 1.2 wt.% europium and along the grain boundaries in the alloys containing 1.44 wt.% europium. The chemical composition of an alloy with 37.44 wt.% europium (melting temperature 1440 ± 10°C) was close to that of a pure $EuNi_5$ compound, which had a microhardness of 620 kg/mm². The

Table II-5 EFFECT OF IRRADIATION ON THE MECHANICAL PROPERTIES OF BORON-CONTAINING (2 WT.%) STAINLESS STEEL*[33]

Test	Approx. thermal flux, 10^{20} neutrons/cm²	Test temp., °F	Ultimate strength, 1000 psi	Yield strength, 1000 psi	Elongation in 1 in., %	Bend angle, deg	Deflection at failure, in.	Charpy impact,† ft-lb
Tensile	0	RT	91.2	62.3	10			
Tensile	0	RT	91.4	62.5	10			
Tensile	0	RT	87.0	62.8	11.5			
Charpy	0	RT						0.85
Bend	0	RT				18	0.062	
Tensile	0	525	75.9	53.0	8.5			
Tensile	0	525	72.4	57.1	9.0			
Tensile	1.4	RT	105.0	‡	2.0			
Tensile	1.4	RT	94.6	90.6	1.0			
Charpy	1.4	RT						0.15
Bend	1.4	RT				0	0.023	
Tensile	1.4	525	124.0	‡	2.5			
Tensile	1.4	525	120.0	‡	2.0			
Tensile	8.6	RT	96.0		0			
Tensile	8.6	RT	88.5		0			
Charpy	8.6	RT						§
Bend	8.6	RT				0	0.017	
Tensile	8.6	550	72.5		2.0			
Tensile	8.6	550	88.5		1.0			

*Includes previous test data.
†Average of three or more specimens.
‡Specimen exhibited no appreciable yielding.
§These Charpy impact tests could not be made owing to jamming of the specimens in the holders. Three were broken at Elk River in removal and shipping. No feasible means could be devised, with available time and funds, to remove the specimens from the holders at Southwest Research Institute without breakage because of the low impact value and brittleness.

maximum solubility of europium in nickel in the solid state was 0.78 wt.% (0.3 at.%) at 1100°C and 0 at 20°C. Alloys containing up to 2 wt.% europium were successfully rolled with a maximum reduction of 60 to 80% in two passes with process annealing at 850°C for 30 min. Alloys containing up to 8.03 wt.% europium sustained a 16% reduction in height in upsetting at room temperature.

A series of cerium alloys containing 0 to 76.5 wt.% europium was melted from 99.5% pure cerium in a vacuum induction furnace, and a tentative phase diagram of the Ce–Eu system was plotted. The phase diagram is characterized by a continuous solubility of high-temperature modifications of gamma cerium and europium and by a wide region of solubility of gamma cerium in europium. Vacuum annealing at 400 and 600°C for 200 hr decreased the hardness of Ce–Eu alloys and led to grain growth. Alloys containing up to 10 to 20 wt.% europium appeared to have a single-phase structure. Holmium alloys containing 0 to 49 wt.% europium exhibited single-phase structures which were only slightly affected by annealing at 600°C for 150 hr. The Ho–Eu alloys were characterized by the good solubility of these metals in each other in both the liquid and solid states. Differences in the crystal lattice of these metals made it possible to assume the existence of intermediate phases in the Ce–Eu system. Hardnesses of Yb–30 wt.% Eu and Ca–12 wt.% Eu were 22 kg/mm^2 and 30 kg/mm^2, respectively. Analogous properties made it possible to substitute calcium for ultrarare and expensive europium as a model in preliminary investigations of interaction between europium and other elements. (M. Kangilaski)

Dispersion and Nonmetallic Poison Materials

Boron and Boron Compounds

The self-shielding effect of B_4C particles has been the subject of a research experiment at Idaho Nuclear.[36] In this work, self-shielding in B_4C particles was evaluated both by an experimental program in the Advanced Reactivity Measurement Facility (ARMF) and by first-flight transport calculations. The results obtained by the two evaluation methods agree closely for particle sizes smaller than 85 μ (170 mesh).

The self-shielding factors were determined experimentally from ARMF reactivity measurements on a series of small high-purity aluminum plates that contained 13 mg of B_4C of graded particle sizes and an unborated control plate. The plates were identical in design to fuel plates except they contained no fuel. The reactivity measurements were made in the corner of the ARMF-I central water hole in a position which placed the plates parallel to and 0.57 in. from the fuel elements. The net reactivity effect due to boron was obtained by subtracting the reactivity effect of the unborated control plate. The results of these measurements (shown in Table II-6) clearly indicate that self-shielding does exist. It should also be noted that the standard deviation in the reactivity effects of the plates within a group is small. This shows that control of the amount of B_4C in the plates was very good and increases the confidence in the results of this study.

Table II-6 REACTIVITY AND SELF-SHIELDING FACTORS FOR BORON CARBIDE PARTICLES[36]

Mesh sizes	Number of plates measured	Mean reactivity due to boron, μk*	Standard deviation, μk	Self-shielding factor (f_p)	
				Experimental	Theoretical
−100 +120	4	−88.8†	0.64	0.74	0.68
−170 +200	5	−94.1	0.66	0.79	0.79
−270 +325	4	−101.4	0.38	0.85	0.86
−325	4	−111.3	0.52	0.94	

*$\mu k = 10^{-6}\ \Delta k/k$.
†A fifth plate was measured at −85.31 μk. However, precision based on eight measurements on a single plate was 0.11 μk.

An investigation on the properties of ZrB_2–Mo alloys was made by the Russians.[37] Alloys were prepared by blending and pressing powder compacts of 5, 10, and 15 wt.% molybdenum in ZrB_2. The compacts were sintered in argon at 2000 to 2100°C for 2.5 to 3 hr and furnace cooled to 1200 to 1400°C, followed by cooling in a stream of argon. X-ray diffraction patterns showed that the three alloys thus prepared consisted of a solid solution of molybdenum in ZrB_2 and (for the respective molybdenum contents) 6.13, 6.21, and 6.27 mole % ZrB formed from ZrB_{12} present in the ZrB_2 powder. The alloys had respective microhardness values of 2082 ± 120, 1860 ± 140, and 1470 ± 200 dan (decanewton)/mm^2. The microhardness values of the ZrB_2 and ZrB in all alloys were 2250 ± 100 and 3570 ± 250 dan/mm^2, respectively. After being extruded and sintered at 2200°C, the three alloys exhibited 5.5 to 6.2, 6.8 to 7.5, and 10.2 to 13.1% porosity, respectively, and oxidation rates significantly lower than that of pure ZrB_2. In thermal-shock tests consisting of cyclic quenching in water from 1200°C, the three alloys sustained 8 to 12, 8 to 12, and 10 to 16 cycles, respectively, compared with 2 to 4 cycles for ZrB_2.

In research at the University of Kansas[38] on the V–B system, two new phases, V_5B_6 and V_2B_3, were discovered. X-ray diffraction studies of synthetic samples with compositions between 50 and 67 at.% boron were performed. Langmuir free-evaporation experiments on inductively heated VB_2 samples proved that the diboride vaporizes congruently. Mass spectrometric studies showed that the vaporization of VB_2 produces only gaseous elements.

Rare Earths

Studies have been made at Battelle–Northwest[39] on the fabrication of rare-earth oxides. Sesquioxides of samarium and promethium were hot pressed to densities in excess of 95% of theoretical at temperatures of 1590°C under a pressure of 5100 psi. Slightly lower densities were obtained for Nd_2O_3 and Pm_2O_3 under similar pressing conditions. It was observed that higher calcination temperatures before pressing lower the density obtained with a given set of pressing conditions. The hot-pressed pellets of the rare-earth oxides showed excellent physical strength and were handled readily without damage. The Nd_2O_3 pellets were found to be sensitive to atmospheric moisture; however, the Sm_2O_3 and Pm_2O_3 pellets were stored in air without suffering apparent damage. It was concluded from this study that hot pressing was a more practical method of fabricating Pm_2O_3 than the slip-casting process previously examined.

A Russian[40] investigation of the Eu–Ni alloys containing 93.6 to 99.7 at.% nickel and 81.1 at.% nickel was carried out by X-ray powder analysis of alloys prepared in an atmosphere of purified helium at an ambient pressure of 0.5 atm. The investigation established the existence of Eu_2Ni_{17} (crystal-type Th_2Ni_{17}), with $a = 8.35$ A and $c = 8.06$ A, and $EuNi_5$ (crystal-type $CaCu_5$), with $a = 4.911 \pm 0.004$ A and $c = 3.965 \pm 0.002$ A. (D. E. Lozier)

References

1. I. B. Mason and R. H. Knibbs, The Young's Modulus of Carbon and Graphite Artefacts, British Report AERE-R-5448, May 1967.
2. R. H. Knibbs, Fracture in Polycrystalline Graphite, British Report AERE-R-5447, May 1967.
3. G. B. Engle and K. Koyama, Effect of Irradiation at 300–1500°C on the Thermal Conductivity and Electrical Resistivity of Impregnated Graphites, USAEC Report GA-7812, General Atomic Division, General Dynamics Corp., July 19, 1967.
4. General Atomic Division, General Dynamics Corp., Public Service Company of Colorado 330 Mw(e) High-Temperature Gas-Cooled Reactor Research and Development Program Quarterly Progress Report for the Period Ending June 30, 1967, USAEC Report GA-8038, pp. 160-165, July 28, 1967.
5. R. G. Brown, U. K. Atomic Energy Authority, 1967.
6. Battelle–Northwest, Effect of Impregnation and Crystallite Orientation on the Radiation-Induced Contraction of Graphite, USAEC Report BNWL-380, July 1967.
7. Los Alamos Scientific Laboratory, LASL Rover Program, Quarterly Status Report for Period Ending May 31, 1967, USAEC Report LA-3723-MS, pp. 46-47, June 28, 1967. (Classified)
8. B. B. Lympany, J. G. Theodore, and W. W. Beaver, Research on Effects of High Purity in Wrought Polycrystalline Beryllium Sheet, Progress Report No. 5, November 1, 1966–February 28, 1967, Report BBC-TR-424-251, The Brush Beryllium Co., Mar. 9, 1967.
9. A. R. Kaufmann, Improvement of Beryllium by Splat Cooling, Report NMI-8003.7, Nuclear Metals Division, Whittaker Corp., May 15, 1967.
10. P. M. Jones and R. Gibson, Hydrogen in Beryllium, *J. Nucl. Mater.*, 21: 353-354 (March 1967).
11. Y. Droulers, G. Pleyber, Y. Carteret, R. Lucus, and J. Bareau, Calcul et Mesure des Quantites d'Helium Produites par Reactions $(n,2n)$ et (n,α) dans le Beryllium Irradie, *J. Nucl. Mater.*, 21(3): 337-342 (1967).
12. J. P. Poirier, J. Antolin, and J. M. Dupouy, Dislocations in Beryllium Twinning and Deformation by Climb, *J. Phys. (Paris)*, 27 (Suppl. to Nos. 7–8): C3-98-102 (July–August 1966).
13. K. Tsuya, The Effect of Temperature on the Hardness Anisotropy of Beryllium Single Crystals, *J. Nucl. Mater.*, 22: 148-157 (1967).
14. R. L. Moment, The Elastic Anisotropy of Rolled Beryllium, *Trans. AIME*, 239: 542-546 (April 1967).
15. D. O. Harris and H. L. Dunegan, Fracture Toughness of Beryllium, USAEC Report UCRL-70255, University of California Lawrence Radiation Laboratory, Jan. 4, 1967.
16. H. H. Hausner (Ed.), *The Beryllium Metal Handbook*, General Astrometals Corp., 1967.
17. E. F. Westlund and H. G. Lohmann, Vapor-Plating Aluminum on Beryllium for Welding, *Welding J. (N. Y.)*, 46: 207-210 (March 1967).
18. Argonne National Laboratory, Reactor Engineering Division Annual Report, July 1, 1965–June 30, 1966, USAEC Report ANL-7290, pp. 111-112, April 1967.
19. A. L. Danforth and D. Krashes, Polishing Beryllium by Vibration, *Metal Progr.*, 91(2): 115 (February 1967).
20. A. E. Calabra and R. J. Jackson, Metallographic Techniques for Vacuum-Cast Rolled Ingot Beryllium Sheet, USAEC Report RFP-962, Dow Chemical Co., Rocky Flats Division, Aug. 7, 1967.
21. E. R. Blosser and W. M. Henry, Development of Analytical Techniques for the Determination of Minute Quantities of Selected Elements in Beryllium, Final Report, Battelle Memorial Institute, Aug. 12, 1966.
22. S. Kallmann and F. Collier, Analytical Techniques for the Determination of Trace Metal Impurities in Beryllium, Report AD-808345 (AFML-TR-66-183), Ledoux & Co., April 1966.
23. K. R. Blake, L. D. England, and D. L. Kellog, Charged Particle Activation Analysis for Surface Impurities in Beryllium, Molybdenum, and Tungsten, Report AFML-TR-67-11, Texas Nuclear Corp., April 1967.
24. U. K. Atomic Energy Authority, Atomic Energy Research Establishment Ceramics Division, unpublished.
25. G. G. Bentle, Diffusion of Zirconium in Zirconium Hydride, *J. Amer. Ceram. Soc.*, 50(3): 166-167 (March 1967).
26. Atomics International and Combustion Engineering, Inc., Heavy Water Organic Cooled Reactor, Quarterly Technical Progress Report, July–September 1965, USAEC Report AI-CE-4, p. 0453-2, Aug. 15, 1967.
27. A. Oka, Production of Stoichiometric Titanium and Zirconium Hydride Powders, British Patent 1,070,022, May 24, 1967.
28. W. E. Kessler, R. E. Prael, and L. N. Weydert, Jr., Analysis of SNAPTRAN Reactor Behavior, USAEC Report IDO-17204, Phillips Petroleum Company, June 1967.
29. E. Catalano, D. D. Kingman, and E. W. Wrenn, Notes on the Growth of Lithium Hydride Single Crystals, USAEC Report UCID-15143, University of California Lawrence Radiation Laboratory, May 31, 1967.
30. B. G. Koehl, W. Hodge, D. N. Williams, and E. S. Bartlett, Continuation of the Investigation of the Reaction of Titanium with Hydrogen, Report NASA-CR-65638, Battelle Memorial Institute, May 15, 1967.
31. J. D. Will and R. G. Barnes, Activation Energies for Hydrogen Diffusion in Thorium Hydrides, *J. Less-Common Metals*, 13(1): 131-132 (July 1967).
32. W. J. O'Donnell and J. G. Weinberg, Low-Cycle Fatigue Properties of Irradiated Hafnium, *Trans. Amer. Nucl. Soc.*, 10: 138 (June 1967).
33. R. D. Wylie, Inspection of the Control Rod Blades (of

the) Elk River Power Plant, April 24–May 22, 1966, USAEC Report SWRI-1228-9-9, Southwest Research Institute, June 22, 1966.
34. Austenitic Stainless Steel Alloy, British Patent 1,056,938, Feb. 1, 1967.
35. E. M. Savitskii, V. F. Terekhova, and R. S. Torchenova, Europium Alloys, *Metalloved. Term. Obrab. Metal.*, 33(2): 25-31 (February 1967).
36. D. R. deBoisblanc, W. C. Francis, and R. G. Fluharty, Nuclear Technology Branches Quarterly Report, October 1–December 31, 1966, USAEC Report IN-1083, pp. 1-2, Idaho Nuclear Corp., May 1967.
37. P. S. Kislyi and M. A. Kuzenkova, Properties of Zirconium Diboride–Molybdenum Alloys, *Izv. Akad. Nauk SSSR, Neorg. Mater.*, 2: 2139-2144 (December 1966).
38. K. E. Spear II, The Chemical and Thermodynamic Properties of Vanadium Borides and Related Systems, USAEC Report COO-1140-157, University of Kansas, Apr. 17, 1967.
39. H. T. Fullam and C. J. Mitchell, Hot Pressing of Rare Earth Oxides, USAEC Report BNWL-448, Battelle–Northwest, June 1967.
40. V. F. Terekhova, P. I. Kripyakevich, D. P. Frankevich, and R. S. Torchinova, The Compounds of Eu_2Ni_{17} and $EuNi_5$ and Their Crystal Structures, *Izv. Akad. Nauk SSSR, Metal.*, No. 1: 205-207 (January–February 1967).

Section

III

Reactor Materials

Cladding and Structural Materials

Corrosion by Aqueous and Gaseous Media

Corrosion of Zirconium Alloys

AQUEOUS CORROSION

Research on the radiation-enhanced oxidation of Zircaloy-2 in *p*H 10 LiOH- and NH_4OH-treated water at 280° C has been summarized by Battelle–Northwest.[1] The following results were obtained. In LiOH-treated water containing about 1 ppm oxygen, corrosion rates ranged up to 3 mg/(dm^2)(day); in-pile weight gain and fluence (>1 Mev) exhibited a linear relation; oxidation rates were higher at a fast flux of 1×10^{14} than at 3.3×10^{13} neutrons/(cm^2)(sec); and hydrogen absorption increased linearly with increasing fluence (percent uptake was in the low range of that observed for out-of-pile exposure under similar conditions). Specimens transferred from *p*H 10 LiOH water with about 1 ppm oxygen to *p*H 10 NH_4OH water with <0.05 ppm oxygen continued to oxidize at the same rate. New specimens exposed to the NH_4OH-treated water oxidized at a rate an order of magnitude lower. The results suggested a synergistic effect between neutron flux and the environmental conditions (particularly oxygen).

The pressure dependence of the zirconium-alloy oxidation in steam has been studied by Chalk River.[2] The results for Zircaloy-2, summarized in Fig. III-1, revealed a marked increase in oxidation rate as the pressure was increased from 1 atm to 5000 psi, particularly at 500 and 600° C. The results for a Zr–2.5 wt.% Nb alloy showed relatively little effect of pressure; i.e., a twofold increase in oxidation rate was observed between atmospheric pressure and 5000 psi at 600° C.

The corrosion behavior of Zircaloy-2 in a fog-cooled (water-cooled) reactor environment has been examined by Italian scientists.[3] Experiments were conducted for 70 days in a steam–water mixture containing 0.5 ppm hydrogen and 3 ppb oxygen at 280° C and 66 kg/cm^2 with a neutron flux of 3.5×10^{12} neutrons/(cm^2)(sec), >1 Mev. The results revealed a projected transition in reaction kinetics after only 320 days, compared with 3250 days in out-of-pile tests. Similar increases in corrosion of Zircaloy due to irradiation in high-temperature liquid water have also been noted by Hanford and Harwell. Hydrogen pickup ratios for these tests were similar to those obtained out of pile.

HYDRIDING

Hydriding and attendant lowering of ductility in Zircaloy-2 tubes in two Hanford production reactors have been described by Douglas United Nuclear.[4] Hydride layers about 0.004 in. thick were found on the inside diameter (water side) of the tubes. The sources of hydrogen were found to be the corrosion reaction between galvanically coupled Zircaloy and aluminum-clad fuel elements or aluminum dummy spacers. Laboratory studies revealed that insulating the two materials and anodizing (oxalic acid) the aluminum essentially eliminated gross hydriding of the Zircaloy.

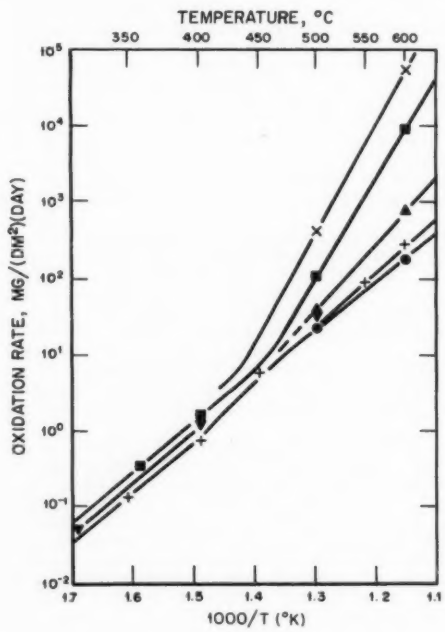

Fig. III-1 Pressure dependence of Zircaloy-2 oxidation in steam.[2] ●, 1 atm; ▲, 500 psig; ▼, 1000 to 1500 psig; ■, 2500 to 3000 psig; ×, 5000 psig; +, AERE data (mean).

Intentional hydriding of Zircaloy-2 by corrosion in 300°C water containing 5 to 72 g/liter LiOH has been investigated by Culcheth.[5] The most useful solutions were found to contain 32 and 50 g/liter LiOH. Uniform hydrogen concentrations (to 3400 ppm) were obtained at hydriding rates of less than 1.4 ppm/hr by cycling to room temperature every time the hydrogen concentration in the metal increased by 60 ppm.

OXIDATION

The reaction of oxygen with beta-phase crystal-bar zirconium has been studied by the French.[6] On samples 0.5 mm thick, oxygen pickup rates of 2.1 ppm/hr and 19 ppm/hr at 1.5×10^{-7} and 2×10^{-6} torr, respectively, were obtained at 1050°C. The oxidation kinetics were linear, which suggested oxidation without formation of an oxide layer or of alpha zirconium. A chemisorbed oxygen layer was found as striations or facets on the surface of beta grains in samples containing more than 400 ppm oxygen. An equilibrium between the dissolved oxygen in the metal and the density of the absorbed layer was suggested.

OXIDE FILMS

A theoretical treatment of zirconium–zirconium oxide epitaxy has been presented by Chalk River.[7] It was concluded that, owing to the relatively low symmetry of the monoclinic (4 ZrO_2) unit cell, at least 24 different ZrO_2 crystallite orientations should exist on oxidized zirconium (0 0 0 1) planes. The relative orientations of these crystallites were defined by the substrate-metal symmetry. Where oxygen transport along easy paths of diffusion is rate controlling, it was anticipated that the greater the symmetry of atom packing in the metal parallel to the oxide–metal interface, the greater would be the oxidation rate. Monoclinic ZrO_2 *d*-spacings, interplanar angles, and unit translation vectors for the cell were also summarized.

An oxygen plasma technique is being developed at Chalk River[2] to measure the electrochemical properties of oxidizing zirconium alloys without the introduction of a liquid or solid electrolyte into the system. The electron- and ion-collecting properties of a zirconium specimen in an oxygen plasma change as the specimen undergoes oxidation. Initial experiments with anodized crystal-bar zirconium have demonstrated that both the a-c and d-c electrical properties of the film formed during oxidation can be followed. (W. E. Berry)

Corrosion of Stainless Steels

OXIDATION IN STEAM

The oxidation of high-purity stainless steel in 500°C steam at 50 kg/cm^2 is being studied by French scientists.[8] After a 1000-hr exposure, an 18/12 steel containing 20 ppm carbon corroded at a slightly lower rate than did a comparable commercial-grade alloy (400 ppm carbon) but exhibited intergranular attack to a depth of about one grain. Additions of 3% molybdenum to the high-purity stainless steel eliminated the intergranular attack but did not reduce the corrosion rate. In contrast, a 3% platinum addition to the high-purity stainless steel not only eliminated intergranular attack but also produced a marked reduction in corrosion rate. A parallelism in susceptibility to intergranular corrosion between the observed behavior of high-purity stainless steel in steam and that of high-purity aluminum in high-temperature water was suggested.

Research on the susceptibility of nonsensitized stainless steels to intergranular attack in boiling $5N$ $HNO_3 - 0.46N$ Cr^{+6} solutions is continuing at GE–Vallecitos.[9] The effects of the following impurity levels in high-purity Fe–14 wt.% Cr–14 wt.% Ni alloys were studied:

	Impurity level, ppm
Carbon	40 to 1500
Manganese	5 to 26,000
Sulfur	80 to 1500
Nitrogen	10 to 450
Oxygen	170 to 880
Phosphorus	15 to 900
Silicon	40 to 40,000

Intergranular attack in boiling $HNO_3 - Cr^{+6}$ was observed only with those alloys containing >100 ppm phosphorus or 1000 to 20,000 ppm silicon. Commercial-purity alloys low in phosphorus and silicon did not exhibit intergranular attack. These latter alloys were recommended for testing as fuel-cladding materials in a boiling-water reactor.

STRESS-CORROSION CRACKING: IRRADIATION

The intergranular stress-corrosion cracking behavior of 304 and 348 stainless steels in 650°F (343°C) water containing 0.1 g/liter $FeCl_3$ has been investigated by Westinghouse.[10] Both mill-annealed and cold-worked materials were included in this study. In the nonirradiated condition, 348 stainless steel was much less susceptible to cracking than was 304 stainless steel. However, after irradiation to $\sim 1 \times 10^{21}$ neutrons/cm^2(>1 Mev), both materials were quite susceptible and cracked within 1 to 3 days. Since 348 stainless steel has performed well in the Yankee reactor (pressurized water), whereas 304 stainless steel has cracked in the VBWR (boiling water), the results of these tests suggest that other factors such as water environment and cladding operating stresses were responsible for the difference observed.

Additional work on stress-corrosion cracking of irradiated 316 stainless steel in boiling $MgCl_2$ has

been conducted at Harwell.[11] Previous results indicated an increased susceptibility to cracking in irradiated specimens and no effect of stress (5000 to 22,000 psi) on the time at which cracking occurred. Further studies at stresses below 5000 psi have shown a marked effect of stress on time to failure. At 3000 psi, specimens did not fail after an exposure of more than 18 hr, compared with failures in 1 to 2 hr at stress levels > 5000 psi. It was concluded that the irradiation effect was due to fast-neutron damage in the metal rather than in the oxide film.

(W. E. Berry)

Corrosion of Nickel-Base Alloys

The composition of oxide films formed on Hastelloy X during exposure to air at 1600 and 1750°F (871 to 954°C) has been determined by Aerojet-General.[12] X-ray diffraction and microprobe analyses revealed an outer layer of $MnCr_2O_4$ and an inner layer of Cr_2O_3. Little or no nickel was found in either layer.

The oxidation behavior of Hastelloy X and Inconel 600 in CO_2 has been investigated by the British.[13] Hastelloy X exhibited less than a cubic oxidation rate at 800°C, a cubic rate at 900°C, and a parabolic rate at 1000°C. On the other hand, Inconel 600 exhibited considerable oxide spalling at 800°C and somewhat less spalling at 900°C; at 1000°C it exhibited no spalling and lower oxidation kinetics than did Hastelloy X. The rate-determining step on both alloys appeared to be cation diffusion outward through the chromic oxide phase that formed in the initial stage of oxidation. This resulted in the subsequent formation of an outer spinel oxide of variable composition.

Oak Ridge[14] has described a materials development program for a molten-salt breeder reactor. The reactor will use uranium-bearing fluoride fuel, a thorium-bearing fluoride blanket, and fluoride-salt coolant for transferring heat to supercritical steam. Expected service temperatures are 100 to 1300°F (38 to 704°C). After the present state of development was reviewed, it was concluded that the core areas would require a better grade of graphite than is now available. Vacuum-melted Hastelloy N modified with 0.5 wt.% titanium was selected for all parts of the system (except the core) on the basis of its known resistance to fluoride salts, air oxidation, steam oxidation, nitriding, and radiation effects. Additional research deemed necessary to fully establish the utility of graphite and Hastelloy N was outlined.

Corrosion of Miscellaneous Alloys

The cavitation damage of a number of alloys has been studied by Pratt & Whitney and University of Michigan scientists.[15] Specimens were rotated in 100°F (38°C) degassed and deionized water at velocities of 128 to 207 ft/sec on a disk containing 1/4-in.-diameter cavitating holes. The alloys, in decreasing order of cavitation resistance, were (in wt.%) Ta–8 W–2 Hf, Nb–18 W–8 Hf, Ta–10 W, 316 stainless steel, Mo–0.5 Ti, Nb–1 Zr, Al–4 Cu–0.7 Mn–0.5 Mg, and Al–2.5 Mg–0.25 Cr. The damage-resistance order did not follow the variation of any single property but appeared to be related to a combination of mechanical properties and phase structure. The Mo–0.5 Ti alloy exhibited predominantly intergranular cracking, whereas the other alloys showed transgranular erosion and cracking.

(W. E. Berry)

Corrosion of Refractory Metals

Aerochem Research[16] has studied the kinetics of metal-atom removal from polycrystalline molybdenum, Mo–TZM alloy, and tungsten filaments in the presence of atomic oxygen at 725 to 1925°C and at pressures of 10^{-3} to 5×10^{-2} torr. Experimental techniques involved a microwave discharge, high-velocity (2×10^4 cm/sec) system coupled with resistance heating and monitoring of the reacting specimens. Under these conditions molybdenum and tungsten oxides volatilize nearly as rapidly as they are formed and thus leave the metal surface vulnerable to linear oxidation. Reaction probabilities were found to be up to 140 times those for oxygen attacking the same surface, were independent of atomic oxygen pressure, and exhibited a much weaker temperature dependence than those for oxygen. These observations were in accord with a Rideal type of mechanism in which oxygen atoms from the gas phase strike chemisorbed oxygen atoms, leading either to oxidation-product formation and desorption or to surface catalyzed oxygen-atom recombination.

Vacuum microbalance analysis of fast gas–metal reactions has been studied by Westinghouse.[17] Oxidation of rhenium and Re–8 wt.% Ti was investigated at oxygen pressures of 1 to 10 torrs, temperatures of 800 to 1400°C, and flows of 0.2 to 2.5×10^{19} oxygen molecules/sec. Below 1100°C the activation energies for oxidation were 21 kcal/mole for the alloy and 16.8 kcal/mole for rhenium and were independent of oxygen pressure. Oxidation appeared chemically controlled by mobile adsorption of oxygen modified by thickness or structural changes at the reaction interface. Above 1100°C the oxidation rates were similar for both metals and were controlled by gas diffusion. Oxidation of molybdenum was investigated at oxygen pressures of 9×10^{-3} to 49 torrs, temperatures of 900 to 1600°C, and flows of 0.07 to 8.5×10^{19} oxygen molecules/sec. Above 1 torr oxygen pressure, the data indicate mobile adsorption of oxygen. At lower pressures a high activation energy for oxidation (41 kcal/mole at > 0.1 torr compared with 19.7 kcal/mole at > 1 torr) and variation in oxidation rate with pressure suggest that a more complex mechanism was operative. High-voltage electron diffraction on the

metal surface indicated that MoO_2 was the predominant oxide formed and that molybdenum did not oxidize directly to the volatile species.

Corrosion of refractory metals in flowing helium in a clean high-temperature loop has been determined by Battelle–Northwest.[18] The helium atmosphere was zirconium gettered and contained <1 ppm total impurities, including 0.3 ppm oxygen. Tests were conducted at 300 psi for 500 hr at 1150°C at a flow rate of 130 ft/sec and included four startup cycles involving the access of air. The results of one test indicated that inleakage of air at the test temperature and 300 psi was negligible. Molybdenum and tungsten samples showed no evidence of attack, whereas niobium and tantalum were contaminated, as indicated by a weight gain of about 2 mg/cm^2, with most of the contamination occurring in the first cycle.

A comprehensive description of the fundamental aspects and reaction mechanism encountered in high-temperature oxidation of metals and alloys has been compiled.[19]

The oxidation behavior of Hf–27 wt.% Ta, Hf–20 wt.% Ta–2 wt.% Mo, and Hf–20 wt.% Ta–2 wt.% Zr has been examined in air or $He-O_2$ mixtures at temperatures of 1175 to 2075°C (Ref. 20). Oxygen partial pressures ranged from 35 to 152 torrs with flow rates of 0.1 to 0.2 ft/sec. Oxidation was parabolic up to 1725°C for times up to 2 hr, and the oxidation rates were found to be about the same for all three alloys.

The oxidation of binary alloys of hafnium with 10 to 50 wt.% niobium and alloys containing ternary additions of 5 to 20 wt.% Cr, Ti, V, and W has been studied at 800 to 1300°C (Ref. 21). The oxygen pressure was generally 10 torrs except for the Hf–34 wt.% Nb alloy, which was exposed to pressures of 10^{-3} torr to 1 atm. Experimental work included thermogravimetric measurements of oxidation rates and X-ray diffraction and electron-microprobe studies. The major reaction products were HfO_2, Nb_2O_5, and $Nb_2O_5 \cdot 6HfO_2$, with the relative amounts of these products being a function of temperature, oxygen pressure, and time. Above 10 torrs oxygen the oxidation rate increased with temperature up to 900 to 1000°C, decreased up to 100°C, and again increased above 1100°C. This maximum was interpreted as a result of interplay between relative rates of HfO_2 and Nb_2O_5 formation and subsequent reaction to form $Nb_2O_5 \cdot 6HfO_2$. Below 0.1 torr oxygen the maximum was not present. The binary Hf–Nb alloys exhibited oxidation rates similar to those of unalloyed niobium within a factor of about 1 to 3. The ternary additions did not significantly affect oxidation rate.

In British work[22] the origin of nonlinear oxidation kinetics of vanadium has been investigated at 700 to 1000°C at oxygen pressures of 100 to 350 torrs. Single-crystal specimens exhibited the same functional time dependence as did polycrystals, indicating that grain-boundary effects were unimportant. Oxygen solution in the metal did not contribute to the overall oxygen flux after the first 2 or 3 min of exposure. It appeared that the rate was controlled by diffusion through the residual liquid-oxide layer on the surface and that the nonlinearity was due to the large changes in surface temperature in the early part of the reaction.

The corrosion of molybdenum and BM-1 alloy (similar to Mo–TZM) in fused LiF and CaF_2–10 wt.% LiF contained in graphite crucibles under argon at 1250 to 1350°C has been investigated.[23] Both metals were attacked and exhibited corrosion rates of about 10 g/(m^2)(hr). Some Mo_2C formed and was insoluble in the molten salt.

Using capacitance and voltage measurements, Sprague Electric[24] has studied the spontaneous growth of oxide films 6 to 20 A thick on tantalum immersed in aqueous solutions of H_2SO_4, NaCl, and NaOH near room temperature. A rapid initial oxide growth rate in NaOH was noted until a thickness of about 12 A was reached. Beyond this thickness and over the entire thickness range in the other electrolytes, the oxide-film thickness increased roughly in proportion to the logarithm of time. There was a small but well-established dependence of "oxide capacitance" on the *p*H of the electrolyte and a rather large, reversible temperature dependence of the oxide capacitance. This behavior indicates these thin oxide films do not behave as an ordinary dielectric.

(B. C. Allen)

Corrosion by Nonaqueous Liquids

Stainless Steels in Sodium or NaK

A set of basic equations governing the corrosion rate of fuel-cladding materials in sodium-cooled reactors has been developed at Atomics International.[25] Attempts to evaluate certain mass-transfer coefficients which appear in these equations led to the conclusion that no loop studies ever run provide the data needed. In a reactor system there is a permanent driving force for corrosion owing to the difference between cladding surface and bulk sodium temperature, whereas in a conventional laboratory loop the driving force is established by the deposition of metal in the cold leg, and there is no way of determining the local bulk liquid concentration of corrosion products in the hot zone. This difficulty was eliminated by utilizing a 304 stainless-steel loop with high-heat-flux heaters capable of maintaining a 675°C surface temperature in 650°C sodium. Preliminary tests show that a ferritic layer, ~0.4 mil thick, forms on the heated section only, and the bulk

liquid becomes saturated with respect to corrosion products throughout the loop.

After accumulating 44,000 hr of sodium flow time at 300 to 1030°F (150 to 560°C), the Sodium Reactor Experiment (SRE) was shut down for modifications involving disassembly of the entire 304 stainless-steel primary system and much of the secondary system. All items removed from the system were examined visually, in search for evidences of wear, erosion, deposits, and carburization. No erosion, cracking, or impending failure was found. Several types of deposits and reaction layers were observed, including appreciable carbonaceous material in the hot leg of the system stemming from the accidental introduction of Tetralin during service. The degree of corrosion was insignificant. These findings, the details of which are contained in a summary report,[26] demonstrate that large sodium systems operated under SRE conditions can be expected to have a long, reliable life.

At Atomics International a program has been in progress to determine the effects of environment on mechanical properties of alloys for use in sodium-cooled reactors. Work to date[27] includes biaxial stress-rupture tests of well-characterized 316 and 304 stainless-steel specimens immersed in static isothermal sodium (<10 ppm oxygen) and in helium. Some of the data are shown in Figs. III-2 and III-3. The following observations were made:

1. The surfaces of the 316 stainless-steel specimens following the 730°C tests showed a 2-mil reaction layer slightly enriched in chromium and molybdenum and slightly depleted in nickel, with some sigma phase present.
2. Exposure of 316 stainless-steel tubing to 730°C sodium appeared to increase its creep rate, decrease both the time to rupture and creep strength, and have little or no effect on its strain at fracture.
3. A large amount of uniformly distributed sigma phase and a loss of carbon were noted in the 304 stainless-steel specimens following 760°C tests in sodium.
4. The stress-rupture curves for 304 stainless steel in sodium at both 705 and 760°C are steeper than those in helium (Fig. III-3).

These results do not confirm earlier work by MSA Research Corp.,[28] in which it was found that high-purity sodium had no effect on the stress-rupture life of 316 stainless-steel specimens. However, several important differences may account for the discrepancy. Tests at MSA were done at 650°C in a dynamic loop, whereas Atomics International's were at 705 to 760°C in a static retort.

A schedule-40 pipe–elbow–pipe (304–348–316 stainless steel) welded assembly that had carried NaK-78 for about 4400 hr below 540°C and almost 10,000 hr above 540°C (760°C peak) was examined at Idaho Nuclear[29] using metallographic, analytical, and mechanical techniques. This assembly had been in the return line from a calciner, and the NaK had apparently been relatively free of contamination during its service life.

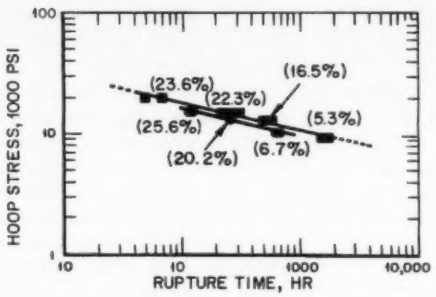

Fig. III-2 Biaxial stress-rupture data for 316 stainless steel in static low-oxygen sodium and in helium at 730°C (Ref. 27). ■, helium; ●, sodium; ductility values are given in parentheses.

General corrosion damage was nil. Carbide precipitation at grain boundaries was most prevalent in the 316, less in the 304, and least in the 348 stainless steel. Sigma phase (Fe–Cr intermetallic) was prominent in the 348, barely detectable in the 304, and not found at all in the 316 stainless steel. The 304–348 stainless-steel weld was harder (25 R_C) than the 316–348 stainless weld (95 R_B) and the wrought materials (90 to 96 R_B). Tensile and bend tests revealed some embrittlement but no loss in strength of the 348 material. It was concluded that sigma phase does not affect the serviceability of a steel if the intermetallic inclusions are small and not too numerous. Where sigma-phase growth is undersirable, it was suggested that a low-carbon fully austenitic stainless steel be used.

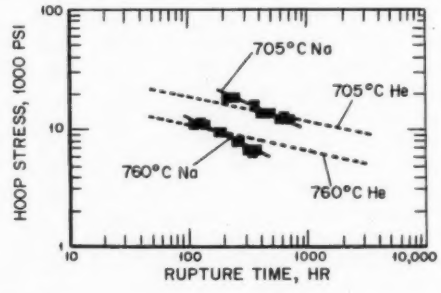

Fig. III-3 Biaxial stress-rupture data for 304 stainless steel in static low-oxygen sodium and in helium.[27]

Miscellaneous Cladding Materials in Sodium

Weight changes resulting from 1024-hr exposures of specimens of fast reactor cladding materials to

hot-trapped sodium (<5 ppm oxygen) by workers at Los Alamos[30] are summarized in Table III-1. These results agree with Argonne data,[31] which also show small weight gains for V–Ti alloys in low-oxygen sodium.

Table III-1 WEIGHT CHANGES OF ANNEALED (1 HR) SPECIMENS IN HOT-TRAPPED SODIUM AFTER 1024 HR AT 750°C (REF. 30)

Material	Annealing temp., °C	Weight change, mg/cm²
Vanadium	900	+0.25
V–10 wt.% Ti	900	+0.47
V–20 wt.% Ti	900	+0.44
V–40 wt.% Ti	900	+0.39
V–15 wt.% Ti–7.5 wt.% Cr	850	+0.83
Zirconium	850	+0.54
Niobium	1200	+0.07
304 stainless steel	1000	−0.23

Diffusion of Sodium and Potassium in Molybdenum

Confirming and extending work reported previously[32] on the diffusion of potassium in molybdenum, the latest Soviet compatibility-oriented studies[33] with ^{24}Na and ^{42}K as tracers in single-crystal and polycrystalline molybdenum and niobium at temperatures to 1100°C revealed the following:

1. The diffusion coefficients were about the same when liquid metals were used to saturate the refractory metals as when molten chlorides of sodium and potassium were used.
2. The rate of diffusion of the alkali metals into molybdenum was somewhat lower than that in niobium, presumably because of the smaller lattice parameters and higher melting point of molybdenum.
3. Potassium has a higher activation energy for diffusion and a lower diffusion coefficient into both metals than does sodium, probably because of the larger radius of the potassium atom.
4. The diffusion coefficients measured in single crystals were lower than those found in polycrystalline specimens, leading to the conclusion that diffusion is enhanced along grain boundaries.

Refractory Metals in Lithium

The search for a suitable container material for lithium at 1600°C is continuing at Battelle–Columbus.[34] Capsules made of unalloyed molybdenum and of TZM (Mo–0.5 wt.% Ti–0.08 wt.% Zr) were charged with lithium and specimens of W–26 wt.% Re and heated with a temperature gradient (1600°C, dropping to ~1400°C in 1.3 cm) for periods up to 1000 hr. For most of the tests, the lithium contained 290 ppm carbon and 50 ppm nitrogen. In a few of the short-time tests, excessive contamination of the lithium caused Mo_2C to form on the molybdenum-capsule walls. Grain-boundary pores were noted in the molybdenum, which had been heated 1000 hr, but not in the corresponding TZM can. No other significant incompatibility or corrosion effects were observed. Typical lithium-exposed surfaces of a W–26 wt.% Re specimen and a molybdenum-capsule wall are shown in Fig. III-4.

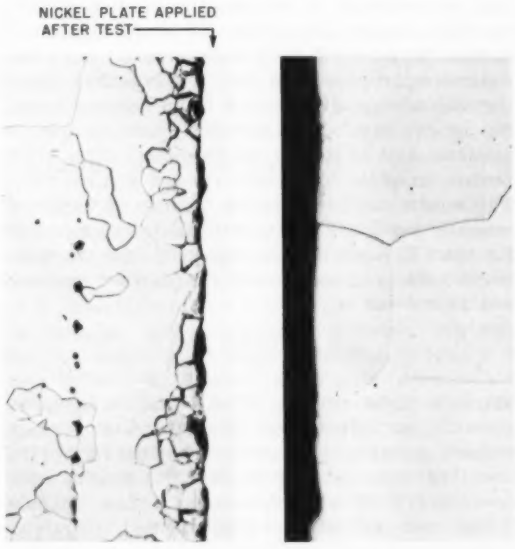

(a) (b)

W–26 wt.% Re specimen surface after 462 hr; fine black particles are sigma; surface unaffected by lithium, except for slight roughening. Magnification, 250 ×.

Molybdenum capsule wall after 174 hr; surface roughness shown is comparable to that in as-received tubing. Magnification, 250 ×.

Fig. III-4 Capsule and insert surfaces[34] after exposure to lithium under a thermal gradient (hot end, 1600°C; cool end, 1450°C).

Graphite in Cesium Vapor

The compatibility of graphite with cesium is of interest for such purposes as predicting the interaction of fission-product cesium with moderator graphite in a high-temperature gas-cooled reactor, studying the retention of fission-product cesium by graphite components in such a reactor, or evaluating graphite as a cesium-storage reservoir from which the cesium could be released by heating for use in an MHD generator. It is known that cesium reacts with graphite to produce distinct compounds characterized by the formula $C(n-1)a \cdot C_aCs$, where n is the number of graphitic layers between the nearest cesium layers and a is the number of moles of carbon per mole of cesium in each filled layer. Which com-

pound forms is governed by the temperature and pressure. Known phases include C_8Cs, $C_{10}Cs$, $C_{12} \cdot C_{12}Cs$, $C_{24} \cdot C_{12}Cs$, $C_{36} \cdot C_{12}Cs$, etc.

Vapor-pressure measurements made by Salzano and Aronson[35] on lamellar compounds in the known two-phase regions were used to calculate heats and entropies of reaction, which can, in turn, be used to predict behavior at pressure–temperature–composition combinations in the range of the data. Unfortunately almost all systems of practical interest involve higher graphite temperatures and lower cesium-vapor pressures than those studied. Using their knowledge of the nature of the bonding forces, the authors developed a method for extrapolating the available data to predict the conditions under which cesium–graphite compounds will and will not form. The results are based on the fact that, in the initial reaction product, the cesium-filled layers are very far apart ($n \rightarrow \infty$), and the expression for the equilibrium vapor pressure of the earliest reaction product reduces to

$$\ln P = -\frac{38{,}000}{RT} + \frac{18.75}{R}$$

which is plotted in Fig. III-5. Thus, at any given pressure, no reaction will occur when cesium vapor contacts graphite at temperatures to the right of the line. The few experimental observations that have been made at several sites on the cesium–graphite system have verified these predictions.

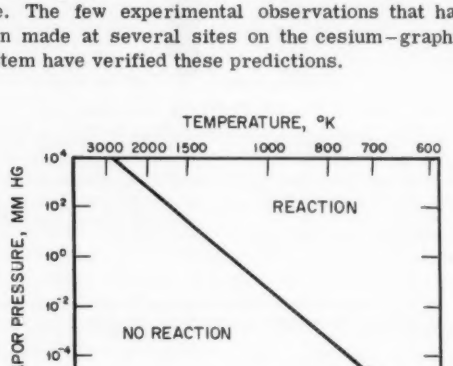

Fig. III-5 The theoretical threshold pressure for reaction between cesium and graphite.[35]

Corrosion by Lead–Bismuth

A small 430 stainless-steel thermal-convection loop, through which a lead–bismuth eutectic inhibited with 100 ppm zirconium was circulated, was sectioned and found to be only slightly attacked after 1300 hr of continuous operation at hot-leg temperatures as high as 700°C and ΔT's of 150°C. These results, obtained at Ames Laboratory,[36a] indicate considerable promise for zirconium as a corrosion inhibitor.

Corrosion by Molten Uranium Fuels

Workers at Ames are studying possible container materials for eutectics of uranium with manganese (U–6 wt.% Mn) and chromium (U–5 wt.% Cr), which have been proposed as liquid-metal fuels. From isothermal capsule tests it was found[36b] that, in spite of slight solution attack, yttrium surfaces still showed machining marks after 3000 hr of exposure to U–Cr eutectic at 950°C. Solution attack was also noted in tests with the U–Cr at 850°C. However, a saturation effect was apparently operative during the first 200 hr, as the amount of precipitated yttrium along the interface did not change much with time. Tantalum was not as resistant as yttrium, since the former formed intermetallic compounds in contact with the eutectics at 850 and 950°C. The U–Mn fuel seemed to be considerably worse in this regard than the U–Cr.

In a continuing quest for containers for molten uranium, 250-hr tests with yttrium capsules at 1300°C, described in a previous review,[37] have been extended to 936 hr (Ref. 36*b*). As with the shorter tests, yttrium precipitated and a U–Y eutectic built up near the meniscus in < 50 hr and did not increase in quantity thereafter. Also, the amount of uranium diffusing along the boundaries of the large yttrium grains to the outer surface of the capsule increased only slightly with test duration, amounting to only a "faint trace" or "very weak" indications. Because of such saturation effects, yttrium is a promising container for molten uranium to 1300°C.

Tantalum in Liquid Tin

To check out the rotating-disk method of studying dissolution kinetics in liquid-metal–solid-metal systems, workers at Argonne made a detailed investigation[38] of the tantalum–liquid tin system at temperatures up to 1200°C. The solubility of tantalum in liquid tin was measured (Fig. III-6), and the diffusion coefficient of ^{182}Ta in liquid tin was determined by the capillary-reservoir method. The values were used in a convective-diffusion model to calculate a diffusion-controlled dissolution flux. The latter was found to be in good agreement with experimental values in the region of diffusion control.

Corrosion by Organic Coolants

Magnesium with small additions of aluminum, beryllium, or zirconium has been used successfully as the fuel cladding for gas-cooled reactors at temperatures up to 500°C. However, these alloys are not suitable for use with terphenyl coolants, being rapidly attacked as a result of interaction with the

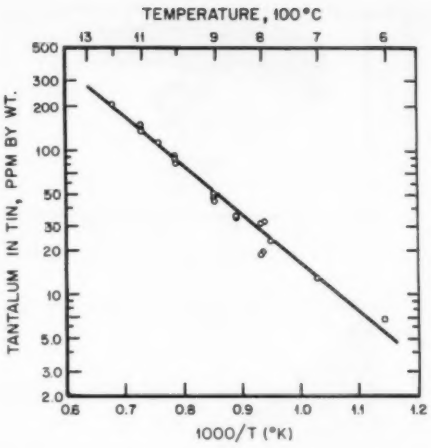

Fig. III-6 Solubility of tantalum in liquid tin.[38]

oxygenated organic compounds or with the 100 to 200 ppm water normally found in terphenyls. Under Euratom auspices, DeBeni[39] exposed Al-80 (Mg–0.8 wt.% Al–0.005 wt.% Be), Zr-55 (Mg–0.02 wt.% Al–0.55 wt.% Zr–0.01 wt.% Zn–0.01 wt.% Si), and several other magnesium alloys to 400°C terphenyl doped with various amounts of CO_2 and NH_3 as inhibitors. In the presence of only a few hundred ppm of these inhibitors, the corrosion rates in wet terphenyl were found to be reduced by factors of 100 and more. Magnesium oxide formed on the surfaces of the magnesium alloys and was compact and adherent. The ammonia appeared to neutralize any acidic compounds formed by reactions involving mineral impurities.

In 1960 the Canadians initiated operation of a 38 gal/min carbon-steel loop, designated X-7, in the NRX reactor for the purpose of testing fuels and organic coolants. It was cooled by the terphenyl mixture Santowax OM, spiked with 30% high boilers obtained from distillation residues of the OMRE (Organic Moderated Reactor Experiment). A review of the coolant-chemistry history of this loop has been published.[40] This describes the use of Attapulgus clay and 5-μ filters to reduce fuel-element fouling to the tolerable film-buildup rate of <10 μ/year. Also, rigid exclusion of chlorine (a fouling promoter) and removal of residual traces of chlorine by passing the Santowax through a bed of magnesium ribbon and alumina pellets covered with a thin layer of palladium are thought to be effective. Hydriding rates of zirconium-alloy specimens and test sections have been low.

Six UO_2 fuel elements, three Zircaloy-2 clad and three Zr–2.5 wt.% Nb clad, were irradiated[41] in the Santowax OM-cooled X-7 loop to 3500 Mwd per metric ton of uranium (117 days at power) at cladding temperatures in the neighborhood of 460°C (fuel-pin center line ~2000°C). Hydrogen absorption by the Zircaloy-2 occurred at about twice the rate of absorption by the Zr–2.5 wt.% Nb. Surface fouling was negligible. Surface oxidation and fission-gas release from the fuel were both small. These results indicate that such elements clad with Zr–2.5 wt.% Nb will perform satisfactorily in the WR-1 (Whiteshell) reactor to their target burnup.

A general review of Soviet work on organic coolants and moderators, containing a summary of findings on interactions with fuel and structural materials, is now available as an English-language translation.[42]

Corrosion by Fused Salts

Studies of molten fluoride mixtures for reactor applications began in the early 1950's, and extensive work has been done on the compatibility of these salt mixtures with structural materials. A pointed review of the materials research, leading to the development of Hastelloy N* for improved corrosion resistance and acceptable mechanical properties, operation of the Molten Salt Reactor Experiment (MSRE), and possible application of the findings to a molten-salt breeder reactor (MSBR), has been published.[14]

Several strings of Hastelloy N test specimens were irradiated[43a] in the MSRE in contact with flowing fuel (64 LiF–30 BeF_2–5.2 ZrF_4–0.8 UF_4, mole %) at ~650°C to thermal fluences in the range 10^{20} to 10^{21} neutrons/cm^2 and fast (>1.2 Mev) fluences about one-fourth of the thermal. Postirradiation metallography of the specimens revealed no evidence of major changes in structure, corrosive attack, or mass transfer as a result of exposure to the salt. As can be seen in Fig. III-7, the observed reductions

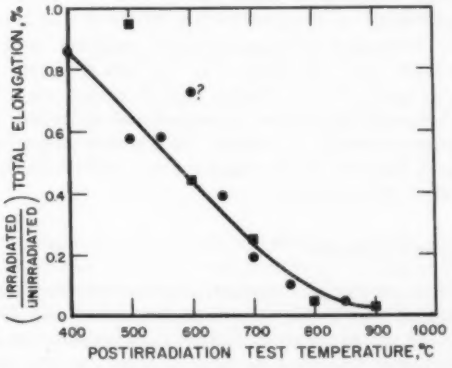

Fig. III-7 Effect of comparable irradiations at 650 to 700°C on the tensile ductility of Hastelloy N in the presence (●) and absence (■) of molten fluoride salts.[43a]

*Composition, wt.%: 16 Mo–7.5 Cr–6 Fe–0.14 C–bal. Ni.

in ductility were comparable with those found in specimens given similar radiation exposures with no salt present. This suggests that the salt plays little or no role in the radiation-induced loss of ductility of Hastelloy N.

IAEA Symposium Proceedings

In a previous review,[44] highlights of papers presented at the November 1966 symposium on "Alkali Metal Coolants — Corrosion Studies and System Operating Experience" were discussed. The proceedings are now available in the form of a 786-page book[45] containing all of the papers in their original languages (mostly English) and discussions. This book, constituting a rather complete state-of-the-art compendium as of mid-1966, is available for $16.00 in the USA through the National Agency for International Publications, Inc., 317 E. 34th Street, New York, N. Y. 10016. (E. M. Simons)

Radiation Effects in Structural Materials

Zirconium and Zirconium Alloys

Four of the six Zircaloy-2 safety-rod guide tubes in the Heavy Water Components Test Reactor failed after operating for 6000 hr at about 200°C (Ref. 46). During irradiation these tubes received fast fluences of 7×10^{18} to 7×10^{19} neutrons/cm^2. The failure was believed due to low cyclic straining that originated from the stress pulses associated with the rapid insertion of control rods during reactor operation. Tube-burst tests were performed on sections of the failed control-rod guide tubes, and the results of these tests are shown in Fig. III-8. It can be seen that increased hydrogen content resulted in lower strength upon irradiation at low fast fluences, but, upon irradiation at higher fast fluences, the effect of hydrogen content was overshadowed by irradiation-induced strength increases. The ductility of the tubes was a function of hydrogen content regardless of the degree of fast fluence.

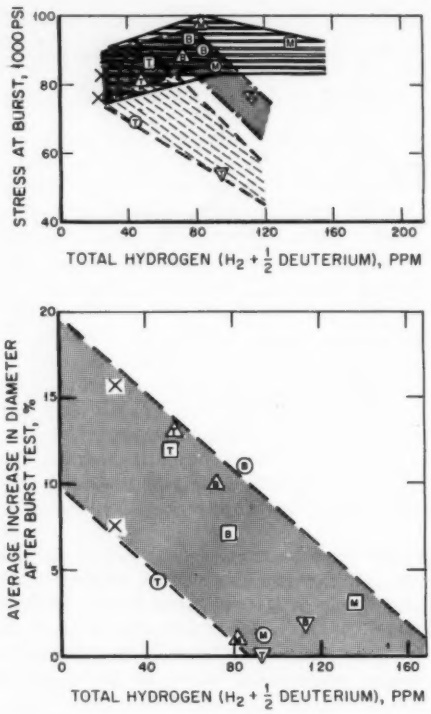

Fig. III-8 Burst strength and ductility of irradiated sections of Zircaloy-2 tubes as a function of hydrogen content and fast fluence.[46] *×, unirradiated sample; △, tube 1; □, tube 2; ○, tube 3; ▽, tube 4. T, top section, 7×10^{18} neutrons/cm^2; M, middle section, 7×10^{19} neutrons/cm^2; B, bottom section, 2×10^{19} neutrons/cm^2.*

Stainless Steel

Both in-pile and postirradiation creep-to-rupture tests at 650°C have been performed at Oak Ridge on 304 stainless steel.[47] The fluence of the in-pile specimens depended on their rupture life. The thermal fluence of the specimens tested after irradiation was 2×10^{20} neutrons/cm^2, whereas the fast fluence was 2×10^{19} neutrons/cm^2. Results of these creep tests are summarized in Tables III-2 and III-3 along with the test results on unirradiated control specimens. The minimum creep rate of the irradiated specimens was 2 to 5 times that of the unirradiated specimens. The in-pile and postirradiation creep tests resulted in similar creep rates, and the increased creep rate in these tests was attributed to failure while still in the primary creep stage. Irradiation was also found to cause large reductions

Table III-2 MINIMUM CREEP RATE OF 304 STAINLESS STEEL AT 650°C (REF. 47)

Stress, 1000 psi	Minimum creep rate,* % hr		
	Unirradiated	In-reactor†	Postirradiation‡
35	2.26 (7.7)		
30	0.92 (9.0)		0.50 (12.0)
27	0.33 (44.1)		
25	0.048 (122.8)	0.138 (17.1)	0.139 (24.4)
22.25	0.042 (157.7)		0.014 (123.4)
20	0.0073 (366.6)	0.016 (98.0)	
17		0.0035 (423.0)	0.006 (314.4)
15	0.00032	0.0014	0.0018 (956.9)

*Numbers in parentheses are rupture life in hours.

†Instantaneous thermal and fast fluxes of 6×10^{13} and 5×10^{12} neutrons/(cm^2)(sec), respectively.

‡Fast and thermal fluences of 2×10^{19} and 2×10^{20} neutrons/cm^2, respectively.

Table III-3 STRESS-RUPTURE DUCTILITY OF 304 STAINLESS STEEL AT 650°C (REF. 47)

Stress, 1000 psi	Elongation, %			Reduction in area, %		
	Unirradiated	In-reactor*	Postirradiation†	Unirradiated	In-reactor*	Postirradiation
35	37.2			35.1		
30	17.2		8.4	25.7		9.1
27	26.6			28.0		
25	17.2	6.7	4.9	22.3	11.1	4.2
22.25	18.4		2.9	19.9		4.0
20	17.5	2.6		13.9	3.0	
17			3.7			
15			2.8			0.2

*Instantaneous thermal and fast fluxes of 6×10^{13} and 5×10^{12} neutrons/(cm^2)(sec), respectively.
†Fast and thermal fluences of 2×10^{19} and 2×10^{20} neutrons/cm^2, respectively.

in elongation at failure. Consequently the rupture time of specimens was significantly reduced by irradiation.

In-pile creep tests on 304 stainless steel have also been conducted at Battelle–Northwest.[48] These test results are in agreement with those obtained at Oak Ridge, i.e., irradiation reduced the ductility and consequently the rupture life, as shown in Fig. III-9. However, it was noted that the creep rates were not affected by irradiation at 500 to 750°C. The Larson–Miller correlations for in-pile and out-of-pile creep tests are shown in Fig. III-10. It was also found that the elongation at rupture was about the same for the irradiated stainless steels regardless of test temperatures.

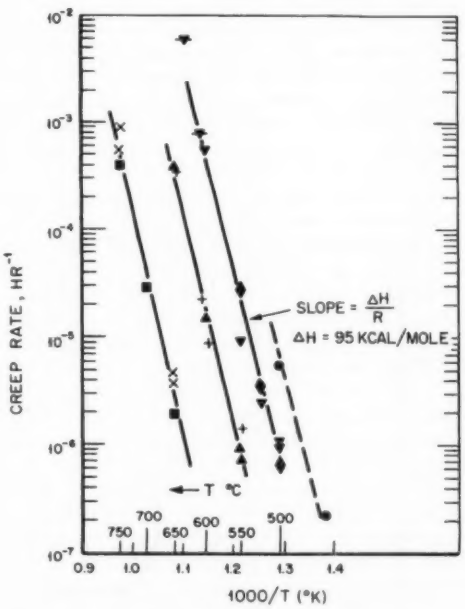

Fig. III-9 Arrhenius plot of in-reactor and ex-reactor creep rates of annealed 304 stainless steel.[48] 10,000 psi: ×, in-reactor; ■, ex-reactor. 20,000 psi: +, in-reactor; ▲, ex-reactor. 30,000 psi: ◆, in-reactor; ▼, in-reactor (activation-energy study rate); ▼, ex-reactor. 40,000 psi: ●, ex-reactor.

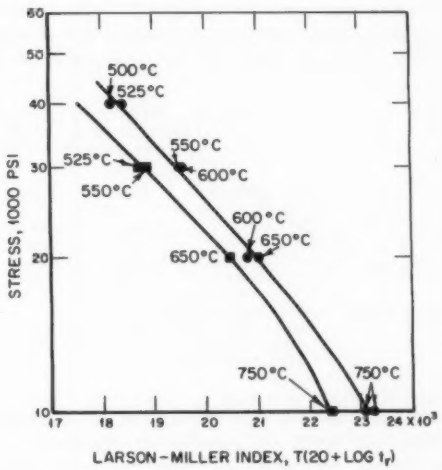

Fig. III-10 Larson–Miller correlation of creep-rupture life for in-pile and out-of-pile 304 stainless steel.[48] T = absolute temperature, °K; t_r = rupture time, hr. ●, ex-reactor; ■, in-reactor.

To duplicate the irradiation-induced embrittlement observed at elevated temperatures, workers impregnated 304 stainless-steel specimens with helium nuclei by cyclotron bombardment.[49] The yield-strength and total-elongation values determined for the helium-injected stainless steel are given in Table III-4. These test results show that helium caused a significant reduction in the elevated-temperature elongation but had no effect on the yield strength. It was further postulated that the helium atoms caused the reductions in elongation by accelerating cavity formation during fracture at grain boundaries.

Table III-4 EFFECT OF HELIUM ON THE MECHANICAL PROPERTIES OF 304 STAINLESS STEEL AT ELEVATED TEMPERATURES[49]

Test temp.* °F	Atom fraction of helium	0.2% yield strength, 1000 psi	Total elongation, %
1000	0	17.5	26.9
1000†	10^{-7}		
1000†	3×10^{-5}	17.8	24.8
1200	0	15.6	31.3
1200†	10^{-7}	16.1	33.8
1200	3×10^{-5}	16.1	22.6
1400	0×10^{-5}	14.5	41.7
1400†	10^{-7}	14.2	25.5
1400†	3×10^{-5}	14.2	13.1

*Stainless steel was annealed for 5 hr at 1010°C before helium impregnation.
†Annealed for 10 hr at 760°C before testing at a strain rate of 0.02 min^{-1}.

Helium has also been injected into 304 stainless steel modified by a 0.2 wt.% titanium addition.[50] This titanium addition was found to minimize the degree of irradiation-induced embrittlement when the specimen was tested in tension at elevated temperatures.[51] Table III-5 shows that the elongation of the titanium-modified stainless steel was not adversely affected by helium, whereas the elongation of unmodified 304 stainless steel was significantly reduced at the same testing temperatures. The improved performance of the titanium-modified 304 stainless steel was attributed to anchoring of the helium atoms as small bubbles by TiC particles.

Researchers at Battelle–Columbus determined that irradiation induced embrittlement in the narrow temperature range of 525 to 575°C (Ref. 52). This was determined by tensile tests on 347 stainless-steel specimens irradiated to a fast fluence of 2.1×10^{22} neutrons/cm^2 and a thermal fluence of 4.0×10^{22} neutrons/cm^2. This embrittlement is illustrated in Fig. III-11. It was observed that, at testing temperatures up to 500°C, the preirradiation tensile properties were recovered by annealing for 1 hr at 980°C. However, at 600°C and above, the preirradiation tensile properties could not be recovered by the same annealing treatment. Since large decreases in uniform elongation were noted in this study, and cyclotron impregnation of stainless steel with helium caused decreases in total elongation only,[49,50] it is suggested that another mechanism besides the helium mechanism may be causing the embrittlement at 575°C.

Tensile tests were performed on 304 stainless-steel specimens that had been irradiated in the EBR-II to a fast fluence of 5×10^{21} neutrons/cm^2 at 538 to 704°C (Ref. 53). Test results at room temperature and at 400, 550, and 650°C are given in Table III-6. The maximum strength increase occurred at a testing temperature of 400°C. Irradiation caused ductility decreases at all testing temperatures, compared with that of the thermal control specimens. However, no drastic reductions in ductility were found at 650°C such as those reported by other investigators. A possible explanation for the absence of embrittlement at 650°C is that these specimens were irradiated in a predominantly fast flux, whereas those which showed embrittlement were irradiated in a mixed thermal and fast flux. Therefore it appears that the elevated-temperature embrittlement may originate from thermal neutrons.

The irradiation-induced change in fracture mode of stainless steel at elevated temperature has also been studied by the British.[54] Specimens of 20 wt.% Cr–25

Table III-5 EFFECT OF ALPHA-PARTICLE BOMBARDMENT ON THE TOTAL ELONGATION OF STAINLESS STEEL AT ELEVATED TEMPERATURES[50]

Stainless steel	Type	Total elongation, %, at indicated temperature				
		500°C	600°C	700°C	800°C	900°C
304*	Control†	45.4–47.8	40.9–41.9	48.3–52.5	34.1–49.1	36.1–39.5
304*	10^{-7} He‡	44.3	42.7	31.0	19.9	13.9
0.2% Ti–304L§	Control	33.4	34.4	55.5	55.3	>33.7
0.2% Ti–304L§	10^{-7} He	32.0	33.7	56.9	65.9	58.4

*ASTM grain size 5.
†Range of values obtained by testing three to five specimens.
‡Impregnated with 10^{-7} atoms of helium per atom of metal.
§ASTM grain size 7.5.

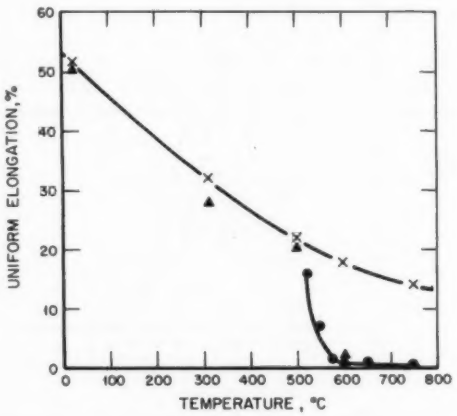

Fig. III-11 Uniform elongation of unirradiated and irradiated 347 stainless steel as a function of test temperature.[52] ×, unirradiated; ●, 2.1×10^{22} neutrons/cm^2; ▲, 2.1×10^{22} neutrons/cm^2 (annealed for 1 hr at 982°C).

Table III-6 TENSILE PROPERTIES* OF 304 STAINLESS STEEL IRRADIATED TO A NOMINAL FLUENCE OF 5×10^{21} NEUTRONS/CM^2 BETWEEN 538 AND 704°C (REF. 53)

Condition	Test temp., °C	0.2% offset yield strength, 1000 psi	Ultimate tensile strength, 1000 psi	Total elongation, %
Unirradiated	Room	64.6	103	64.8
	Room	64.8	103	65.8
	400	53.1	69.2	24.8
	550	49.4	68.4	33.2
	550	51.3	67.6	25.7
	650	47.5	64.1	30.1
	650	51.1	67.6	29.5
Unirradiated, 30 days at 550°C	Room	62.0	106	84.2
	400	47.5	69.9	37.2
	550	47.6	71.4	32.4
	650	48.4	71.3	33.5
Irradiated	Room	78.0	112	82.1
	Room	77.6	110	80.4
	400	66.1	84.8	23.0
	400	71.6	84.8	21.8
	550	68.9	83.6	24.2
	650	67.2	82.0	25.2
	650	67.5	81.1	25.4

*Tested at crosshead speed of 0.05 cm/min, ~2.5%/min.

wt.% Ni stainless steel were irradiated to a thermal fluence of 5×10^{19} neutrons/cm^2 at 40°C and tensile tested at 600 to 900°C. The results indicated that the irradiation did not affect the elongation at 600 and 700°C. With increasing temperature, the elongation of the irradiated specimens remained the same and that of the unirradiated specimens increased. Therefore it was concluded that, at temperatures above 700°C, irradiation causes a reduction in elongation. Metallographic examination of the fractured specimens revealed that irradiation promoted wedge-type cracking at the expense of cavitation-induced cracking. This effect accounts for the reduced ductility in irradiated specimens, since the specimens which failed by cavitation-induced cracking exhibited higher ductilities than did those which failed by wedge-type cracking. It should be noted that these specimens exhibited elongations of 30%, whereas specimens irradiated to higher fluences in other investigations have shown ductilities of less than 1%.

Preirradiation annealing of Incoloy 800 for 96 hr at 1500°F (816°C) resulted in improved postirradiation ductility when tested[55] at 1300 and 1500°F (704 and 816°C). This improved ductility occurred only with carbon contents above 0.07 wt.% at testing temperatures of 1300°F and with carbon contents above 0.04 wt.% at testing temperatures of 1500°F. Tensile specimens were irradiated to fast and thermal fluences of 1.6×10^{21} and 3.0×10^{21} neutrons/cm^2, respectively. The improved postirradiation ductility was attributed to formation of coarse carbide particles near the grain boundaries.

A preirradiation heat-treatment was developed for improving the high-temperature ductility of austenitic stainless steel after irradiation.[56] The metal was first worked and then annealed at a temperature in the range 800 to 900°C. This working–annealing process was then repeated at least once. This procedure allowed the formation and coarsening of a precipitate of all insoluble materials at the temperature of the anneal and prevented the formation of fine precipitates under subsequent irradiation conditions. It has been found that irradiation at 550°F (288°C) increased the room-temperature yield strength of stainless steel as a function of the square root of fast fluence up to about 1×10^{21} neutrons/cm^2 (Ref. 57). At higher fluences a saturation of radiation-induced mechanical-property changes takes place. Previous studies have indicated[58] that a similar saturation in mechanical-property changes in stainless steels occurs upon irradiation to a fast fluence of about 2×10^{20} neutrons/cm^2 at an irradiation temperature of 100°F (38°C).

Postirradiation fatigue life of 347 stainless steel can be predicted from postirradiation tensile data by use of empirical relations.[59] The correlation of the fatigue life with the predicted fatigue life is shown in Figure III-12.

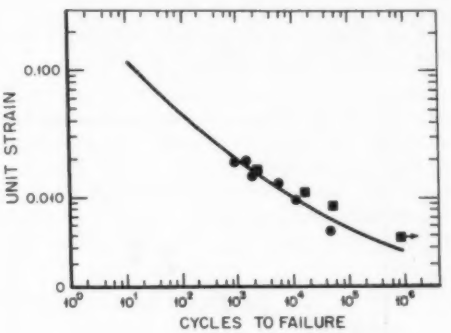

Fig. III-12 Correlation of measured fatigue life to predicted fatigue life for irradiated 347 stainless steel.[59] ●, 11×10^{21} neutrons/cm^2; ■, 5.5×10^{21} neutrons/cm^2; —, predicted.

Nickel- and Cobalt-Base Alloys

An extensive evaluation of irradiated Hastelloy N is being conducted at Oak Ridge[43b] in support of the MSRE (Molten Salt Reactor Experiment). The mechanical properties of unirradiated and irradiated Hastelloy N are compared in Fig. III-13. The specimens were irradiated at 645°C to a thermal fluence of 1.3×10^{20} neutrons/cm^2 and a fast fluence of 3×10^{19} neutrons/cm^2. The yield strength does not appear to be changed by irradiation, whereas the ultimate strength is somewhat reduced. Radiation-induced losses in elongation occur at all test temperatures, with especially severe losses above 600°C. The reduced elongation at low temperatures was attributed to aging during irradiation and that at elevated temperatures was related to helium-induced

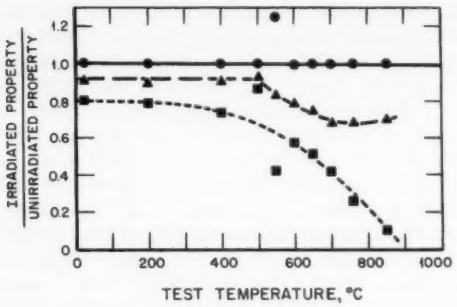

Fig. III-13 Comparative tensile properties of unirradiated and irradiated Hastelloy N specimens.[43b] Specimens irradiated to thermal and fast fluences of 1.3×10^{20} and 3×10^{19} neutrons/cm^2, respectively. ●, yield stress; ▲, ultimate stress; ■, total elongation. Strain rate, 0.05 min^{-1}.

embrittlement. The strain-rate dependence of elongation in irradiated Hastelloy N in tensile tests is not apparent at 400°C, but it becomes significant at 500°C and very evident at 650°C and above. Figure III-14 illustrates the strain-rate dependence of elongation in irradiated Hastelloy N at 760°C.

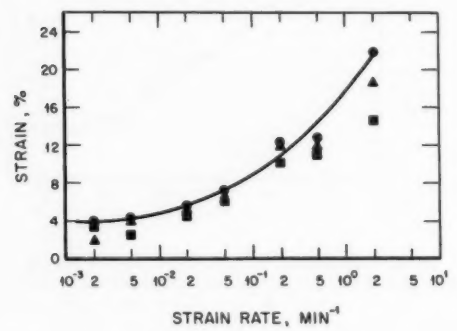

Fig. III-14 Influence of strain rate on the ductility of Hastelloy N specimens irradiated at 760°C to thermal and fast fluences of 1.3×10^{20} and 3×10^{19} neutrons/cm^2, respectively.[43b] ▲, uniform elongation; ●, total elongation; ■, reduction in area.

To establish the effect of helium on the postirradiation stress-rupture properties of Hastelloy R-235, workers investigated specimens with constant boron contents but various ^{10}B contents.[60a] These experiments were based on the theory that more helium will be generated by neutron irradiation in the alloy that contains the most ^{10}B. Figure III-15 shows that the preirradiation stress-rupture properties at 870°C are not influenced by the different amounts of ^{10}B; however, the postirradiation rupture life is significantly decreased by higher ^{10}B contents, which result in more helium generation.

Canadian investigators at Chalk River have performed elevated-temperature postirradiation tensile tests on nickel and various nickel alloys.[61] The alloys that were irradiated and tested included Inconel X-750, Inconel 600, commercial nickel, Monel, 304 stainless steel, and various Fe–Ni–Cr alloys. These alloys were irradiated to fast fluences of 2.5×10^{18} to 5.8×10^{19} neutrons/cm^2 and thermal fluences about 3 to 4 times higher. It was found that all alloys tested suffered a postirradiation ductility loss above 550°C which was not significantly affected by pre- or postirradiation heat-treatments. The ductility loss increased with decreasing strain rates, but no grain-size dependence was evident. The sharp ductility loss in the 550 to 600°C range was difficult to explain by a helium-induced embrittlement model. It was suggested that the irradiation-induced ductility loss may be related to the ductility minima that have been found in many unirradiated alloys.[62]

Hastelloy X irradiated in EBR-II (Ref. 53) to a fast fluence of 5×10^{21} neutrons/cm^2 at temperatures of 538 to 704°C was tensile tested at room temperature and at 400, 550, and 650°C. The test results given in Table III-7 indicate that irradiation did not significantly affect the ultimate strength and elongation, but the yield strength was increased. These test data are in disagreement with those of other investigators who report significant irradiation-induced ductility losses at these temperatures for nickel-base alloys.[43b,60,61] It is suggested that the irradiation-induced ductility loss may not take place if the irradiation is in a predominantly fast flux.

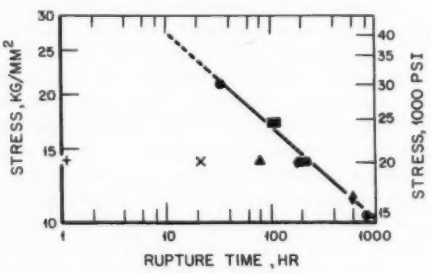

Control	Boron* isotope	Irradiated†
●	^{N}B	×
■	^{10}B	+
◆	^{11}B	▲

*50 ppm (by weight) total boron, 98% isotopic enrichment when other than ^{N}B.
†Irradiation conditions:
Fast fluence, 5.5×10^{19} neutrons/cm^2 ($E_n > 1$ Mev)
Thermal fluence, 1.6×10^{20} neutrons/cm^2

Fig. III-15 Stress-rupture strength at 870°C of irradiated and unirradiated Hastelloy R-235 containing various ^{10}B contents.[60a]

Table III-7 TENSILE PROPERTIES* OF HASTELLOY X IRRADIATED TO A NOMINAL FLUENCE OF 5×10^{21} NEUTRONS/CM^2 AT TEMPERATURES BETWEEN 538 AND 704°C (REF. 53)

Condition	Test temp., °C	0.2% offset yield strength, 1000 psi	Ultimate tensile strength, 1000 psi	Total elongation, %
Unirradiated	Room	46.1	98.3	71.0
	Room	47.7	100.8	67.7
	400	31.2	86.3	67.4
	400	34.1	93.3	69.4
	550	34.1	93.3	69.4
	550	34.9	89.8	70.5
	650	32.7	82.5	69.5
Unirradiated, 30 days at 550°C	Room	53.8	110.2	58.3
	400	37.9	90.4	61.2
	550	35.2	89.9	65.8
	650	37.3	89.6	56.9
Irradiated	Room	70.3	113.6	58.8
	400	57.3	96.8	55.7
	400	57.3	95.5	60.2
	550	57	89.8	49.4
	550	58.1	93.6	50.4
	650	56.4	94.1	51.7
	650	55.2	94.6	58.6

*Tested at crosshead speed of 0.02 in./min, ~2.5%/min.

Postirradiation burst tests were conducted on Incoloy 800 and Inconel 625 tubes irradiated at 1000 and 1300° F (538 and 704°C) to fast fluences of 1.1 to 1.6×10^{21} neutrons/cm^2 (Ref. 55). The thermal fluence in these irradiations was about twice the fast fluence. Results of the burst tests, given in Table III-8, show that the ductility (measured by diameter change) of the unirradiated tubes was considerably reduced by heating at the irradiation temperature. Irradiation at elevated temperatures caused further decreases in ductility to levels of less than 1.0%. Irradiation was also shown to cause significant reductions in the hoop stress at failure.

Tensile properties of Hastelloy X, Inconel 625, and 347 stainless-steel sheet specimens after thermal fluences of 5×10^{17} to 1×10^{19} neutrons/cm^2 have been determined by Aerojet Nuclear.[63] The tensile tests were performed at 1040, 1290, and 1540° F tests were performed at 1040, 1290, and 1540° F (560, 700, and 838°C). The yield and ultimate strengths were not affected at any fluence level or testing temperature. However, measurable losses in elongation were found at all testing temperatures and thermal fluence levels.

The effect of fast-neutron irradiation on the mechanical properties of cobalt-base alloys has been studied at Brookhaven.[64] Specimens of Multimet (Co–20 wt.% Ni–21 wt.% Cr–3 wt.% Mo–2.5 wt.% W–1.0 wt.% Nb) and Haynes 25 alloy (Co–10 wt.% Ni–20 wt.% W–3 wt.% Fe) were irradiated to fast fluences of 2×10^{20} neutrons/cm^2 at 100°C. Results of tensile tests are shown in Table III-9. At 800°C the yield strengths for both materials are increased, but tensile strength values are not affected by irradiation. However, irradiation causes a drastic ductility loss at elevated temperatures, which is also exhibited by stainless steels and nickel-base alloys.

The effect of fast-neutron irradiation on the relaxation of springs at 1000 to 1150° F (538 to 621°C) has been determined.[65] Springs of René 41 (Ni–18 wt.% Cr–10 wt.% Mo–10 wt.% Co) and Stauffer 880 (Ta–12 wt.% W) were irradiated and tested. The results, summarized in Fig. III-16, indicate that René 41 springs underwent relatively less relaxation. The

Table III-8 BURST TESTS ON UNIRRADIATED AND IRRADIATED INCOLOY 800 AND INCONEL 625 TUBULAR SPECIMENS*[55]

Specimen condition	Exposure temp., °F	Test temp., °F	Burst pressure, psi	Time to burst, min	Hoop stresses, psi	Net diameter change, %
Incoloy 800						
Irrad.	1300	1100	3280	7.6	38,790	15.2
Irrad., aged	1300	1100	3200	5.8	45,390	10.2
As received	None	1300	3000	1.2	39,780	12.0
Control†	1000	1300	3000	0.9	39,780	11.3
Control	1300	1300	2750	1.8	36,470	12.9
Irrad.‡	1300	1300	1800	2.4	24,990	0.9
Irrad., aged	1300	1300	1750	1.8	25,120	0.8
As received	None	1500	2010	0.5	26,650	19.3
Control	1000	1500	2150	0.7	28,510	17.3
Control	1300	1500	2100	0.7	27,850	13.2
Irrad.	1300	1500	1425	2.3	18,500	3.6
Irrad., aged	1000	1500	1550	3.4	21,730	2.7
Inconel 625						
Irrad.	1300	1100	9550	3.6	125,930	0.7
As received	None	1300	6650	1.8	86,720	17.0
Control	1000	1300	6200	1.0	80,850	6.1
Control	1300	1300	7800	1.7	101,710	0.6
Irrad.	1300	1300	7480	7.6	95,520	0
As received	None	1500	5500	1.0	71,720	13.4
Control	1000	1500	5350	1.2	69,760	5.2
Control	1300	1500	7000	1.7	91,280	3.9
Irrad.	1000	1500	3150	1.1	39,390	0.4
Irrad.	1300	1500	3725	6.6	47,570	0.4

*Tubing size: 0.280-in. outside diameter by 0.010-in. wall.
†Controls: 4500 hr at temperature.
‡Irradiation period: 4300 hr.

Table III-9 EFFECT OF IRRADIATION ON THE TENSILE PROPERTIES OF HAYNES 25 ALLOY AND MULTIMET[64]

(All Specimens Are Solution Treated at 1175°C. Strain Rate of Tensile Test is 0.002 in./min. Irradiation Temperature is 100°C)

Alloy	Fluence,* 10^{20} neutrons/cm^2	Test temp., °C	Yield strength, psi	Tensile strength, psi	Total elongation, %
Haynes 25	0	25	67,000	152,000	55
Haynes 25	2	25	139,000	142,000	15
Haynes 25	0	800	35,900	41,500	10.5
Haynes 25	2	800	39,200	41,100	2.3
Multimet	0	25†	71,000	121,000	43
Multimet	2	25	116,000	138,000	31
Multimet	0	800	23,600	32,900	55
Multimet	2	800	30,000	31,300	6.7

*Estimated fluence ($E > 1$ Mev).
†Tested at 0.02 in./min.

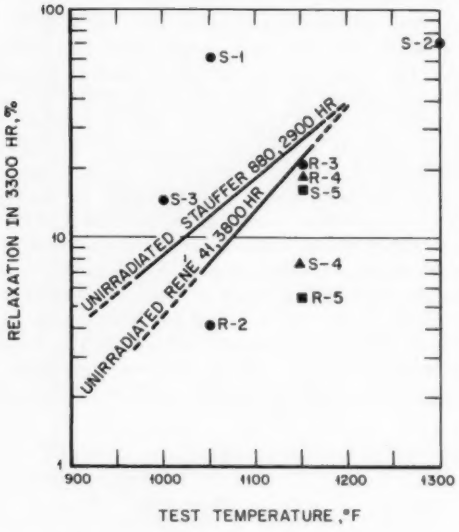

Fig. III-16 Comparison of spring force relaxation for irradiated and unirradiated René 41 and Stauffer 880 at 40,000 psi (Ref. 65). ●, 1 to 2 × 10^{19} neutrons/cm^2; ▲, 3 to 4 × 10^{18} neutrons/cm^2; ■, 2 to 3 × 10^{17} neutrons/cm^2. S, Stauffer 880; R, René 41; numbers are specimen numbers.

irradiated René 41 springs were found to undergo less relaxation than the unirradiated springs. However, with increasing fluence the René 41 relaxation values approached those of the unirradiated springs. It appears that small fluences are beneficial to René 41 springs through a hardening effect that results in less relaxation. The data for springs made of Stauffer 880 showed considerable scatter.

Pressure-Vessel Steels

Boron-containing specimens of Fortiweld steel (bainitic boron–molybdenum steel) undergo larger irradiation-induced shifts of the ductile-to-brittle transition temperature (DBTT) than do steels without boron.[66] To establish whether the ^{10}B $(n,\alpha)^7$Li reaction was responsible for the increased shift, workers irradiated specimens that had the same boron content but varying amounts of ^{10}B and ^{11}B. Figure III-17

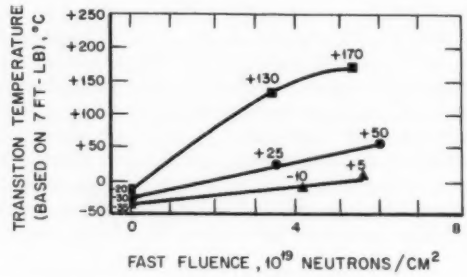

Fig. III-17 The transition temperature in Fortiweld steel as a function of fast-neutron irradiation at 265°C and boron content.[65] ●, natural boron (20 wt.% ^{10}B); ■, ^{10}B; ▲, ^{11}B.

shows that the ^{10}B reaction is probably responsible for the observed behavior, since the transition-temperature shift increased with increasing ^{10}B content in the various steels.

An Fe–9 wt.% Ni alloy steel offers advantages over low-alloy steels in pressure-vessel construction because of higher strength and lower ductile-to-brittle transition temperatures. However, both thermal-stability and irradiation tests indicate large increases in the DBTT.[67] It was hypothesized that, after a few years of operation at 300° C in a nuclear environment, the original advantage of low transition temperature would be lost.

Basic Irradiation Mechanisms

The electron microscope was used to observe the behavior of helium-gas bubbles in cold-worked Al–Li alloys upon postirradiation heating.[68] The bubbles

appeared occasionally along the grain boundaries in the Al–2.7 wt.% Li specimen irradiated to a thermal fluence of 4.1×10^{19} neutron/cm^2 and then heated to about 300°C. Upon heating to higher temperatures, up to 450°C, the bubbles in the specimen grew, and there was a gradual growth in the recrystallized grains. When the bubbles reached sizes of 0.3 to 0.6 μ, upon heating to 500°C, the grain boundaries migrated and were detached from the bubbles. In the Al–0.4 wt.% Li specimen, the bubbles migrated along with the grain boundaries out of the specimen surface when heated to temperatures above 450°C. The grain sizes of the irradiated Al 2.7 wt.% Li specimen heated for 1 hr to 450°C were smaller than those of an unirradiated specimen heated for 1 hr to 400°C. In the displacement of grain boundaries caused by grain growth, the gas bubbles were swept together to form larger bubbles until they reached a certain critical size. As they became larger, they detached themselves from the moving boundary. The bubbles impeded the grain-boundary movement but did not suppress it completely. The bubbles found on the grain boundaries differed in shape from those that had grown in the grain interior.

A theoretical study on the effect of irradiation with fast neutrons on the processes of deformation and failure of metals has been presented by the Russians.[69] Equations were derived which showed that coagulation of vacancies into complexes played a significant part in the process of deformation and failure. Stress-rupture tests with a 20 wt.% Cr–28 wt.% Ni stainless steel showed that irradiation increased the creep rate and accelerated failure. Specimens strained to rupture in the reactor failed in a brittle manner without necking and with numerous cracks along the grain boundaries. The relative decrease in the rupture life of stainless steel subjected to stress-rupture tests and irradiation at various temperatures under a constant load was given by $\epsilon = \tau_0/\tau_r$, where τ_0 is the rupture life of the original stainless steel and τ_r is the rupture life of irradiated stainless steel. The determination of mechanical characteristics of materials after, instead of during, irradiation may lead to significant errors in estimating the service life of nuclear reactor components at elevated temperatures. (M. Kangilaski)

Metallurgy of Refractory Metals

Chromium

A program to develop chromium-base alloys for use in fast breeder reactors is being conducted at General Electric.[60b] Tensile data at 550 and 750°C for a number of alloys tested in argon are given in Table III-10. Yield strengths obtained were based on crosshead travel and cannot be considered as absolute values. A wide range of tensile properties was realized in chromium-base alloys by adjusting the rolling and annealing procedures. In these alloys, short-time strengths at 750°C can be achieved which exceed those for austenitic stainless steels. Of the primary alloys in the warm-rolled or warm-rolled plus 750°C annealed condition, Cr–TZC–Y was the strongest and the Cr–Y alloy was the weakest of the three.

Initial stress-rupture tests at 750°C were conducted on as-warm-rolled Cr–Hf–Th–Y alloy sheet specimens. An argon-filled test capsule was employed

Table III-10 TENSILE PROPERTIES* OF CHROMIUM-BASE ALLOYS IN ARGON†[60]

Alloy	Condition†	Test temp., °C	Yield strength		Tensile strength		Elongation, %	Hardness,‡ DPH
			1000 psi	kg/cm^2	1000 psi	kg/cm^2		
Cr–Y	Warm rolled plus 750°C anneal	750	28.5	2000	37.4	2630	3.4	227
Cr–Y	Warm rolled plus 750°C anneal	750	31.4	2200	38.0	2670	2.0	227
Cr–Y	Hot rolled plus 750°C anneal	750	10.2	720	22.5	1680	41.4	153
Cr–Hf–Th–Y	Warm rolled	750	45.5	3200	54.7	3850	3.3	240
Cr–Hf–Th–Y	Warm rolled	550	48.3	3400	57.8	4060	2.9	240
Cr–Hf–Th–Y	Warm rolled plus 750°C anneal	750	50.3	3540	57.0	4010	3.1	258
Cr–Hf–Th–Y	Warm rolled plus 750°C anneal	750	52.3	3680	56.7	3990	2.9	258
Cr–Hf–Th–Y	Hot rolled plus 750°C anneal	750	40.2	2830	41.2	2900	6.1	203
Cr–TZC + Y	Warm rolled	750	43.8	3080	61.9	4350	1.9	266
Cr–TZC + Y	Warm rolled	550	62.6	4390	66.4	4670	2.9	251
Cr–TZC + Y	Warm rolled plus 750°C anneal	750	53.3	3820	62.0	4360	4.1	266
Cr–TZC + Y	Hot rolled plus 750°C anneal	750	13.2	930	20.1	1410	8.1	139
Cr–20 V–1 Y	As extruded, 2500°F	750	32.4	2280	39.0	2740	1.7	287
Cr–20 V–1 Y	As extruded, 2500°F	750			39.1	2750	2.3	287
AISI 304		750			30.0	2110		
AISI 304		550			55.0	3870		
AISI 316		750			40.0	2810		
AISI 316		550			65.0	4570		

*Specimens were 0.076 cm thick with a 1.27-cm-wide reduced section and a 2.54-cm gauge length. The major axis of all specimens parallels the rolling direction. Crosshead speed was 0.071 cm/min.
†Warm rolled from 850°C; 2-hr anneal. Hot rolled from 1100°C; 2-hr anneal.
‡Hardness measured on specimen ends.

which was identical to that used for the tensile tests. Data for these tests are plotted in Fig. III-18, which also includes literature data[70] for 304 and 316 austenitic stainless steels for comparison. A significant strength advantage is apparent for the chromium-base alloy.

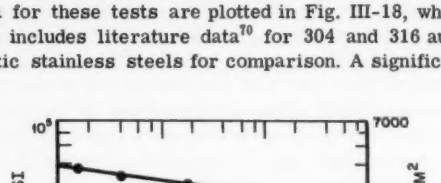

Fig. III-18 Stress-rupture data on Cr–Hf–Th–Y alloy and 316 and 304 stainless steels.[60b] ●, Cr–Hf–Th–Y (M-314), as warm rolled, 750°C; ■, 316 stainless steel, 732°C; ▲, 304 stainless steel, 732°C.

Sheet bend tests were performed on the three primary alloys and a Cr–20 V–1 Y alloy in various conditions. Testing was accomplished in a tensile machine at a crosshead speed of 0.075 cm/min over a 2*T* radius. Bending continued until either fracture occurred or a 90° bend was achieved. The results as a function of heat-treatment are presented in Table III-11. As can be seen, the DBTT for the Cr–Y alloy in the warm-rolled condition was about 100°C and did not change with annealing at 750, 870, and 980°C. The DBTT for the Cr–Hf–Th–Y and Cr–TZC–Y alloys in the as-warm-rolled condition was not determined; however, that for Cr–Hf–Th–Y was about 200°C after a 750°C anneal, whereas that for Cr–TZC–Y appeared to exceed 200°C after 750 and 870°C anneals. Limited data on the warm-rolled Cr–20 V–1 Y alloy after vacuum annealing at 750°C indicate a DBTT in excess of 200°C.

Table III-11 BEND DATA FOR CHROMIUM-BASE ALLOYS AS A FUNCTION OF VACUUM-ANNEALING CONDITIONS*[60]

Alloy and condition	Vacuum-annealing conditions	Hardness, DPH	Temp.,† °C	Bend angle, deg	Comment
Cr–Y, W/R*	As rolled	195	RT	9	Fractured
Cr–Y, W/R	750°C, 2 hr	195	RT	6	Fractured
Cr–Y, W/R	980°C, 2 hr	127	RT	9	Fractured
Cr–Y, W/R	As rolled	195	106	90	No fracture
Cr–Y, W/R	750°C, 2 hr	195	104	90	No fracture
Cr–Y, W/R	870°C, 2 hr	178	104	90	No fracture
Cr–Y, W/R	980°C, 2 hr	127	100	90	No fracture
Cr–Y, W/R	750°C, 10 hr	200	110	90	No fracture
Cr–Y, W/R	870°C, 10 hr	136	106	90	No fracture
Cr–Y, H/R	750°C, 2 hr	140	109	5	Fractured
Cr–Hf–Th–Y, W/R	980°C, 2 hr	175	RT	90	No fracture
Cr–Hf–Th–Y, W/R	870°C, 10 hr	197	RT	90	No fracture
Cr–Hf–Th–Y, H/R	980°C, 3.5 hr	145	RT	90	No fracture
Cr–Hf–Th–Y, W/R	750°C, 2 hr	232	100	9	Fractured
Cr–Hf–Th–Y, W/R	750°C, 2 hr	232	150	10	Fractured
Cr–Hf–Th–Y, W/R	750°C, 2 hr	232	204	90	Fractured
Cr–Hf–Th–Y, W/R	750°C, 10 hr	222	110	72	Fractured
Cr–Hf–Th–Y, W/R	870°C, 2 hr	216	110	18	Fractured
Cr–Hf–Th–Y, W/R	870°C, 10 hr	197	110	90	No fracture
Cr–Hf–Th–Y, W/R	870°C, 2 hr	216	150	90	No fracture
Cr–Hf–Th–Y, W/R	870°C, 2 hr	216	209	90	No fracture
Cr–Hf–Th–Y, W/R	980°C, 2 hr	175	108	90	No fracture
Cr–Hf–Th–Y, W/R	1090°C, 2 hr	140	110	90	No fracture
Cr–Hf–Th–Y, H/R	750°C, 2 hr	196	105	7	Fractured
Cr–Hf–Th–Y, H/R	980°C, 3.5 hr	145	109	90	No fracture
Cr–TZC–Y, W/R	980°C, 2 hr	154	RT	7	Fractured
Cr–TZC–Y, W/R	1090°C, 2 hr	129	RT	90	No fracture
Cr–TZC–Y, H/R	980°C, 3.5 hr	142	RT	5	Fractured
Cr–TZC–Y, W/R	750°C, 2 hr	259	RT	12	Fractured
Cr–TZC–Y, W/R	750°C, 2 hr	259	150	7	Fractured
Cr–TZC–Y, W/R	750°C, 2 hr	259	204	9	Fractured
Cr–TZC–Y, W/R	750°C, 10 hr	252	110	15	Fractured
Cr–TZC–Y, W/R	870°C, 2 hr	227	110	5	Fractured
Cr–TZC–Y, W/R	870°C, 2 hr	227	150	18	Fractured
Cr–TZC–Y, W/R	870°C, 2 hr	227	204	9	Fractured
Cr–TZC–Y, W/R	870°C, 10 hr	211	106	9	Fractured
Cr–TZC–Y, W/R	980°C, 2 hr	154	108	90	No fracture
Cr–TZC–Y, H/R	750°C, 2 hr	181	114	7	Fractured
Cr–TZC–Y, H/R	980°C, 3.5 hr	142	108	90	No fracture
Cr–V–Y, W/R	750°C, 2 hr	366	110	9	Fractured
Cr–V–Y, W/R	750°C, 2 hr	366	152	10	Fractured
Cr–V–Y, W/R	750°C, 2 hr	366	204	9	Fractured

*W/R, warm rolled from 850°C. H/R, hot rolled from 1100°C.

†For tests above room temperature, the specimens were heated in test position in a resistance furnace.

Niobium

Improvement in the properties of niobium and tantalum through alloying has been investigated by workers at the Bureau of Mines.[70] Resistivity measurements using standard techniques were made on tensile specimens in the as-worked and annealed condition at room temperature. As indicated in Table III-12, the small difference in resistivity of the samples in the as-worked and heat-treated conditions showed little evidence of a phase transformation. The Nb–90 at.% Zr alloy, however, showed considerable decrease in resistivity after annealing.

Table III-12 ELECTRICAL-RESISTIVITY DATA FOR NIOBIUM AND TANTALUM ALLOYS[70]

Alloy composition, at.%	Resistivity, 10^{-5} ohm-cm	
	As rolled	Annealed
Nb–33 Hf–10 W–10 Ti	6.72	6.86
Nb–33 Hf–5 Zr–5 W	5.95	6.06
Nb–33 Hf–10 Zr	6.12	6.27
Nb–70 Hf	7.83	7.99
Nb–80 Hf	7.34	7.19
Nb–10 Hf–5 Mo	2.82	2.84
Nb–20 Hf–5 Mo	3.97	3.98
Nb–30 Hf–5 Mo	5.12	5.23
Nb–5 V–5 Mo–1 Hf	1.98	1.96
Nb–20 Hf–10 V	4.83	4.85
Nb–70 Zr	8.02	8.03
Nb–80 Zr	8.63	8.82
Nb–90 Zr	10.85	7.46
Ta–70 Hf	5.42	4.98
Ta–70 Zr	4.21	3.95
Ta–82 Zr	4.79	4.65

Tensile data for these alloys are shown in Table III-13. The high-hafnium and -zirconium alloys were tested at 1000°C only because of testing-machine limitations. Strength data on unalloyed niobium are included for comparison purposes. Of the alloying elements studied, hafnium and tungsten appear to be the most effective strengtheners for niobium.

The influence of nitrogen on the properties of niobium has been studied at the Naval Research Laboratory.[71] The effect of nitrogen on mechanical properties at elevated temperatures was found to depend principally on phase structure and test temperature, i.e., whether the latter was below or above one-half the absolute melting temperature ($0.5T_m$). Nitrogen in solid solution increased the strength of niobium at temperatures below approximately one-half the melting temperature, but at higher temperatures it showed no significant effect. When the nitrogen concentration was such that the structure was two phase, then strength at all test temperatures increased with increasing nitrogen content. In the area near the boundary between the single-phase and two-phase regions, a sharp transition in the strength of the material generally occurred.

Tensile strength at 1900°F (1038°C), which is approximately one-half the melting temperature of niobium, was improved with increasing nitrogen content in both the single-phase and two-phase regions, as shown in Fig. III-19. At 2600°F (1427°C), solid-solution strengthening occurred only for amounts above 0.24% nitrogen.

Creep-rupture properties were affected by nitrogen in a consistent manner, the magnitude of the effect being dependent upon the test conditions. Nitrogen in solid solution increased rupture life at 1700°F (927°C); at 2300 and 2600°F (1260 and 1427°C), it had no distinct effect. At 1900°F (1038°C), which is approximately $0.5T_m$ of niobium, both effects were observed.

Nitrogen in solution had no significant influence on rupture life at 6300 psi, but at 6600 psi it markedly increased strength. The effect of nitrogen at the higher stress was the same as that below $0.5T_m$, whereas the effect at the lower stress corresponded to that above $0.5T_m$. When present in a two-phase structure, nitrogen in increasing amounts substantially improved rupture strength at all test temperatures.

When solid-solution strengthening occurred, as at 1700 and 1900°F, an abrupt reduction in rupture life took place in the region of the boundary between the single-phase and two-phase structures. Although the two-phase alloy in the region of the boundary showed a rupture life lower than that of the single-phase material, its strength nevertheless was higher than that of pure niobium.

Although there was no strongly discernible effect of nitrogen in solid solution at 2300 and 2600°F, the rupture life of the alloy nearest the phase boundary tended to be the lowest. The transition from a single-phase structure to a two-phase structure at these temperatures was marked by a substantial increase in rupture life, contrary to the accompanying decrease in rupture life at the phase boundary at the lower temperatures.

In both niobium and niobium alloys containing 19 to 33 wt.% zirconium, German investigators[72] noted an anomalous temperature dependence of Young's modulus after heavy cold deformation. The bulk modulus decreased initially and then increased sharply with increasing temperature. Annealing treatments at 600°C led to a transition to the normal behavior, which was due to recovery in the unalloyed niobium and to a decomposition of the beta phase in Nb–Zr alloys. Suitable heat-treatment of the alloys produced heterogeneous microstructures that exhibited areas of decomposition and areas with deformation and rolling texture in juxtaposition. Alloys treated in this way exhibited a large temperature range (approximately 0 to 200°C) with an anomalously small temperature dependence of Young's modulus. This effect was ascribed to a superposition of the

Table III-13 TENSILE PROPERTIES OF NIOBIUM AND TANTALUM ALLOYS AT ELEVATED TEMPERATURES[70]

Alloy composition, at.%	Test temp., °C	Annealing temp., °C	Tensile strength, 1000 psi	Yield strength, 1000 psi	Elongation, %
Nb–15 Hf–5 W	1000	1300	59.1	43.6	16
	1095	1300	57.0	44.8	9
	1200	1300	42.0	37.6	26
	1315	1300	35.2	34.6	7
	1480	1300	27.4	25.5	41
Nb–10 V–5 W	1095	1300	51.0	42.0	9
	1315	1300	28.4	28.1	16
	1480	1300	19.9	17.4	39
	1650	1300	13.9	12.3	
Nb–33 Hf	1000	1300	62.8	53.9	24
	1200	1300	44.2	43.7	47
Nb–15 Hf–5 W–10 Ti	1095	1300	50.0	46.0	4
	1315	1300	17.8	15.9	
	1480	1300	17.5	14.7	24
Nb–15 Hf–10 W–10 Ti	1095	1300	64.9	58.4	3
	1480	1300	23.8	22.0	0
Nb–20 Hf–5 W–10 Ti	1000	1300	61.4	55.4	11
	1200	1300	44.0	43.0	14
Nb–10 V	1095	1450	31.4	23.9	25
Ta–30 V	1000	1300	108.0	96.0	12
	1400	1300	23.0		25
Ta–20 Hf	1200	1300	52.7	47.7	3
	1400	1300	23.3	23.3	65
	1480	1300	23.9		147
100 Nb	1200		3.6		37
Nb–33 Hf–10 W–10 Ti	1200	1300	44.3	44.3	49
	1300	1300	23.6	22.3	60
	1400	1300	16.5	14.3	43
Nb–35 Hf–5 Zr–5 W	1200	1300	38.5	38.5	21
	1300	1300	25.4	25.1	30
	1400	1300	11.1	9.1	34
Nb–33 Hf–10 Zr	1200	1300	31.5	30.8	33
	1400	1300	8.8	8.5	67
Nb–70 Hf	1000	1000	9.3	9.3	
	1200	1000	4.4	4.1	19
Nb–80 Hf	1000	1000	3.9		
Nb–10 Hf–5 Mo	1200	1300	31.0	25.5	39
	1300	1300	22.6	19.6	11
	1400	1300	19.3	19.2	41
Nb–20 Hf–5 Mo	1200	1300	35.7	33.2	8
	1300	1300	25.6	25.4	7
	1400	1300	20.7	19.8	65
Nb–30 Hf–5 Mo	1200	1300	38.9	38.9	10
	1300	1300	29.9	29.9	63
	1400	1300	17.8	16.1	61
Nb–5 V–5 Mo–1 Hf	1200	1300	26.2	22.1	32
	1400	1300	14.3	13.4	34
Nb–20 Hf–10 V	1200	1300	24.7	21.8	1
	1400	1300	10.8	10.5	41
Nb–70 Zr	1000	1000	17.5	15.2	
Nb–80 Zr	1000	1000	6.8	5.8	74
Nb–90 Zr	1000	1000	9.2	8.4	47

positive values of the temperature coefficient in the deformed areas and the negative values in the decomposed areas.

It was shown that the anomalous effect after heavy cold deformation was independent of the rolling texture present and of the effect arising from the recrystallization texture. The reason for the anomaly after heavy cold deformation was thought to be the very high dislocation densities in niobium and Nb–Zr alloys and the temperature-dependent interactions between dislocations and impurity atoms.

The effects of impurity content, structural state, and deformation rate on the mechanical properties of Nb, Ta, Mo, and W were investigated by the Russians.[73] At temperatures less than $0.2T_m$, molybdenum and tungsten had higher transition temperatures than

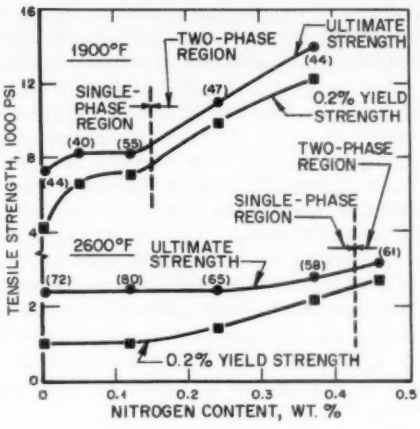

Fig. III-19 Influence of nitrogen on the tensile strength of niobium at 1900°F (1038°C) and 2600°F (1472°C) (Ref. 71). Numbers in parentheses are elongation-at-fracture values.

did niobium and tantalum. An increase in deformation rate increased this transition temperature more for molybdenum and tungsten than for niobium and tantalum. The transition from the intermediate-temperature (0.2 to $0.5T_m$) region to the high-temperature region ($>0.5T_m$) was determined empirically by the deformation rate as follows: $T_{tr} = (0.57 + 0.03 \log \dot{\epsilon})\ T_m$. Here T_{tr} is the transition temperature, $\dot{\epsilon}$ is the deformation rate in sec^{-1}, and T_m is the melting temperature. Impurity content and structural state had essentially no effect on the transition temperature. At temperatures above $0.5T_m$, the strength properties did not depend on the nature of the metal, impurity content, or initial structure. The strength of various metals as a function of temperature was given by the general equation: $\sigma = a' \exp(-m'T/T_m)$. Here a' and m' are coefficients depending on the method of testing and the rate of deformation.

Molybdenum

The fatigue curves for a TZC molybdenum alloy at 1800, 2000, and 2200° F (982, 1093, and 1204°C) for both notched and smooth specimens are presented in Fig. III-20 (Ref. 74). A well-defined endurance limit was not present at any of the test temperatures. At 2200° F and an A ratio (peak-to-mean stress) of approximately ∞, a fatigue strength as low as 16,000 psi was observed at 10^9 cycles. The fatigue strength–tensile strength ratios for the alloy are shown in Table III-14 for each of the test temperatures. The ratios are considerably lower than the 0.5 to 0.4 usually observed in materials such as steels which possess a well-defined endurance limit or the 0.7 value obtained for molybdenum when tested below 875° F (468°C), where dislocation locking can occur. At the lower A ratios, the specimens tested at 2000 and 2200° F (1093 and 1204°C) exhibited comparable fatigue behavior; the strength at 1800° F (982°C) was significantly greater when the data were plotted in a modified Goodman diagram.

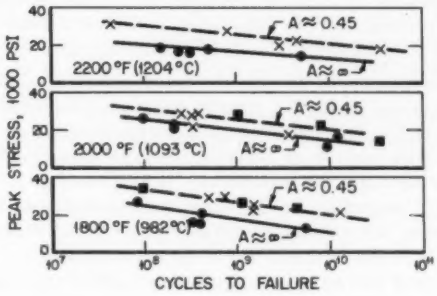

Fig. III-20 Fatigue data for TZC alloy recrystallized at 3092°F (1700°C) and tested at ~20 kHz in vacuum environment of $< 1 \times 10^{-7}$ torr.[74] ×, smooth specimens ($A \approx 0.45$); ■, notch specimens ($A \approx 0.45$); ●, notch specimens ($A \approx \infty$).

Russian investigators[75] have studied the properties of polycrystalline unalloyed molybdenum produced by electron-beam fusion without the use of deoxidizers. The Rockwell hardness was found to be 153 for the cast material, 167 after cold working, and 154 kg/mm² after recrystallization. The corresponding microhardness values were 204, 215, and 203 kg/mm², respectively. The electrical resistance was 0.0557 ohm-mm²/m for recrystallized molybdenum. The elastic modulus was 31,180 for the cold-worked material and 33,170 kg/mm² for the recrystallized material. The shear moduli for these materials were 12,340 and 12,475 kg/mm², respectively. With molybdenum deformed at a rate of 3 mm/min, the strength decreased with an increase in annealing temperature. A maximum of 16.4% relative elongation was obtained at an annealing temperature of 800°C.

Molybdenum foil containing 0.5 wt.% titanium and subjected to 80% deformation was examined by X-ray diffraction analysis by the Russians.[76] The texture of the deformed foil was chiefly described by the orientation (1 0 0) [0 1 1] as well as (1 1 2) [1 1 0], with rotation through 4 to 6° with respect to the direction of

Table III-14 RATIO OF FATIGUE-TO-TENSILE STRENGTH FOR A TZC MOLYBDENUM ALLOY*[74]

Test temp.		Tensile strength		Fatigue strength at 10^9 cycles		Ratio of fatigue-to-tensile strength
°F	°C	1000 psi	N/m²	1000 psi	N/m²	
1800	982	63.0	4.34×10^8	18	1.24×10^8	0.29
2000	1093	60.8	4.19×10^8	17	1.17×10^8	0.28
2200	1204	54.2	3.71×10^8	16	1.10×10^8	0.30

*Tested in vacuum of 1×10^{-7} torr, $A \approx \infty$, 20,000 cps.

rolling. The temperature dependence of the growth rate of nuclei of primary recrystallization was investigated at 1050 to 1150°C. Subsequent annealing of the recrystallized foil at >2000°C led to continued recrystallization and gradual enlargement of grains. The texture of primary recrystallization was described by the same orientations as for the deformation texture and was obtained by a similar rotation of 12 to 15° relative to the direction of rolling.

The kinetics of the formation and growth of anomalous grains in the foil greatly resembled the kinetics of primary recrystallization in polycrystalline material. The texture of secondary recrystallization was described by the orientation (1 0 0) [0 0 1] or (1 1 0) [0 0 1], depending on the annealing atmosphere. The shape of the anomalous grains was evidently associated with the original metallographic texture of the deformed foil and with the characteristic distribution of impurities along the boundaries of the extended grains, and thus grain growth in the direction perpendicular to the direction of rolling was impeded. In thicker specimens that had not been subjected to prior deformation by rolling, the shape of anomalous grains was equiaxed.

On the basis of X-ray and microstructural analyses and measurements of the hardness of alloys after quenching from the equilibrium state at 750 and 600°C, isothermal sections of the Mo–Ti–Zr phase diagram were constructed by Russian workers.[77] A sizable region of beta solid solution, extending continuously from the Mo–Ti binary system to the Ti–Zr binary system and bounded by a heterogeneous region on the Mo–Zr side, was found in the section at 600°C. The heterogeneous region occupied a small part of the concentration triangle and protruded toward the titanium corner. Decomposition of the beta solid solution into two solid solutions occurred at an equiatomic content of molybdenum in zirconium and 61 at.% titanium. Two three-phase regions, $\beta_1 + \beta_2 + \delta$ and $\alpha + \beta_2 + \delta$, existed inside the heterogeneous region. The δ phase extended up to 13 at.% titanium at 33.3 at.% zirconium in the ternary system, and no appreciable solubility was noted in this phase. The isothermal section at 750°C was similar to the section at 600°C, but the region of the beta solid solution increased considerably, both at the expense of the heterogeneous region (on the side of the Mo–Zr system) and at the expense of the two-phase $\alpha + \beta$ regions adjacent to the titanium and zirconium corners of the section. Decomposition of the beta solid solution occurred at 57 at.% titanium and 19 at.% zirconium. At 750°C the δ-phase region was represented as a line (as it was at 600°C) and existed in this section up to 15 at.% titanium at 33.3 at.% zirconium.

Eleven sections of the ternary phase diagram of the Mo–Ti–Zr system were plotted by Russian investigators.[78] The phase boundaries were determined with homogenized alloys quenched from 600 to 1200°C, annealed at 1400°C, and furnace cooled. In all the isothermal sections, β_1 and β_2 solid solutions were found on the molybdenum and zirconium bases, respectively. The critical temperature for the saturated solid solution (27.5 at.% titanium and 37.5 at.% zirconium) was 1620 ± 25°C. At 1575 ± 10°C a peritectic-type compound and delta phase formed. At 600°C the homogeneous area of β^s solid solution extended from the molybdenum corner to the zirconium corner, and separate α^s and β^s phases, adjacent to the titanium corner, extended from the Mo–Zr side. The same area of α^s phase in the titanium and zirconium corners propagated in the range 0.2 to 0.3 at.% molybdenum. The δ^s phase was observed in an alloy with 13 at.% titanium and 33.3 at.% zirconium. The solubility of titanium and zirconium in molybdenum changed significantly with temperature.

To increase the oxidation resistance of molybdenum at high temperatures in air, the Japanese developed a coating method.[79] Commercially pure molybdenum rods were coated by casting with a Nimonic 90 nickel-base alloy that is hot workable and oxidation resistant. After the composite cast materials were hot swaged, they were creep-rupture tested at 1000°C with a stress of 5 to 10 kg/mm² in air. It was possible to work the hard and brittle diffusion zone formed in the interface between molybdenum and the covering alloy without cracking. The creep-rupture strength of the composite cast materials at 1000°C in air was improved as the relative amount of the molybdenum core was increased. It was demonstrated that the new coating method using the Nimonic 90 alloy protected molybdenum from oxidation in air at elevated temperatures.

Tantalum

Russian workers[80] investigated the effect of oxygen on recrystallization temperature of high-purity tantalum. Electron-beam-melted ingots of 99.362%-pure tantalum containing 0.0007 wt.% oxygen were cold forged and rolled into 1.0 mm-thick sheets, after which the oxygen content was increased to 0.1 wt.%. Annealing in air at 500°C for 5 or 10 hr, followed by homogenizing at 1200°C in a vacuum, increased the oxygen content to 0.4 or 0.7 wt.%, respectively, which was below the limit of solubility in tantalum at 20°C. The sheets were then cold rolled with a reduction of 59% and vacuum annealed at 800 to 2000°C for 1 hr. The recrystallization temperature of both materials, as determined by X-ray diffraction analysis and by hardness measurements, was 1200°C regardless of the oxygen content. Annealing at temperatures above 1200°C and below 1600°C brought about no noticeable changes in hardness. However, annealing at 1800°C lowered the hardness in direct proportion to the initial oxygen content to roughly the same value. Thus, after annealing at 1800°C, both the low- and high-oxygen-content materials had the same microhardness and

also the same lattice parameters. This effect indicated that the embrittlement of recrystallized Ta, Mo, W, and Cr is due to interstitial, not substitutional, elements.

Vanadium

Preliminary tube-burst tests on a V–15 wt.% Ti–7.5 wt.% Cr alloy were performed by Argonne.[31] The tubes were irradiated to a maximum fluence of 6×10^{21} neutrons/cm^2 at a temperature of 600 to 650°C. The results for the alloy, both irradiated and unirradiated, are shown in Table III-15. At 550°C the maximum increase in burst strength was 27%, at 650°C it was 13%, and at 750°C (one specimen) there was no increase in strength due to the irradiation. At both 650 and 750°C, the unirradiated specimens showed about twice the ductility of the irradiated samples. Presumably the shattered unirradiated specimens tested at 550°C had negligible ductility. One specimen tested at 650°C split open along its entire length.

Table III-15 BURST STRENGTH AND DUCTILITY OF V–15 WT.% Ti–7.5 WT.% Cr TUBING[31]

Test temp., °C	Specimen location*	Max. tangential stress, 1000 psi	Max. tangential stress, kg/mm^2	Diameter change, %$\Delta D/D$, Range	Diameter change, %$\Delta D/D$, Av.	Time at test temp., min
550	Unirradiated	100.1	70.4	†	†	60
	Unirradiated	101.3	71.3	†	†	60
	–10 to –20 cm	113.8	80.0	0.8–2.3	1.4	130
	0 to –10 cm	128.0	90.0	1.8–2.4	2.0	90
	+50 to + 60 cm	110.5	77.7	2.2–3.6	2.8	30
650	Unirradiated	97.8	68.8	7.4–8.8	8.1	45
	–10 to –20 cm	111.0	78.1	2.6–3.2	2.9	35
	0 to –10 cm	112.0	78.8	1.2–1.7	1.4	120
	+50 to +60 cm	88.0	61.9	†	†	60
750	Unirradiated	90.2	63.4	6.9–8.6	7.8	60
	+50 to +60 cm	89.3	62.8	2.2–6.8	3.7	95

*Specimen location above or below reactor midplane in centimeters.
†Shattered or split so that no diameter measurements were possible.

The French[81] have conducted preliminary research on a series of vanadium-base alloys for use as canning material in fast reactors. The alloys included (wt.%) V–5 Cr, V–5 Mo, V–0.5 Si, V–5 Nb, V–2 Zr, V–20 Ti, V–10 Al, V–10 Sn, and V–10 Ti. Transformation by forging at about 1000°C and rolling between 200°C and room temperature was satisfactory for all types of alloys except V–10 wt.% Sn and V–10 wt.% Al. Tensile strength on alloy samples annealed 1 hr at 1050°C in a vacuum showed that, in general, the addition elements led to an improvement in mechanical properties.

The room-temperature tensile properties for a number of vanadium-base alloys were determined. Large increases in strength were achieved, as shown in Table III-16 (Ref. 81).

Several vanadium-base alloys intended for possible application as fuel cladding in liquid-metal-cooled fast breeder reactors were investigated by Westinghouse.[82] The effects of compositional variations on mechanical properties of vanadium were emphasized, particularly the creep properties at 700 and 800°C. Limited investigations on the effects of heat-treatment on mechanical properties were also carried out. The mechanical properties of these materials are summarized in Table III-17, along with data for several stainless steels. It can be seen that the 0.2% offset yield strength of the vanadium alloys at both room and elevated temperatures is, in general, much higher. The ultimate strength is comparable, if not better, and the ductility of the vanadium alloys, although

Table III-16 MECHANICAL CHARACTERISTICS OF VANADIUM ALLOYS BEFORE SODIUM CORROSION[81]

(Tensile Tested in Air at Room Temperature)

Alloy, wt.%	Top yield point, kg/mm^2	Lower yield point, kg/mm^2	Breaking stress, kg/mm^2	Elongation, % Total	Elongation, % Uniform
Unalloyed vanadium	27.62	25.50	34.8	30.3	17.1
V–5 Mo	52.8	50.3	59.1	24.9	14.6
V–20 Ti	62.7	61.00	68.2	26.3	16.5
V–5 Nb	46.6	46.2	55.0	23	14
V–10 Al	77.5			15.4	
V–5 Cr	49	46.4	55.4	28.4	16.7
V–0.5 Si	46.6	43.2	51.6	24.5	14.6
V–2 Zr			30.2	27.2	16.4

Table III-17 MECHANICAL PROPERTIES OF VANADIUM ALLOYS[82]

Composition, wt.%	Test temp., °C	0.2% offset yield strength, 1000 psi	Ultimate strength, 1000 psi	Elongation in 2 in., %	Minimum creep rate, %/hr, for stress indicated	
					30,000 psi	10,000 psi
V–10 Ti*	RT	56.6	72.2	32.5		
	700	36.8	68.1	24	0.006	
	800	29.5	52.4	33		0.18
V–20 Ti†	RT	83.1	100.2	27		
	700	61.3	87.0	21	0.09	
	800	48.4	62.0	20		0.09
V–15 Ti–7.5 Cr‡	RT	92.4	106.6	29		
	700	54.0	79.6		0.0027	
	800	41.2	56.9	50		
V–9.1 Cr–3.3 Fe–1.3 Zr–0.05 C (HSV 27)	RT	50.9	75.1	32		
	700	28.1	56.2	22	0.0031	
	800	24.9	45.2	28		0.0017
V–6.4 Fe–5.3 Cb–1.3 Zr–0.05 C (HSV 41)	RT					
	700				0.0008	
	800					0.0002
V–8.49 Cr–9.85 Ta–1.24 Zr–0.05 C (HSV 29)	RT	53.4	77.6	31		
	700				0.002	
	800	30.5	56.5	24		0.0011
AISI 304	RT	33.0	83.0	64		
	700	14.0	34.5	35	65.0	
	800	10.6	20.0	37.5		2.16
AISI 316	RT	35.0	80.0	65		
	700	19.0	50.3	42.8	0.154§	
	800	16.6	31.5	42		0.0892¶

*Material annealed at 900°C for 1 hr prior to test; tensile-test-chamber vacuum, 6×10^{-7} torr.
†Material annealed at 1200°C for 1 hr prior to test; tensile-test-chamber vacuum, 6×10^{-7} torr.
‡Material annealed at 850°C for 1 hr prior to test; tensile-test-chamber vacuum, 6×10^{-7} torr.
§Stress level, 24,000 psi.
¶Stress level, 9000 psi.

lower than that of the stainless steels, is more than adequate for ease of fabrication. Creep properties were compared using minimum creep rates at stress levels of 30,000 and 10,000 psi for temperatures of 700 and 800°C. It is clear from the results that the minimum creep rates, particularly for the alloys, were several orders of magnitude lower than those for the 304 and 316 stainless steels under the same conditions. (J. A. DeMastry)

Metallurgy of Common Cladding and Structural Materials

Zirconium and Zirconium Alloys

Grain-growth phenomena in recrystallized zirconium were studied by using industrially pure Kroll and very-high-purity van Arkel zirconium.[83a] Topological relations of the metal remained unaltered during annealing treatments despite changes in the structure. The mean diameter of the crystals increased linearly as a function of the number of their sides. The crystals were most frequently hexagonal in form. In addition, an equilibrium relation was observed between the frequency of crystals with more than six sides and that of crystals with less than six sides. From a statistical point of view, the distribution of the grains as a function of their mean diameter approximated the log-normal law when the grains were divided into categories that represented a geometric progression. From the isothermal annealing study, grain growth was described by the relation:

$$D^2 - D_0^2 = Kt^n$$

where D = final grain size
D_0 = original grain size
t = annealing time
K,n = constants

The value of n was found to be 0.25, which was considerably lower than the theoretical value of 0.5.

The recrystallization behavior of high-purity zirconium prepared by zone melting crystal-bar material 10 times in ultrahigh static vacuum was also examined.[83b] Purified zirconium recrystallized at 170°C, as opposed to the starting metal that recrystallizes at 295°C, and exhibited a resistivity ratio of 36×10^{-4}. A determination of the preferential orientation of zone-melted zirconium sheets in the cold-worked state (reduction ratio of 98%) and after annealing at increasing temperatures showed that recrystallization occurs without texture modification. The pole-figure diagrams in both the initial state of the sheet and after annealing at 200°C are the same. Texture modifica-

tion accordingly does not occur during recrystallization, but during grain growth.

Numerous patents have been issued for zirconium alloys that possess corrosion resistance and creep strength superior to those of Zircaloy-2 in superheat environments in the 400 to 600°C temperature range. The compositions of these new zirconium alloys are as follows: Zr–0.5 wt.% Nb–0.02 to 0.5 wt.% Ce or Y (Ref. 84), Zr–0.5 to 3.0 wt.% V–0.5 to 3.0 wt.% Cu (Ref. 85), and Zr–0.5 wt.% Nb–0.2 wt.% Ca (Ref. 86).

The specific heats of Zircaloy-2 and low-nickel Zircaloy-2 have been determined at temperatures from 0 to 1050°C (Ref. 87). The specific-heat values, shown in Fig. III-21, illustrate that no difference exists between the two Zircaloys. The heat of transformation for both alloys was found to be 10.6 cal/g for the alpha–beta transformation. It has been found that the terminal solid solubilities of hydrogen in Zircaloy-2 and Zircaloy-4 are identical up to 550°C (Ref. 88). These solubilities were determined by a diffusion-sample method. The solubilities of hydrogen

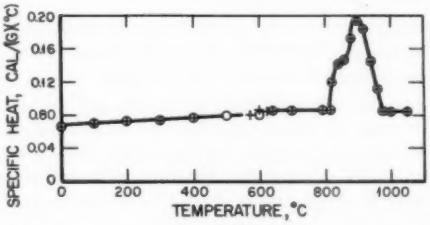

Fig. III-21 Interpolated instantaneous specific heat of Zircaloy-2 and low-nickel Zircaloy-2 (Ref. 87). ○, Zircaloy-2; +, low-nickel Zircaloy-2.

in both sponge and iodide zirconium are close to those of the Zircaloys and are represented by the same curve in Fig. III-22. Grain-size variations were found to have no effect on this solubility, and the effects of residual cold work on hydrogen solubility were minor. The terminal solid solubility of hydrogen in Zircaloy-2 and Zr–2.5 wt.% Nb was also determined by thermal-diffusion techniques.[89] The results showed that the solubility of hydrogen was identical in both alloys and were in excellent agreement with the results of Kearns.[7] It was further noted that the hydrogen solubility was not affected by heating into the alpha + beta phase.

For a texture in which the majority of the grains in Zircaloy tubing are oriented in the axial direction, either cold drawing or tube reducing can be used.[90] If tubing is required wherein the majority of the grains are oriented perpendicular to the tube axis, then shear forming or tube reducing must be employed. This can also be accomplished by making the tube undersize and then expanding it by pulling a plug through the inside. The strength and ductility proper-

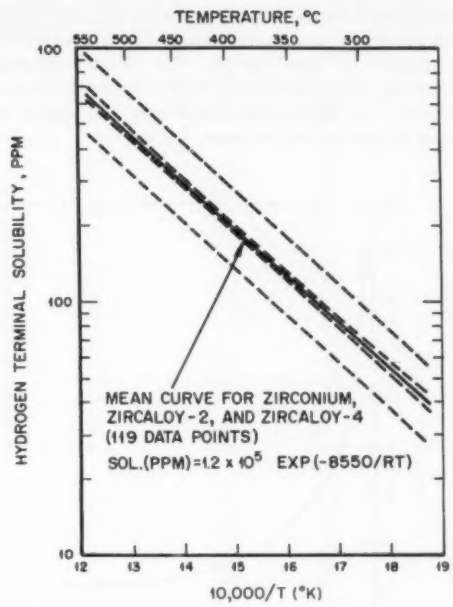

Fig. III-22 Combined data for zirconium; Zircaloy-2, and Zircaloy-4. Inner and outer dashed lines represent, respectively, the 95% confidence band on the mean and the 95 to 99% tolerance band.[88]

ties of Zircaloy-2 tubing were found to depend mostly on residual cold work.[91] The anisotropy in mechanical properties and deformation behavior in highly textured Zircaloy-2 can be predicted by using the known slip and twinning modes. It was further noted that the yield strength of Zircaloy-2, in tube-burst tests, could be predicted from axial tensile tests and Knoop hardness measurements. The tubes with the best overall mechanical properties were those which had only radial basal poles.

Twelve $3\frac{1}{4}$-in.-ID cold-worked Zr–2.5 wt.% Nb pressure tubes were evaluated by mechanical testing and metallographic examination.[92] Tubes made by extrusion and cold drawing (~22% reduced) were found to be stronger than tubes that were annealed between extrusion and drawing. The ultimate tensile strength of the strongest tubes exceeded 70,000 psi at 300°C. Generally the back ends of tubes were stronger than front ends, and the transverse strengths were higher than in the longitudinal direction. These mechanical properties correlated well with the textures resulting from the fabrication. A postfabrication anneal at 400°C for 72 hr had little effect on the ultimate strength of the strongest tubes, but the 0.2% yield strength decreased by up to 24%. Annealing at 500°C for 10 hr weakened all tubes.

The plane-strain fracture toughness (K_{Ic}) of Zircaloy-4 as a function of hydrogen content has been

determined.[93] In the determination of K_{Ic}, single-edge notch sheet specimens were used, and the test results are shown in Fig. III-23. The K_{Ic} is decreased drastically with increasing hydrogen contents up to 400 ppm. No subsequent decreases take place with further increases in hydrogen content.

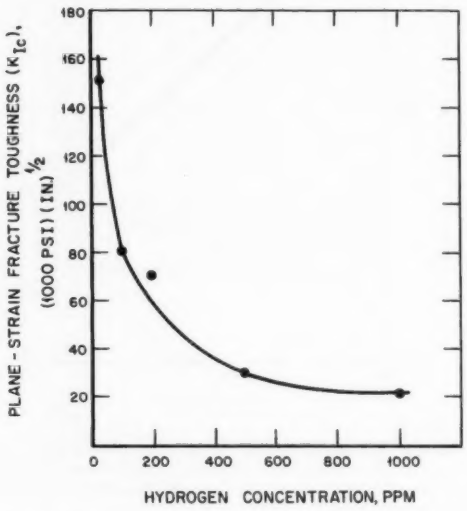

Fig. III-23 The effect of hydrogen on the plane-strain fracture toughness (K_{Ic}) of Zircaloy-4 (Ref. 93).

Workers at Chalk River[94] have been studying fabrication techniques and corresponding properties of Zr–Y_2O_3 dispersions to develop improved stress-rupture properties. The best properties were achieved with a 5 vol.% dispersion of fused, crushed, and sized (<0.5 μm) Y_2O_3 particles. These dispersions were subjected to a double fabrication cycle with an intermediate rehydriding step. The rupture time and minimum creep rate of this material at 500°C were improved by a factor of about 10 over the corresponding properties of sintered zirconium. This improvement was attributed to the stabilization effects of particles on the grain structure. No strength contribution from direct dislocation–particle-interaction was detectable.

Stainless Steels and Nickel Alloys

The fracture of ductile austenitic stainless steel in the temperature range 20 to 700°C is attributed to the carbide particles.[95] These carbide particles in the stainless steel fracture after about 5 to 10% tensile strain owing to concentrated local stresses from matrix slip lines. With further strain the voids formed from the fractured carbide particles link up and cause fracture. This theory was substantiated by showing that fracture occurred after less strain in stainless steel containing carbide particles than in comparison specimens where most of the carbon was in solution.

Additions of 0.15 wt.% titanium to 304 stainless steel were found to cause significant decreases in creep rates in the temperature range 704 to 816°C (Ref. 96). The fracture mode for the titanium-modified 304 stainless steel was a mixture of transgranular and intergranular fracture, whereas the commercial 304 stainless steel failed completely by intergranular fracture. Aging of the titanium-modified stainless steel at 600 and 700°C resulted in large increases in creep rates at 704 and 816°C. Aging at similar temperatures had only minor effects on the creep rate of the commercial steel at test temperatures of 704 and 816°C. The behavior of these materials was explained in terms of the fine TiC particles throughout the matrix, which impede dislocation movement and thus cause lower creep rates in the modified steel. Aging at 600°C and especially at 700°C caused the agglomeration of these fine TiC particles, and consequently the creep rate was increased.

Fatigue tests at 650 and 816°C have been performed on 304 and 348 stainless-steel specimens.[60c] Results of these fatigue tests are given in Table III-18.

It has been established by X-ray diffraction that sigma phase can be precipitated in solid-solution Ni–Fe–Mo alloys (Hastelloy X) by aging at 1300 to 1450°F (704 to 788°C) (Ref. 97). Previously it was believed that sigma formation occurred in only precipitation-hardened Ni–Fe–Mo alloys and that the precipitation of sigma phase had to be preceded by precipitation of the gamma prime or eta phase. Room-temperature tensile tests were performed on sheet specimens of Hastelloy X aged in air at 2000°F (1093°C) for times up to 7500 hr. It was found that the yield and ultimate strengths were decreased after 2500 hr. The ultimate strength was reduced from 110,000 to 120,000 to 80,000 psi, and the yield strength was reduced from 60,000 to 75,000 to 35,000 psi. Further annealing resulted in minor changes in the ultimate strength, but the yield strength was not affected. The specimens reached a ductility maximum after 100 hr of annealing, which was followed by a ductility minimum after 1000 hr. The ductility then gradually increased and started decreasing again after 2500 hr. The room-temperature ductility was reduced from an original value of about 40% to 12 to 25% after 7500 hr in air.

A comparison of bending and tension creep on Hastelloy X at 1800°F (982°C) is presented in Fig. III-24 (Ref. 97). The bending creep curve exhibits a very short primary stage compared with the tensile creep curve. Removal of several mils from the outer surface was found to significantly improve the tensile creep performance.

The development of Hastelloy N as a structural material in the Molten Salt Breeder Reactor has been

Table III-18 PRELIMINARY TEST RESULTS PERTAINING TO EFFECT OF STRAIN RATE ON FATIGUE LIFE OF ANNEALED 348 AND 304 STAINLESS STEELS AT 650 AND 816°C*[60c]

Test identification		Axial strain		Diametral strain		Cyclic rate	Fatigue life	
Material	Test temp., °C	Strain range ($\Delta\epsilon$), %	Strain rate ($\dot{\epsilon}$), sec^{-1}	Strain range ($\Delta\epsilon_d$), %	Strain rate ($\dot{\epsilon}_d$), sec^{-1}	Frequency of loading (f), cycles/sec	Cycles to 5% load reduction point (N_5)	Cycles to fracture (N_f)
348	816	2.04	4.1×10^{-5}	1.01	2.0×10^{-5}	0.001	118	183
		2.06	4.1×10^{-5}	1.00	2.0×10^{-5}	0.001	122	233
		2.11	4.2×10^{-4}	1.01	2.0×10^{-4}	0.01	158	220
		2.08	4.2×10^{-4}	1.00	2.0×10^{-4}	0.01	176	315
		2.11	4.2×10^{-3}	1.00	2.0×10^{-3}	0.1	266	317
		2.09	4.2×10^{-3}	1.00	2.0×10^{-3}	0.1	245	326
		1.08	4.3×10^{-5}	0.50	2.0×10^{-5}	0.002	385	586
		1.07	4.3×10^{-5}	0.50	2.0×10^{-5}	0.002	439	582
		1.09	4.4×10^{-4}	0.50	2.0×10^{-4}	0.02	595	681
		1.09	4.4×10^{-4}	0.50	2.0×10^{-4}	0.02	462	729
		1.11	4.4×10^{-3}	0.50	2.0×10^{-3}	0.2	746	1170
		1.11	4.3×10^{-3}	0.50	2.0×10^{-3}	0.2	682	949
		0.55	4.4×10^{-5}	0.25	2.0×10^{-5}	0.004	1554	1862
		0.56	4.5×10^{-5}	0.25	2.0×10^{-5}	0.004	1613	1892
		0.57	4.6×10^{-4}	0.25	2.0×10^{-4}	0.04	1874	2465
		0.58	4.6×10^{-4}	0.25	2.0×10^{-4}	0.04	2718	3160
		0.57	4.6×10^{-3}	0.25	2.0×10^{-3}	0.4	3379	4281
		0.57	4.6×10^{-3}	0.25	2.0×10^{-3}	0.4	4656	4896
	650	2.17	4.3×10^{-5}	1.01	2.0×10^{-5}	0.001	193	217
		2.17	4.3×10^{-5}	1.01	2.0×10^{-5}	0.001	177	208
		2.18	4.4×10^{-4}	1.01	2.0×10^{-4}	0.01	335	370
		2.18	4.4×10^{-4}	1.01	2.0×10^{-4}	0.01	320	329
		2.16	4.3×10^{-3}	1.00	2.0×10^{-3}	0.1	471	550
		2.19	4.4×10^{-3}	1.01	2.0×10^{-3}	0.1	585	596
		1.13	4.5×10^{-5}	0.50	2.0×10^{-5}	0.002	760	871
		1.13	4.5×10^{-5}	0.50	2.0×10^{-5}	0.002	680	950
		1.12	4.5×10^{-4}	0.50	2.0×10^{-4}	0.02	989	1259
		1.13	4.5×10^{-4}	0.50	2.0×10^{-4}	0.02	1133	1360
		1.13	4.5×10^{-3}	0.50	2.0×10^{-3}	0.2	2412	2635
		1.15	4.6×10^{-3}	0.50	2.0×10^{-3}	0.2	2607	2685
304	816	2.07	4.1×10^{-5}	1.00	2.0×10^{-5}	0.001	80	130
		2.07	4.1×10^{-4}	1.00	2.0×10^{-4}	0.01	117	145
		2.08	4.2×10^{-3}	1.00	2.0×10^{-3}	0.1	226	260
		1.05	4.2×10^{-5}	0.50	2.0×10^{-5}	0.002	204	307
		1.07	4.3×10^{-4}	0.50	2.0×10^{-4}	0.02	379	429
		1.07	4.3×10^{-3}	0.50	2.0×10^{-3}	0.2	529	784
		0.53	4.2×10^{-5}	0.25	2.0×10^{-5}	0.004	591	788
		0.54	4.3×10^{-4}	0.25	2.0×10^{-4}	0.04	1055	1338
		0.56	4.5×10^{-3}	0.25	2.0×10^{-3}	0.4	2346	2477

*Control mode: diametral strain.
Cyclic mode: triangular with zero mean strain.
Heat numbers: 55700 (348) 55697 (304).
Specimen: Push-pull type, hourglass gauge section, longitudinal surface finish.

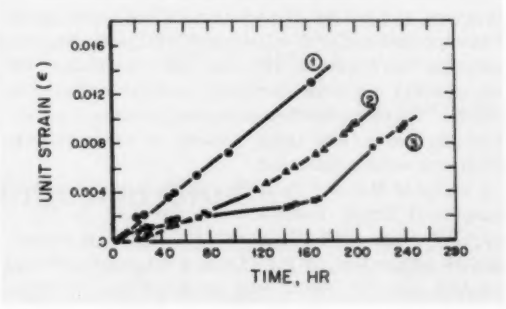

Fig. III-24 Comparison of strain vs. time for Hastelloy X subjected to bending and tensile creep at $\sigma_c = 1165$ psi (Ref. 97). A, bending creep, surface removed, as-received, T = 1800°F; B, tensile creep, surface removed, as-received, T = 1814°F; C, tensile creep, surface not removed, as-received, T = 1814°F.

reviewed.[14] The areas covered are general properties, mechanical properties, effects of irradiation on mechanical properties, corrosion by molten salts and gaseous environments, welding, and remote fabrication. The effect of strain rate on the total elongation of Hastelloy N at elevated temperatures is illustrated in Fig. III-25 (Ref. 43*c*). It is apparent that the elongation does not depend on the strain rate at 400, 500, and 760°C. Dependence of elongation on strain rate occurs in tensile tests at 650°C and to a slight degree at 850°C.

In TD nickel (Ni – 2 vol.% ThO_2), detachment of ThO_2 particles from the matrix is difficult to initiate during fatigue and tensile tests at room temperature.[98] Although some softening occurred during fatigue testing, the microstructure was found to remain relatively stable. TD nickel has a tendency to fail by shear fracture in either tension or fatigue.

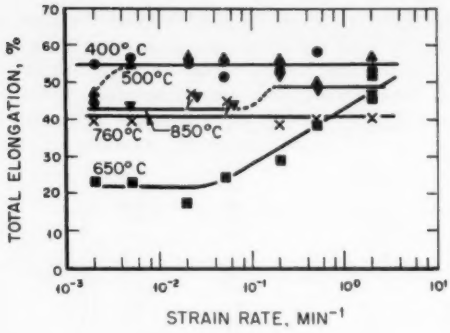

Fig. III-25 Influence of strain rate on the ductility of MSRE surveillance control specimens made of Hastelloy N (Ref. 43c). Test temperature: ●, 400°C; ▲, 500°C; ■, 650°C; ×, 760°C; ▼, 850°C.

Pressure-Vessel Steels

A joint ASTM–ASME symposium on the elevated-temperature mechanical properties of pressure-vessel alloy steels was held at New Orleans in September 1966 (Ref. 99). The symposium was especially directed toward properties of thick sections of alloy steels at elevated temperatures. The steels discussed at the meeting included the following (wt.%): 2.25 Cr–1 Mo, 0.5 Mo–B, 3.5 Ni–1.5 Cr–0.3 Mo–0.1 V, and SSS-100. The stress-rupture strength of silicon–aluminum deoxidized 1 Cr–0.5 Mo steel has been determined at 1000° F (538° C) for possible application as a pressure-vessel steel for the EBOR (Ref. 100). These stress-rupture properties at 1000° F are illustrated in Fig. III-26.

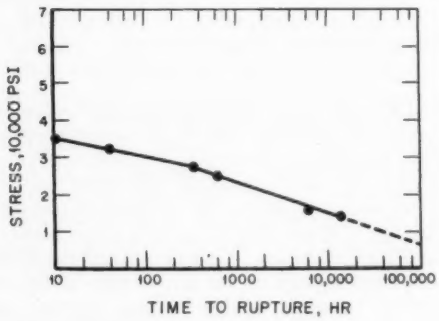

Fig. III-26 Stress rupture characteristics of 1 Cr–0.5 Mo steel at 1000°F (Ref. 100).

Additions of Ce, La, Pr, and Nd to ferritic steels have been found to restrain grain growth during annealing.[101] Figure III-27 illustrates the effect of various rare-earth-metal additions on the grain size as a function of annealing temperature.

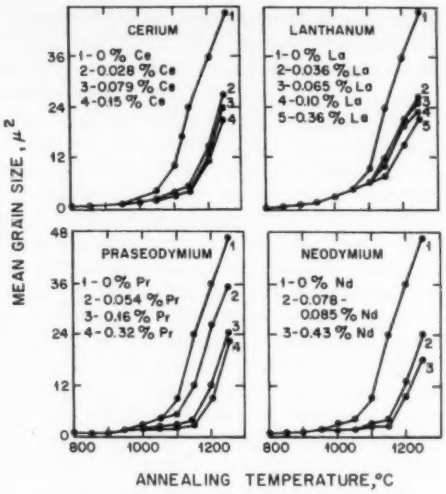

Fig. III-27 Influence of rare-earth additions and annealing temperature on the grain size of ferritic steel.[101]

Miscellaneous Alloys

Electron fractography was performed on SAP alloys (aluminum containing 6 to 8 wt.% Al_2O_3) which had been tensile tested at –200 to 450° C or creep tested at 450° C (Ref. 102). In all cases the failure occurs by a ductile fracture mode. The high-temperature fracture was usually initiated at a single oxide particle by initial separation and propagation by tearing, followed by shear to the specimen surface. The low-temperature fractures were predominantly of the shear type. Oxide banding and stringering resulted in reduced ductility at high temperatures. The mechanical properties of blended and ball-milled Al_2O_3 - Al alloys were found to be better than those of the commercial SAP alloys.[103] The improved mechanical properties were attributed to a more uniform microstructure and better distribution of the oxide phase. In the blended and ball-milled material, the aluminum particles were coated with the Al_2O_3 particles, and subsequently the oxide particles were embedded in the matrix. These embedded particles produced severe work hardening, and large pockets of oxide between the grains were eliminated.

A sintered Mg–0.5 wt.% Zr alloy has demonstrated exceptional creep resistance in the 400 to 450° C range.[104] Figure III-28 shows the relative stress-rupture properties of the cast and extruded material and the material which was sintered and extruded. The better stress-rupture performance of the sintered alloy was attributed to the presence of MgO particles at the grain boundaries. These particles reduced the grain-boundary migration processes and thus restricted both intergranular slide and intergranular shear mechanisms.

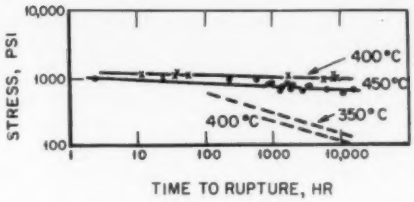

Fig. III-28 Stress-rupture properties of Mg–0.5 wt.% Zr alloy at 350 and 400°C (Ref. 104). ——, sintered and extruded; ---, cast and extruded.

Extremely creep-resistant vanadium-base alloys have been developed for application at 800°C (Ref. 105). The creep resistance was obtained by solid-solution hardening, dispersion hardening, and the use of interstitial additions. The elements utilized as alloying additions were Fe, Nb, Cr, Zr, Ta, and C. Creep curves for these alloys are compared with those for V–10 wt.% Ti and V–20 wt.% Ti in Fig. III-29.

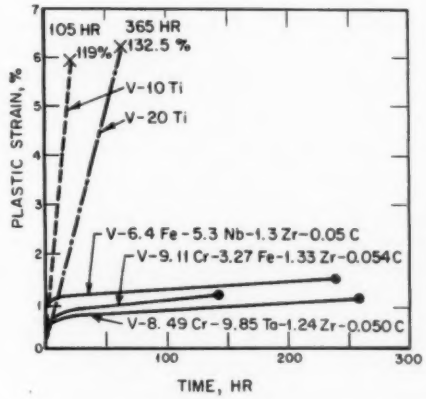

Fig. III-29 Creep behavior of vanadium alloys at 800°C under a stress of 10,000 psi (Ref. 105). Specimens were annealed for 1 hr at 1200°C. ×, ruptured; •, test stopped.

(M. Kangilaski)

Diffusion Studies

In a study of carbon diffusion into body-centered cubic refractory metals,[106] annealed molybdenum, tungsten, and tantalum specimens were coated with a thin layer of ^{14}C and diffusion annealed in vacuum at 1200 to 1600°C. Annealed titanium and niobium specimens were similarly coated and then vacuum diffusion annealed at 1100 to 1400°C. Diffusion coefficients and activation energies for carbon diffusion into these metals were determined as follows:

Metal	Temp., °C	Diffusion coefficient, cm^2/sec	Activation energy, kcal/gram atom
Molybdenum	1200	1.34×10^{-8}	41.0
	1600	4.24×10^{-7}	41.0
Tungsten	1200	8.61×10^{-10}	53.0
	1600	5.15×10^{-8}	53.0
Tantalum	1200	1.05×10^{-8}	43.0
	1600	2.51×10^{-7}	43.0
Niobium	1100	2.49×10^{-8}	35.0
	1400	4.88×10^{-7}	35.0
Titanium	1100	1.75×10^{-6}	20.0
	1400	7.27×10^{-6}	20.0

The activation energies were compared with previous values for carbon diffusion in these metals.

Metal	Activation energy, kcal/mole	Reference
Molybdenum	31.0	107*a*
Tungsten	40.4	107*b*
	23.8	108
Tantalum	38.5	107*a*
	24.6	107*b*
Niobium	33.0	107*a*
Titanium	18.9	107*b*

The diffusion of carbon in tantalum was also studied by the Japanese[109] using ^{14}C over the temperature range 1450 to 2200°C. The diffusion coefficients were described by the equation $D = 0.012 \exp(-40.3 \text{ kcal}/RT)$ cm^2/sec. Values obtained by internal-friction techniques at about 350°C indicated that the activation energy for carbon diffusion in tantalum was about 39 to 40 kcal/mole over a wide temperature range of 300 to 2200°C. It was suggested that the diffusion of carbon occurred by an interstitial mechanism at temperatures as high as 2200°C. The above equation also fits the diffusion data of Nakonechnikov et al., which were compiled at lower temperatures of 1200 to 1600°C. Besides the differences in the activation energies, the calculated value of D_0, the frequency factor, from the Russian data was about 0.024 cm^2/sec, compared with the Japanese value of 0.012 cm^2/sec. From other sources,[107a,108] the D_0 value has been reported as 0.0061 cm^2/sec and as low as 2.78×10^{-3} cm^2/sec, although the activation-energy value in the latter case was much lower than the currently published values of 38 to 43 kcal/mole.

A review[60d] of the work of Gebhardt, Fromm, and Roy[110] indicated that the carbon solubility in rhenium is considerably less than that proposed by Hughes.[111] The diffusion coefficient calculated from permeation-rate data depends upon the accuracy of the solubility values, and large discrepancies in carbon solubilities result in significant differences in carbon diffusion coefficients. The diffusion coefficients based on the results of Gebhardt, Fromm, and Roy are compared

with those determined[60d] from Hughes' data in Table III-19. The activation energy for the diffusion process based on the analysis using Hughes' results is 58 kcal/mole, compared with 77 kcal/mole for Gebhardt's data.

Table III-19 DIFFUSION COEFFICIENTS FOR CARBON IN RHENIUM AT 1500 AND 2300°C (REF. 60*d*)

Temp., °C	Carbon solubility, at.%		Diffusion coefficient, cm^2/sec	
	Hughes	Gebhardt et al.	Hughes	Gebhardt et al.
1500	4.2	0.4	1.11×10^{-8}	1.1×10^{-9}
2300	7.3	3.7	1.89×10^{-6}	9.6×10^{-7}

In a study of ^{14}C diffusion in beta zirconium and in zirconium carbides,[113] radioactive carbon in a glycerin emulsion was applied as a thin layer on the ends of ground samples. The samples were annealed in pairs in a graphite container: zirconium was annealed in a vacuum of 10^{-4} to 10^{-5} mm Hg at 1100 to 1600°C; the zirconium carbide was annealed in purified helium at 1600 to 2100°C. After annealing, the samples were given a radiometric analysis.

The diffusion data were determined by the method of least squares and were fitted to Arrhenius-type equations:

$$D_{C-Zr} = 3.6 \times 10^{-2} \exp [-34.200 \text{ cal/(mole)}(RT)] \quad cm^2/sec$$

$$D_{C-ZrC_{0.96}} = 3.3 \times 10^{2} \exp [-114,000 \text{ cal/(mole)}(RT)] \quad cm^2/sec$$

The values for carbon diffusion in beta zirconium and in zirconium carbide can be compared with data of other Russian investigators who made studies at similar temperatures and obtained the equation $D = 4.8 \times 10^{-3} \exp [-26,700 \text{ cal/(mole)}(RT)] \ cm^2/sec$ for carbon in beta zirconium[114] and $D = 5 \times 10^{2} \exp [-79,900 \text{ cal/(mole)}(RT)] \ cm^2/sec$ for carbon in zirconium carbide.[115]

Screening tests of hydrogen diffusion barriers for zirconium alloys were conducted[116] at 399°C in hydrogen for possible use in the Heavy Water Organic Cooled Reactor (HWOCR). Plasma-sprayed aluminum coatings were very porous and ineffective as barriers. Zirconium oxide, zirconium nitride, and diffused aluminum coatings were found to be effective hydrogen barriers but subject to progressive, catastrophic failure because of their inherent brittleness. An undamaged zirconium nitride coating appeared to be impervious to hydrogen at 750°F (399°C). Figure III-30 shows curves of typical pressure decay which indicate the amounts of hydrogen absorbed with time. Uncoated specimens and the plasma-spray-coated specimen began to absorb hydrogen immediately and at a relatively rapid rate. Oxide-coated specimens began to absorb hydrogen at a relatively low rate and then at a gradually accelerating rate. Nitride-coated specimens were characterized by no detectable absorption for some period of time, followed by rapid absorption. All the pressure-decay curves show evidence of decreasing absorption rate at pressures below 100 mm Hg. The screening tests were more indicative of the integrity of coatings than of their permeability to hydrogen. With the exception of the plasma-sprayed aluminum, all coatings retarded the hydriding of zirconium to some degree. The thin, naturally occurring oxide layer reduced hydriding sufficiently that hydriding occurred preferentially at the fresh metal surfaces exposed at defects. A ductile coating, such as pure, dense aluminum, or coatings that can be continuously repaired in service, possibly a self-healing oxide coating, were suggested for further study.

The trapping of hydrogen ions in several reactor metals was studied[117] by mass-spectrometry techniques as functions of ion-bombardment dose and energy. High trapping coefficients were indicated for titanium, tantalum, and zirconium near room temperature, and these high coefficients were maintained with increased ion bombardment (to 10^{19} ions/cm^2) and energy. The behavior of molybdenum was markedly different; this was explained in part by a thermal-diffusion model and the rate of hydrogen diffusion in these metals.

The interdiffusion of niobium and the Group IV*a*–VI*a* refractory metals, which form continuous solid solutions, has been investigated.[118] Pairs of the metals were heated in a vacuum furnace from 1300 to 1800°C, and the diffusion zone was examined by X-ray diffraction, metallography, and microhardness measurements. The lower melting element diffused preferentially into the more refractory metal, and in several couples a Kirkendall effect was observed. Alloying niobium with higher melting elements, such as tantalum, tungsten, or molybdenum, tended to increase the energy of activation for self-diffusion. Alloying with lower melting elements, such as titanium, vanadium, or zirconium, resulted in an increase in the diffusion coefficient with respect to the self-diffusion coefficient of pure niobium at the same temperatures.

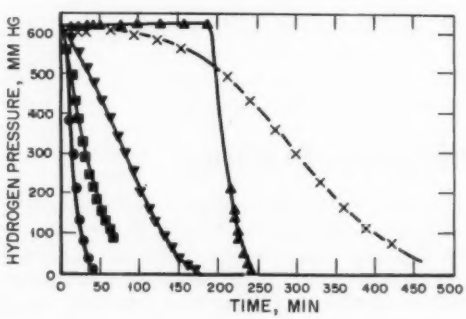

Fig. III-30 Typical hydrogen-pressure-decay curves for zirconium alloys.[116] *●, uncoated Zircaloy-2; ■, aluminum coated by plasma spray; ▼, uncoated 3Z1; ▲, nitrided 8 hr at 800°C; ×, oxidized in oxygen at 450°C.*

The region near the surface of a metal has sometimes exhibited anomalous diffusion characteristics, such as enriched and depleted concentrations of atoms where they were not expected. Mortlock investigated this near-surface behavior in gold.[119] Cobalt and nickel were diffused at tracer concentrations in gold at temperatures ranging from approximately 700 to 950°C. The diffusion penetration profiles were determined by serial sectioning techniques; the gold was first anodized and then the anodic layer was dissolved in acid. Sections as thin as 250 A could thus be removed reproducibly. The region close to the specimen surface was characterized by irregular behavior, i.e., the logarithm of concentration vs. the square of the penetration distance was not linear. The near-surface concentration anomaly was explained in terms of the chemical potential for diffusion. Solute atoms that tend to lower the surface tension and, by their diffusion to the surface, cause a decrease in the change of surface free energy result in what appears to be an anomalously high concentration at the surface. If such is the case, the concentration of solute atoms in the region away from but near the surface is therefore anomalously low. Conversely, if the solute atoms tend to increase surface tension and cause an increase in the change of surface free energy, the concentration of solute atoms *at* the surface would be expected to be anomalously low. (A. N. Ashurst)

Nonfuel Refractories

Rudy and Windisch[120] studied the phase relations in the W–C system at 2000, 2200, 2400, and 2600°C to determine whether ordered types of W_2C other than the CdJ_2 antitype occur in the intermediate-temperature range. Powder-diffraction patterns of all specimens quenched from 2000°C were indexed on the basis of the hexagonal close-packed unit cell previously reported for W_2C. X-ray patterns of all specimens quenched from higher temperatures revealed splitting of certain diffraction lines, with the reflections being somewhat diffuse in the alloy series quenched from 2650°C but very sharp in the series quenched from 2200 and 2400°C. Excellent agreement between the observed and calculated reflections was obtained by indexing the patterns on the basis of an orthorhombic unit cell analogous to the structure of Mo_2C. There was evidence that W_2C exists in three forms, which cannot be considered distinct phases but merely different states separated by homogeneous transitions of the second order.

Russian investigators[121] have shown that finely dispersed powders of refractory-carbide solid solutions activate the sintering process considerably. The high-temperature elastic and strength properties for compacted and sintered samples of such refractory carbides were somewhat higher than those for materials made from coarser powders.

Other Russian investigators[122] have examined the system W–Cr–C. The phase diagram for this system, as shown in Fig. III-31, was constructed on the basis of chemical, X-ray, and microstructural analysis on samples annealed in vacuum at 1400°C for 100 hr. It was found that the lattice-parameter values

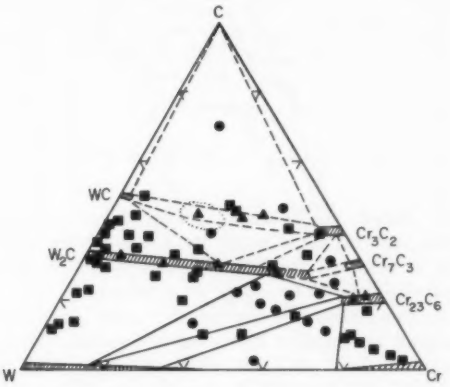

Fig. III-31 Phase equilibrium diagram in the W–Cr–C system.[122] ▲, *single-phase alloys;* ■, *binary alloys;* ●, *ternary alloys;* ═══, *boundary of phase fields at 1400°C;* ·····, *phase with cubic NaCl-type structure in cast alloys.*

for the carbide (W,Cr)C were very close to the extrapolated values for the solid solutions of tungsten in ZrC. The phase (W,Cr)C may represent a solid solution of tungsten in CrC.

Researchers at the Ames Laboratories[36c] are preparing refractory carbides by the reduction of the respective oxide with appropriate amounts of carbon. The melting temperature and lattice parameters of the individual monocarbides are given in Table III-20.

Table III-20 MELTING TEMPERATURES AND LATTICE PARAMETERS OF FIVE MONOCARBIDES[36c]

Carbide	Melting point, °C	Lattice parameter, A
HfC	3880	4.6375
TaC	3870	4.4545
NbC	3505	4.4703
ZrC	3495	4.6985
UC	2610	4.9595

The binary systems TaC–HfC and TaC–ZrC exhibited complete solid solubility, and the solidus curves for these systems varied almost linearly between the melting points of the pure components.

Ordan'yan[123] investigated the system Zr–C–Nb and established the ZrC–Nb polythermal profile shown in Fig. III-32. An isothermal section was also constructed for the Zr–C–Nb alloy system at 2273°K. No triple compounds were discovered; however, there

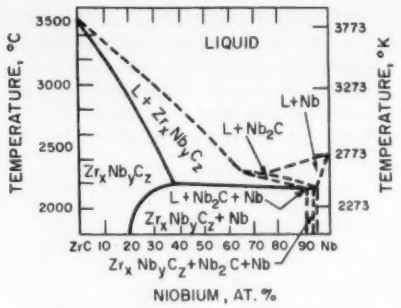

Fig. III-32 ZrC–Nb polythermal profile.[123]

were three single-phase fields, three two-phase fields, and one three-phase field. The lattice parameters of complex nonstoichiometric carbides and the melting points of the alloys were examined.

Denbnovetskaya[124] studied the solid solutions of complex carbides of the transition metals. Alloys of Mo_3C_2–ZrC, Mo_3C_2–NbC, WC–TiC, WC–ZrC, WC–HfC, WC–VC, and WC–TaC were prepared by powder-metallurgy methods involving sintering, hot pressing, or synthesis in vacuum furnace. On the basis of cubic carbides, the formation of wide-range solid solutions was confirmed in all systems. Concentration dependence of crystal-lattice parameters for all systems was also investigated.

The Albany Metallurgy Research Center has continued studies of practical methods and equipment to spin cast high-melting-point metal–carbon alloys.[125] Carbon–refractory-carbide compositions are being evaluated with respect to thermal-shock resistance, thermal expansion, bend rupture, hot hardness, oxidation resistance, and electrical resistivity. Numerous NbC castings with carbon contents ranging from 14 to 18.3 wt.% were fabricated to densities of 94 to 95% of the theoretical. The microstructure of transverse sections generally consisted of an all-eutectic core surrounded by a hypereutectic shell, which was in accordance with the carbon variation. Air oxidation tests performed on TiC castings revealed oxidation rates at 900, 948, and 1000°C of 1.1, 2.6, and 5.75 mg/(dm^2)(min), respectively. The coefficients of linear thermal expansion measured for CbC, HfC, ZrC, and TiC are shown in Table III-21.

Denbnovetskaya[126] has shown a concentration dependence of the properties of solid solutions in the system NbC–Mo_3C_2. Changes in the electron structure of the solid solution were related to the increase in molybdenum carbide content.

Other Russian investigators have examined physical properties of the solid solutions HfC–MoC and TaC–MoC.[127] Alloys of HfC–MoC and TaC–MoC, both with MoC contents ranging from 0 to 100 mole %, were synthesized from a mixture of HfO_2, TaC, molybdenum powders, and carbon black. The mixtures were hot compacted at 2000 to 2200°C for 15 min and were then vacuum annealed at 2000°C for 1 to 2 hr and slowly cooled. All alloys were found to be homogeneous single-phase solid solutions with a free-carbon content of less than 0.5 wt.%. The dependence of the temperature of transition to the superconducting state (T_{cr}), melting temperature, resistivity, microhardness, and lattice constant on the composition or valency electron concentration was shown. The $(HfC)_{0.90}$ $(MoC)_{0.10}$ and $(HfC)_{0.95}$ $(MoC)_{0.15}$ alloys have a melting temperature higher than 3900°K, which made them the most refractory in the systems investigated. The results also showed that in solid solutions of groups IV and V metal carbides with WC, the most refractory compounds should be at electron concentrations of about 4.2 valence electrons/atom. The alloys of the HfC–WC system should have the highest melting temperature. Superconducting compounds (with high T_{cr}) should have electron concentrations of 4.8 to 4.9 valence electrons/atom.

Table III-21 COEFFICIENTS OF LINEAR THERMAL EXPANSION OF FUSED HYPOEUTECTIC CARBIDES[125]

Material	Carbon, wt.%	Expansion coefficient, 10^{-6}/°C	
		200–1000°C	200–1600°C
NbC	14.4	7.2	7.6
HfC	10.3	6.22	7.0
HfC	12.0	5.9	7.21
ZrC	17.6	6.9	8.14
ZrC	19.4	6.0	7.64
ZrC	20.3	6.45	7.14
TiC	18.5	7.78	9.0
TiC	22.1	5.1	7.15

Kuchma and Samsonov[128] have studied the resistance change, thermoelectromotive force, and superconductivity of the monocarbides and mononitrides of Ti, Zr, Hf, Nb, and Ta. Dependence of the specific electrical resistance of several carbides and nitrides on atomic ratios is illustrated in Fig. III-33. The carbides of tantalum (TaC) niobium (NbC) and molybdenum (Mo_2C and MoC) were noted to be superconductive with T_k values of 9.7, 11.1, 2.78, and 9.26°K, respectively. Most of the transition-metal nitrides, TiN, ZrN, and HfN exhibit superconductivity with T_k values of 5.6, 10.7, and 6.2, respectively.

Plastic deformation in hot-pressed polycrystalline specimens of TiC, UC, NbC, TaC, and WC was evaluated by testing in four-point bending and under compression to 2100°C (Ref. 129). Table III-22 illustrates the results of the ductile-to-brittle temperature measurements. Above the ductile-to-brittle temperature for these materials, their yield strengths decreased exponentially with increasing temperature, as shown in Fig. III-34. Between the ductile-to-brittle transition temperature and about 1900°C, the apparent activation energy for flow in the carbides with a rock-salt structure was near 0.5 ev/atom. Above 1900°C the value was approximately 2 ev/atom. The value for

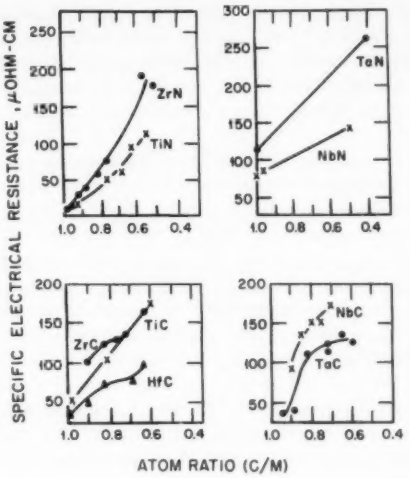

Fig. III-33 Dependence of the specific electrical resistance of several transition carbides and nitrides.[128]

Table III-22 DUCTILE-BRITTLE TEMPERATURES FOR CARBIDES TESTED IN FOUR-POINT BENDING[129]

Material	Ductile–brittle temp., °K	Melting point, °K	T_{DB}/T_M
$TiC_{0.745}$	1800	3073	0.59
$VC_{0.61}$	1500	3000	0.50
$NbC_{0.95}$	1750	3673	0.48
TaC	2000	4073	0.49
WC	1500	2873	0.52

WC was apparently 0.3 ev/atom to 2070°C. The VC and TiC recovered extensively on annealing for short times near 2000°C, whereas no recovery occurred in the WC under these conditions.

The relation between the microhardness and microbrittleness of refractory compounds and their electron structure was examined by Samsonov and Stasovskaya.[130] The microhardness and microbrittleness were measured on the individual powder particles of refractory compounds prepared by reduction of the appropriate oxides or synthesis from their elements. The composition of the test compounds was checked by chemical and X-ray phase analyses. Table III-23 gives the optimum loads and the respective microhardness values. The resultant overall degree of brittleness for several refractory materials is given in Table III-24. The load at which about 50% of the impression showed crazings was used as a failure criterion. However, this total degree of brittleness alone was insufficient to characterize the brittleness of a given material. The rate of increase in failure with increasing load was characterized by the derivative of the overall degree of brittleness with respect to the applied load. For each material the variation in total degree of brittleness as its optimum load increased to 10 g was

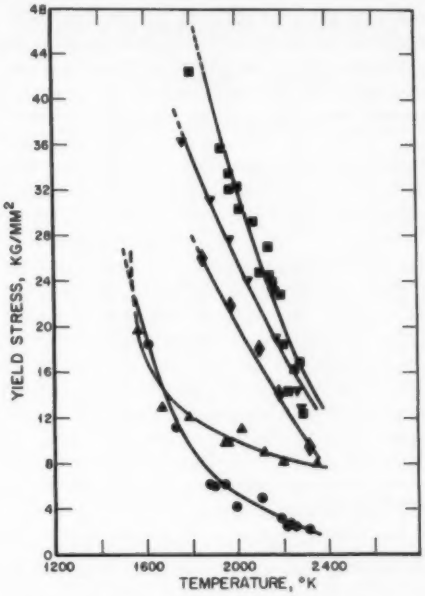

Fig. III-34 Yield strength vs. absolute temperature for carbides tested in four-point bending.[129] ●, $VC_{0.61}$; ▲, WC; ◆, $NbC_{0.88}$; ▼, $NbC_{0.95}$; ■, $TiC_{0.745}$.

Table III-23 MICROHARDNESS OF REFRACTORY COMPOUNDS[130]

Refractory compound	Optimum load ($P_{opt.}$), g	Microhardness at $P_{opt.}$, DPH/mm²	Microhardness, DPH/mm²
TiC	70	3022	2985
ZrC	100	2723	2925
HfC	50	1932	2913
VC			2094
NbC	50	2003	1961
TaC	150	1536	1600
$Cr_{23}C_6$	100	1663	1650
Cr_7C_3	200	1882	1336
Cr_3C_2	150	1800	1350
Mo_2C			1499
WC	150	1300	1780
TiB_2	50	2970	3370
ZrB_2	40	2774	2252
HfB_2	20	3356	2900
VB_2	10	2300	2800
NbB_2	20	1862	2600
TaB_2	30	2475	2500
CrB_2	60	1901	2100
Mo_2B_5	40	2239	2350
W_2B_5	50	2260	2663

determined. The brittleness index γ of the material, reflecting both the time of onset of brittle failure and the rate of increase of that failure with further increase in load, was determined from the following relation:

$$\gamma = \frac{1}{P_{opt.}} \left(\frac{\partial Z}{\partial P} \right)$$

Table III-24 CHARACTERIZATION OF THE MICRO-BRITTLENESS OF REFRACTORY COMPOUNDS[130]

Refractory compound	Optimum load ($P_{opt.}$), g	Overall degree of brittleness at $P_{opt.}$ (Z)	$\frac{\partial Z}{\partial P}$	Brittleness index* (γ)
TiB_2	50	0.5	0.09	0.0180
ZrB_2	40	0.9	0.07	0.0175
HfB_2	20	0.5	0.06	0.0300
VB_2	10	0.4	0.06	0.0600
NbB_2	20	0.5	0.09	0.0450
TaB_2	30	0.4	0.09	0.0300
CrB_2	60	0.5	0.04	0.0067
Mo_2B_5	40	0.5	0.07	0.0175
W_2B_5	50	0.6	0.03	0.0060
TiC	70	0.5	0.04	0.0061
ZrC	100	0.8	0.03	0.0080
HfC	50	0.5	0.03	0.0060
NbC	50	0.7	0.06	0.0120
TaC	150	0.7	0.03	0.0017
$Cr_{23}C_6$	100	0.4	0.01	0.0010
Cr_7C_3				
Cr_3C_2	150	0.2	0.007	0.0005
WC	150	0.9	0.03	0.0019

*Arbitrary units.

It is obvious that borides of the refractory metals exhibit the greatest brittleness, and, in general, the brittleness of transition metal compounds increases in the following order: carbides–nitrides–silicides–borides. Hardness of the refractory compounds generally increased with increasing statistical weight of the stable electron sp^3 configurations and with decreasing statistical weight of the nonlocalized or weakly bound electrons. The microbrittleness of these compounds was strongly influenced by the proportion of nonlocalized electrons, which relax the lattice and thus decrease the microbrittleness.

In neutron-diffraction studies of the Ti–C system by Goretski,[131] face-centered cubic superstructure lines were noted in the concentration range between 32 and 36 at.% C. The phase was found to be stable up to 1900°C at a concentration of 33 at.% C. Specimens with carbon concentrations between 36 and 40 at.% showed the same superstructure lines after annealing in hydrogen at 700°C. The isotype ordering phase was found in the Zr–C systems, where it appeared near the boundary of the B1 phase.

Influences of nuclear irradiation on properties of refractory compounds were studied by Konozenko and Ryzhkov.[132] The radiation stability of solids depends on their structure and on the type of atomic bonds in the lattice. Solids with covalent bonds are less stable than solids with ionic bonds. The relative stability of SiC under radiation makes it attractive as a matrix in nuclear fuels, and the sensitivity of its crystalline lattice structure to radiation permits its use as a neutron-flux monitor. Titanium carbide with a cubic lattice and MoC with a hexagonal lattice suffer greater changes in their structure and properties as a result of irradiation than do solids with an anisotropic crystalline structure. The change in the properties of UC at small fluences shows an effect of saturation. Pure metallic boron and B_4C crack under irradiation, although a series of experimental data indicated the absence of cracks in B_4C and the ceramic $B_4C-Al_2O_3$. The ZrB_2 demonstrated good stability against radiation.

Rudy and Bruko[133] examined the lower temperature modifications of Nb_2C and U_2C. The orthorhombic, low-temperature alpha modification of Nb_2C has a structure similar to that of zeta Fe_2N(a = 12.36 A, $b = 10.89_5$ A, $c = 4.96_3$ A), and transforms at 1200°C into the hexagonal epsilon Fe_2N type. A second transition at approximately 2500°C is associated with destruction of long-range order in the carbon sublattice. The structure of alpha V_2C (orthorhombic, a = 11.49 A, b = 10.06 A, c = 4.55 A) is similar to that of alpha Nb_2C and transforms at 800°C into the hexagonal high-temperature modification. The structures of alpha V_2C and alpha Nb_2C are distorted modifications related to the epsilon Fe_2N type.

Continued studies are being performed by researchers at the Los Alamos[134] on compositions of TaC–NbC. Definite effects of the purity of the starting carbide powders on the final properties of the material were observed. High iron content appeared to cause a grain-boundary network of relatively soft graphite that seemed to facilitate deformation by grain-boundary sliding. Composition appeared to have little effect on resistance to deformation of both NbC and TaC composites over the range investigated. Preliminary results indicated that solid-solution strengthening occurs through the combination of carbides in the TaC–NbC pseudo-binary system. A mixture of 50 wt.% TaC–50 wt.% NbC showed greater resistance to deformation as a function of carbide composition than NbC–C composites of comparable volume percent carbide loading. The Young's modulus and the shear modulus as a function of composition for NbC–C composites are shown in Figs. III-35 and III-36, respectively.

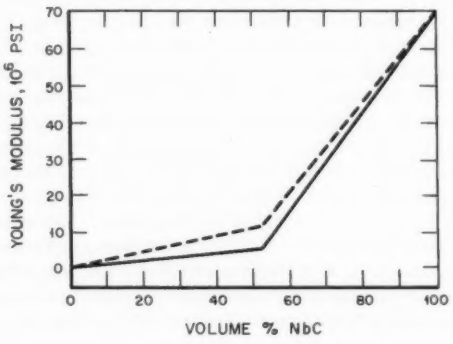

Fig. III-35 Young's modulus as a function of composition for NbC–C composites.[134] ---, perpendicular to direction of pressing; ——, parallel to direction of pressing.

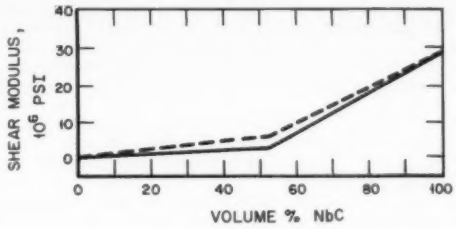

Fig. III-36 Shear modulus as a function of composition for NbC–C composites.[134] ---, perpendicular to direction of pressing; ——, parallel to direction of pressing.

(W. C. Chard)

Concrete

French researchers[135] have studied the effect of neutron irradiation at elevated temperatures on the load-bearing properties and dimensional stability of several reactor concretes. Mortar and concrete specimens containing calcium aluminate cement, with serpentine alumina and rare-earth aggregates, were evaluated after up to 180 days in fast fluences up to 1.05×10^{20} neutrons/cm^2 and thermal fluences up to 3.3×10^{19} neutrons/cm^2. Temperatures up to 280°C were employed, with some thermal cycling tests continuing for up to 165 days. Irradiation caused a swelling in the concrete which tended to compensate for the shrinkage associated with the loss of moisture on heating. The modulus of elasticity and compressive strength of the concrete were not significantly affected by irradiation, although the flexural strength of irradiated specimens was slightly lower than that for unirradiated specimens. (D. R. Lankard)

Ceramic Technology

Russian investigators[136] have identified the two mixed-oxide compounds $SrZrO_3$ and $Sr_5Zr_3O_{11}$ in the $SrO-ZrO_2$ system. The compound $Sr_5Zr_3O_{11}$ was found to melt incongruently at about 2200°C, yielding $SrZrO_3$. Two eutectics, at 80 and 26% SrO, were reported to melt at 2100 and 2270°C, respectively. The same authors also examined the $SrO-Al_2O_3-ZrO_2$ system.[137]

Other Russian investigators studied the $Nb_2O_3-Cr_2O_3$ system in argon and found one compound, $NbCrO_3$, which melted at 2330°C (Ref. 138). The eutectics, at 24 and 78 mole% Cr_2O_3, were observed to melt at 2060 ± 30°C and at 2100 ± 30°C, respectively.

The effects of heating rate, residual gas pressure, specimen size, and magnesia content on the sintering of alumina in vacuum have been described by Warman and Budworth.[139] It was found that swelling occurred on sintering unless these conditions were appropriately chosen. For a particular specimen size and heating rate, there is a critical pressure below which the specimen must be evacuated before firing if complete absence of pores is to be achieved in the sintered ware. Similar effects were noted when firing in a hydrogen atmosphere.

Hasselman and Fulrath[140] made a quantitative investigation of the effect of micromechanical stress concentrations on the strength of two-phase brittle-matrix ceramic systems. A soda borosilicate glass was used as the matrix, with either spherical alumina particles 60 μ in diameter or spherical pores of the same size as those for the discontinuous phase. Stress concentrations were varied under uniaxial and biaxial stress conditions. The experiments showed that the micromechanical stress concentrations strongly affected the macroscopic strength of the composite. Under biaxial tensile stress, either of the dispersed phases studied resulted in a decrease in strength which corresponded to the maximum calculated stress-concentration factor. Under uniaxial stress conditions, however, the reduction in strength for the glass-alumina system was negligible, whereas the glass-pore system gave a reduction in uniaxial strength which did not correspond to the maximum calculated stress-concentration factor. These findings suggest that differences in strength of brittle multicomponent systems can be explained by microstructural features. The authors developed a hypothesis relating the size of the region in the (glass) matrix over which stress concentrations act to the size of Griffith flaws responsible for failure. The hypothesis may also apply to the effects of porosity on the strength of polycrystalline brittle ceramics. (H. D. Sheets, Jr.)

References

1. A. B. Johnson, Jr., and J. E. Irvin, Radiation-Enhanced Oxidation of Zircaloy-2 in *p*H 10 LiOH and *p*H 10 NH_4OH, USAEC Report BNWL-463, Battelle–Northwest, July 1967.
2. Atomic Energy of Canada Ltd., unpublished progress report, January–March 1967.
3. E. Cerrai, F. Gadda, and A. Scaroni, Development Program on the Application of Steam–Water Spray to Reactor Cooling. In-pile Corrosion of Zircaloy-2 in Steam–Water Mixtures, USAEC–Euratom Report EURAEC-1862, Cestro Informazioni Studi Esperienze, October 1966.
4. W. K. Alexander, Hydriding of Hanford Production Reactor Zircaloy Process Tubes, USAEC Report DUN-SA-34, Douglas United Nuclear, Inc., June 16, 1967.
5. R. A. Murgatroyd and J. Winton, UKAEA, unpublished, 1967.
6. L. Rensicci and J. P. Langeron, Oxydation du Zirconium en Phase β Sour Trés Basser Pressions Aspect Superficiel Prensenté par les Allrager Zirconium–Oxygene, *J. Nucl. Mater.*, 23(1): 79-87 (July 1967).
7. Atomic Energy of Canada Ltd., unpublished report, July 1967.
8. G. Chaudron, Behavior of Stainless Steels in Superheated Steam, Quarterly Report No. 5, July 1–September 30, 1966, USAEC–Euratom Report EURAEC-1749, Centre National de la Recherche Scientifique.

9. S. J. Armijo, Effects of Impurity Additions on the Intergranular Corrosion of High-Purity Fe–Cr–Ni Austenitic Alloys, USAEC Report GEAP-5047 (EURAEC-1855), General Electric Company Nuclear Technology Department, October 1966.
10. M. J. O'Boyle (Ed. and Comp.), Yankee Core Evaluation Program Quarterly Progress Report for the Period Ending September 30, 1966, USAEC Report WCAP-6082, pp. 330.12-330.14, Westinghouse Electric Corp., Atomic Power Division, April 1967.
11. C. F. Knights, Stress Corrosion of Irradiated Type 316 Stainless Steel, British Report AERE-M-1899, June 1967.
12. Aerojet-General Corp., Evaluation Study of Hastelloy X as a Nuclear Cladding, Quarterly Progress Report, January 1–March 31, 1967, USAEC Report AGN-8224, May 1967.
13. J. M. Francis, J. A. Jutson, and J. H. Buddery, An Oxidation Study of Ni–Cr–Fe Alloys in Carbon Dioxide at 800 to 1000°C, *J. Mater. Sci.*, 2(1): 78-87 (January 1967).
14. H. E. McCoy, Jr., and J. R. Weir, Jr., Materials Development for Molten-Salt Breeder Reactors, USAEC Report ORNL-TM-1854, Oak Ridge National Laboratory, June 1967.
15. G. M. Wood, L. K. Knudsen, and F. G. Hammitt, Cavitation Damage Studies with Rotating Disk in Water, *J. Basic Eng.*, Series D, 89(1): 98-110 (March 1967).
16. D. E. Rosner and H. D. Allendorf, Kinetics of the Attack of High-Temperature Molybdenum and Tungsten by Atomic Oxygen, *J. Electrochem. Soc.*, 114: 305-314 (April 1967).
17. E. A. Gulbransen, K. F. Andrew, and F. A. Brassart, Studies on the High Temperature Oxidation of Molybdenum, Tungsten, Niobium, Tantalum, Titanium, and Zirconium, USAEC file No. NP-16704, Westinghouse Research Laboratories, Apr. 18, 1967.
18. I. A. Charlot, R. A. Thiede, and R. E. Westerman, Corrosion of Superalloys and Refractory Metals in High Temperature Flowing Helium, USAEC Report BNWL-SA-1137, Battelle–Northwest, March 1967.
19. P. Kofstad, High-Temperature Oxidation of Metals, *Corrosion Monograph Series*, John Wiley & Sons, Inc., New York, 1966.
20. J. B. Berkowitz-Mattuck, L. Kaufman, E. V. Clougherty, and R. Hopper, Oxidation of Hf–Ta Alloys, *Trans. Met. Soc., AIME*, 239: 750-753 (May 1967).
21. P. Kofstad and I. Kvernes, Studies of Oxidation of Niobium Alloys at Very High Temperatures, Report AFML-TR-67-40, Central Institute for Industrial Research, Oslo, Norway, April 1967.
22. W. R. Price, S. T. Kennett, and J. Stringer, The Oxidation of Vanadium in the Temperature Range 700–1000°C: the Non-Linear Rate Law, *J. Less-Common Metals*, 12(4): 318-325 (1967).
23. V. A. Blinova, I. N. Ozeryanaya, G. I. Belyaeva, and E. V. Konstantinova, Molybdenum and BM-1 Alloy Corrosion in Molten Fluorides, *Tr. Inst. Electrokhim., Akad. Nauk SSSR, Ural. Filial*, No. (9): 109-116 (1966).
24. K. Lehovec and J. D'Amico, Kinetics of Tantalum Corrosion in Aqueous Electrolytes: I, *J. Electrochem. Soc.*, 114: 363-367 (April 1967).
25. J. Hopenfeld and D. Darley, Dynamic Mass Transfer of Stainless Steel in Sodium Under High-Heat-Flux Conditions, USAEC Report NAA-SR-12447, Atomics International, July 15, 1967.
26. D. A. Mannas, Effects of Long-Term Sodium Exposure on Materials in the Sodium Reactor Experiment, USAEC Report AI-66-53, Atomics International, June 15, 1966.
27. Atomics International, AEC Unclassified Programs, Quarterly Technical Progress Report, January–March 1967, USAEC Report NAA-SR-12395, pp. 115-122, May 31, 1967.
28. R. C. Andrews and F. Tepper, Mechanical Properties of Materials in Sodium, in Proceedings of Sodium Components Development Program Information Meeting, Chicago, Ill., June 16–17, 1965, USAEC Report CONF-650620, pp. 1-17.
29. T. L. Hoffman, Performance of Types 304, 316, and 348 Stainless Steel in NaK at High Temperatures, USAEC Report IN-1089, Idaho Nuclear Corp., May 1967.
30. Los Alamos Scientific Laboratory, Advanced Plutonium Fuels Program, Quarterly Status Report, April 1–June 30, 1967, USAEC Report LA-3745-MS, p. 55, Aug. 30, 1967.
31. Argonne National Laboratory, Reactor Development Program Progress Report, April 1967, USAEC Report ANL-7329, pp. 48-49, June 16, 1967.
32. E. M. Simons, Corrosion by Liquid Metals, Fused Salts, and Organics, *Reactor Mater.*, 10(1): 30 (Spring 1967).
33. M. G. Karpman, G. V. Shcherbedinskii, G. N. Dubinin, and G. P. Benediktova, Diffusion of Alkali Metals into Molybdenum and Niobium (in Russian), *Metalloved. Term. Obrab. Metal.*, 3: 46-49 (March 1967).
34. J. M. Fackelman, Battelle Memorial Institute, Columbus Laboratories, private communication, Oct. 19, 1967.
35. F. J. Salzano and S. Aronson, The Compatibility of Graphite with Cesium, *Nucl. Sci. Eng.*, 28: 51-54 (1967).
36. Ames Laboratory, Annual Summary Research Report, Ceramics and Mechanical Engineering, Chemical Engineering, Chemistry, Mathematics and Computer Science, Metallurgy, Physics, and Reactor Divisions, July 1, 1966–June 30, 1967, USAEC Report IS-1600, (*a*) CE 3-5, (*b*) pp. C&ME 11-13, (*c*) M 29-32, July 1967.
37. E. M. Simons, Corrosion by Nonaqueous Liquids, *Reactor Mater.*, 10(3): 166 (Fall 1967).
38. T. F. Kassner, Rate of Solution of Tantalum Disks in Liquid Tin, *J. Electrochem. Soc.*, 114(7): 689-694 (July 1967).
39. G. F. DeBeni, Magnesium Alloys in Terphenyls—Corrosion Inhibitors, *J. Nucl. Mater.*, 22: 158-164 (May 1967).
40. J. L. Smee, The Chemistry of the X-7 (Organic) Loop Coolant. Part I, May 1960–April 1965, Canadian Report AECL-2527, January 1966.
41. J. F. Walker, The Behaviour of Zircaloy-2 and Zr–2.5% Nb Clad Uranium Dioxide Fuel in an Organic Coolant (The X-719 Irradiation), Canadian Report AECL-2661, November 1966.
42. Yu. N. Aleksenko and A. M. Brodskiy, Research on the Use of Organic Coolants and Moderators in Nuclear Reactors, Translation No. 2247 from Papers of the Institute of Atomic Energy of the USSR, Paper No. 611 (1964), Oct. 28, 1966, Report AD-645062.
43. Oak Ridge National Laboratory, Molten-Salt Reactor Program Progress Report for Period Ending February 28, 1967, USAEC Report ORNL-4119, (*a*) pp. 95-103, (*b*) pp. 95, 99, and 103-108, (*c*) pp. 103-104, July 1967.
44. E. M. Simons, IAEA Symposium on Alkali-Metal Coolants, *Reactor Mater.*, 10(2): 96-100 (Summer 1967).
45. *Alkali Metal Coolants*, Symposium Proceedings, Vienna, 1966, International Atomic Energy Agency, Vienna, 1967 (STI/PUB/143).
46. R. P. Marshall and C. L. Selby, Failure Analyses and Properties of Safety Rod Guide Tubes from the HWCTR, USAEC Report DP-1077, Savannah River Laboratory, April 1967.
47. E. E. Bloom and J. R. Weir, In-Reactor and Postirradiation Creep-Rupture Properties of Type 304 Stainless Steel, *Trans. Amer. Nucl. Soc.*, 10: 131-132 (June 1967).
48. J. A. Williams and J. W. Carter, The Creep of Annealed 304 Stainless Steel During Irradiation and Its Engineering Significance, USAEC Report BNWL-SA-373, Battelle–Northwest, Mar. 17, 1966.
49. H. Brager, D. Framer, C. G. Rhodes, and A. G.

Pard, High-Temperature Tensile Behavior of Helium-Injected Type 304 Stainless Steel, *Trans. Amer. Nucl. Soc.*, 10: 129-130 (June 1967).
50. J. R. Weir and R. T. King, The Effect of Cyclotron-Injected Helium on the Mechanical Properties of Stainless Steel, *Trans. Amer. Nucl. Soc.* 10: 130-131 (June 1967).
51. W. R. Martin and J. R. Weir, Solutions to the Problems of High-Temperature Irradiation Embrittlement, USAEC Report ORNL-TM-1544, Oak Ridge National Laboratory, June 1966.
52. D. L. Keller, Progress Relating to Civilian Applications During July 1966–June 1967, USAEC Report BMI-1809, pp. B1-16, Battelle Memorial Institute, July 1, 1967.
53. Argonne National Laboratory, Reactor Development Program Progress Report for June 1967, USAEC Report ANL-7349, pp. 81-84, July 31, 1967.
54. J. S. Waddington and K. Loffhouse, The Effect of Irradiation on the High-Temperature Fracture of Stainless Steel, *J. Nucl. Mater.*, 22: 205-213 (May 1967).
55. S. Y. Ogawa and C. N. Spalaris, Burst and Tensile Properties of Irradiated Incoloy 800 and Inconel 625 Tubing Materials, *Trans. Amer. Nucl. Soc.*, 10: 134-135 (June 1967).
56. P. C. L. Pfeil, Improvements in or Relating to Heat Treatment of Steel, British Patent 1,055,317, Jan. 18, 1967.
57. A. E. Powers and E. E. Baldwin, Effect of Neutron Irradiation in 550°F Loop Water on the Mechanical Properties of Ni–Cr–Fe Alloy 600, Ni–Cr–Fe Weld Metal, and Type 347 Stainless Steel, USAEC Report KAPL-3161, Knolls Atomic Power Laboratory, Jan. 27, 1967.
58. J. E. Irvin, A. L. Bement, and R. G. Hoagland, The Combined Effects of Temperature and Irradiation on the Mechanical Properties of Austenitic Stainless Steels, USAEC Report BNWL-1, Battelle–Northwest, January 1965.
59. M. Kangilaski and F. R. Shober, Correlation of Tensile and Fatigue Properties of Irradiated 347 Stainless Steel at Room Temperature, *Trans. Amer. Nucl. Soc.*, 10: 132 (June 1967).
60. General Electric Company, Nuclear Materials and Propulsion Operation, AEC Fuels and Materials Development Program Progress Report No. 67, USAEC Report GEMP-67, (*a*) pp. 123-126, (*b*) pp. 91-100, (*c*) pp. 133-134, (*d*) p. 175, June 30, 1967.
61. V. B. Lawson, The Effect of Neutron Irradiation on the High-Temperature Tensile Properties of Some Nickel-Containing Alloys, Canadian Report AECL-2677, March 1967.
62. F. N. Rhines and P. J. Wraz, Investigation of the Intermediate Temperature Ductility Minimum in Metals, *Trans. Amer. Soc. Metals*, 54: 117-129 (1961).
63. C. E. Dixon, C. W. Funk, and W. Weleff, High Temperature Radiation Embrittlement of Hastelloy X, Inconel 625, and AISI 347, *Trans. Amer. Nucl. Soc.*, 10: 133-134 (June 1967).
64. J. R. Weeks, Brookhaven National Laboratory, unpublished, June 30, 1967.
65. D. S. Cowgill, N. F. Davies, and W. J. Kurzeka, Irradiation Test of SNAP-8 Candidate Spring Materials, USAEC Report NAA-SR-11519, Atomics International, June 30, 1967.
66. M. Grounes, Irradiation Effects in Fortiweld Steel Containing Different Boron Isotopes, Swedish Report AE-288, July 1967.
67. A. Cowan, G. D. Fearnehough, and R. W. Nichols, The Behavior of 9% Nickel Steel in a Reactor Environment, *Weld. J. (N. Y.)*, 46: 97s-104s (March 1967).
68. K. Shiraishi, Grain-Boundary Migration and Growth of Gas Bubbles in Neutron Irradiated Al–Li Alloys, *J. Nucl. Sci. Technol. (Tokyo)*, 4: 136-142 (March 1967).
69. V. S. Karasev, Vacancy Mechanism of the Accelerated Failure of Materials During Irradiation Under Stress (in Russian), *Dokl. Akad. Nauk SSSR*, 171: 84-87 (Nov. 1, 1966).
70. H. R. Babitzke and H. Kato, Columbium and Tantalum Alloy Development, USAEC Report BMI-RI-6964, Bureau of Mines, Albany Metallurgy Research Center, November 1966.
71. J. Stoop and P. Shaninian, The Effect of Nitrogen on the Tensile and Creep-Rupture Properties of Niobium, Report NRL-6464(AD-647889), Naval Research Laboratory, Oct. 31, 1966.
72. A. Helmut and I. Pfeiffer, Anomalies of the Temperature Dependence of Young's Modulus of Niobium–Zirconium Alloys and of Pure Niobium, *Z. Metallk.*, 58: 311-316 (May 1967).
73. B. A. Klypin, A. P. Gulyaev, and N. N. Morgunova, Mechanical Properties of High-Melting-Point Metals (in Russian), *Metalloved. Term. Obrab. Metal.*, 12: 15-21 (December 1966).
74. C. R. Honeycutt, T. F. Martin, J. C. Sawyer, and E. A. Steigerwald, Elevated Temperature Fatigue of TZC Molybdenum Alloy Under High Frequency and High Vacuum Conditions, Report NASA-CR-72241, Thompson Ramo Wooldridge Inc., May 1967.
75. G. F. Zaboronok, V. B. Milova, M. D. Polyakova, and T. V. Simonishvili, Properties of Polycrystalline Unalloyed Molybdenum (in Russian), *Metalloved. Term. Obrab. Metal.*, 12: 49-50 (December 1966).
76. M. N. Belyakova, S. T. Borimskaya, E. E. Zasimuk, and L. N. Larikov, Kinetics of Primary, Cumulative, and Secondary Recrystallization in Molybdenum Foil (in Russian), *Fiz. Metal. Metalloved.*, 23: 101-105 (January 1967).
77. D. A. Prokoshkin and M. I. Zakharova, Isothermal Sections at 600 and 750°C of the Molybdenum–Titanium–Zirconium Phase Diagram, *Izv. Akad. Nauk SSSR, Neorg. Mater.*, 3: 87-93 (January 1967).
78. D. A. Prokoshkin and M. I. Zakharova, Phase Diagram of the Molybdenum–Titanium–Zirconium System, *Dokl. Akad. Nauk SSSR*, 172: 1382-1384 (1967).
79. R. Yoda and T. Arai, On the Creep-Rupture Strength of Molybdenum Composite Cast with Nimonic 90 Alloy, *Nippon Kinzoku Gakkaishi*, 31: 90-94 (1967).
80. M. I. Gavrilyuk and V. A. Konstantinov, Effect of Oxygen on Recrystallization of Tantalum (in Russian), *Fiz. Metal. Metalloved.*, 20: 410-414 (September 1966).
81. M. Conte, Preliminary Studies of Vanadium-Base Alloys Intended for Use in Fabrication of Cans for Fast Reactors, Report EURFNR-269 (English translation of French Report CEA-R-3152), March 1967.
82. W. Pollack, R. W. Buckman, R. T. Begley, K. C. Thomas, and E. C. Bishop, Development of High-Strength Vanadium Alloys, USAEC Report WCAP-3487-16, Westinghouse Electric Corp., Advanced Reactor Division, June 1967.
83. *Étude sur la Corrosion et la Protection du Zirconium et de ses Alliages*, Centre d'Études Nucleaires de Saclay, Gif-sur-Yvette, and Presser Univeritaires de France, Paris, 1966.
    a. J.-C. Colin and P. Lebr, Grain Growth Phenomenon in Zirconium, pp. 77-96.
    b. M. Billion and J. P. Laugeron, Recrystallization, Grain Growth, and Preferential Orientations in Zone Melted Zirconium, pp. 97-105.
84. U. Rosler, Zirconium Alloys Containing Cerium and Yttrium, Canadian Patent 753,191, Feb. 21, 1967.
85. Improvements in/or Relating to Zirconium Alloys, British Patent 1,061,156, Mar. 8, 1967.
86. U. Rosler, Zirconium Alloy, Canadian Patent 755,579, Mar. 28, 1967.
87. E. A. Eldridge and H. W. Deem, Specific Heats and Heats of Transformation of Zircaloy-2 and Low-Nickel Zircaloy-2, USAEC Report BMI-1803, Battelle Memorial Institute, May 31, 1967.
88. J. J. Kearns, Terminal Solubility and Partitioning of Hydrogen in the Alpha Phase of Zirconium, Zircaloy-2,

and Zircaloy-4, *J. Nucl. Mater.*, 22: 292-303 (June 1967).
89. A. Sawatzky and B. J. S. Wilkins, Hydrogen Solubility in Zirconium Alloys Determined by Thermal Diffusion, *J. Nucl. Mater.*, 22: 304-310 (June 1967).
90. B. A. Cheadle, The Development of Texture in Zirconium Alloy Tubes and Its Effect on Mechanical Properties, Canadian Report AECL-2698, March 1967.
91. K. P. Steward and B. A. Cheadle, The Effects of Preferred Orientation on the Mechanical Properties and Deformation Behavior of Zircaloy-2 Fuel Sheathing, *Trans. Met. Soc. AIME*, 239: 504-513 (April 1967).
92. B. A. Cheadle and W. Evans, The Fabrication and Metallurgical Evaluation of 3¼-In.-Diameter Cold-Worked Zirconium–2.5 Percent Niobium Pressure Tubes, Canadian Report AECL-2652, December 1966.
93. Canadian Materials Newsletter, unpublished, July 1967.
94. J. Rezek and B. G. Childs, Fabrication and Mechanical Properties of Sintered Zirconium–Yttria Dispersion, Canadian Report AECL-2633, January 1967.
95. J. T. Barnby, The Initiation of Ductile Failure by Fractured Carbides in Austenitic Stainless Steel, *Acta Met.*, 15: 903-909 (May 1967).
96. E. E. Bloom, Effect of Titanium Additions on the Stress-Rupture Properties of Type 304 Stainless Steel, USAEC Report ORNL-TM-1807, Oak Ridge National Laboratory, June 1967.
97. Aerojet-General Corp., Evaluation Study of Hastelloy X as a Nuclear Cladding, USAEC Report AGN-8214, February 1967.
98. R. K. Ham and M. L. Wayman, The Fatigue and Tensile Fracture of TD-Nickel, *Trans. Met. Soc. AIME*, 239: 721-725 (May 1967).
99. M. Semchyshen, *Symposium on Heat Treated Steels for Elevated Temperature Service*, New Orleans, La., September 19–20, 1966, American Society of Mechanical Engineers, 1966.
100. J. W. Wunderlich, The Creep and Rupture Strength of Silicon–Aluminum Deoxidized 1 Percent Chromium–½ Percent Molybdenum Steel at 1000°F, USAEC Report GAMD-5878, General Atomic Division, General Dynamics Corp., Nov. 12, 1964.
101. M. M. Sandomirskiy and A. S. Zavyalov, Influence of Rare Earth Metals on the Grain Size and the Fine Structure of Structural Steels, *Izv. Akad. Nauk SSSR, Metal.*, No. 2: 107-109 (March–April 1966).
102. D. J. Harman and T. A. Noland, Fracture of Al–Al_2O_3 Alloys: Fracture Analysis of the Commercial SAP Type Alloy XAP-001, USAEC Report ORNL-TM-1826, Oak Ridge National Laboratory, July 1967.
103. N. C. Kothari, Physical and Mechanical Properties of Blended and Ball-Milled Aluminum–Aluminum Oxide Alloys, *J. Nucl. Mater.*, 22: 165-176 (May 1967).
104. G. Greenfield and W. Vickers, The Creep Properties of a Compacted Magnesium Alloy Powder, *J. Nucl. Mater.*, 22: 77-87 (1967).
105. W. Pollack, E. C. Bishop, R. T. Begley, and R. W. Buckman, Development of High Strength Vanadium Based Alloys for LMFBR Core Applications, *Trans. Amer. Nucl. Soc.*, 10: 119-120 (June 1967).
106. A. I. Nabonechnikov, L. V. Pavlinov, and V. N. Bykov, Carbon Diffusion into Refractory Metals with a BCC Lattice, *Fiz. Metal. Metalloved.*, 22: 234-238 (August 1966).
107. International Conference on Diffusion in Body-Centered Cubic Materials, Gatlinburg, Tenn., September 16–18, 1964.
    a. R. Gibala and C. A. Wert, Measurement of Diffusion Coefficient by Internal Friction, Chap. 8, Table 1.
    b. I. I. Kovenskii, Investigation of Diffusion of Carbon in Three Refractory Metals over a Wide Range of Temperatures, Chap. 22, Table 2.
108. J. Askill (Comp.), A Bibliography on Tracer Diffusion in Metals; Part II, Impurity Diffusion in Pure Metals, USAEC Report ORNL-3795, Part II, Oak Ridge National Laboratory, June 1967.
109. P. Son, T. Seiichi, M. Mikake, and T. Sano, Diffusion of Carbon in Tantalum (in Japanese), *Nippon Kinzoku Gakkaishi*, 30: 1137-1140 (1966).
110. E. Gebhardt, E. Fromm, and U. Roy, Die Löslichkeit von Kohlenstoff in Molybdän und Rhenium (in German), *Z. Metallk.*, 57: 732 (October 1966).
111. J. Hughes, A Survey of the Rhenium–Carbon System, *J. Less-Common Metals*, 1: 377 (1959).
112. Reference deleted.
113. R. A. Andrievskii, V. N. Zagriazkin, and N. Meshcheriakov, Study of Diffusion of Carbon in Zirconium and Zirconium Carbide, USAEC Report LA-tr-67-32, translated by Helen J. Dahlby from Report STI/PUB-109 (Vol. II), pp. 172-180.
114. L. V. Pavlinov and V. N. Bykov, Carbon Diffusion into β-Zirconium (in Russian), *Fiz. Metal. Metalloved.*, 19: 397-400 (March 1965).
115. A. N. Ashurst, Diffusion Studies, *Reactor Mater.*, 10(3): 179 (Fall 1967).
116. W. R. Kerr, Screening Tests of Hydrogen Diffusion Barriers for Zirconium, USAEC Report AI-CE-27, Atomics International, Aug. 15, 1967.
117. G. M. McCracken and J. H. C. Maple, The Trapping of Hydrogen Ions in Molybdenum, Titanium, Tantalum, and Zirconium, *Brit. J. Appl. Phys.*, 18: (1967).
118. D. A. Prokoshbin, E. V. Vasileva, and L. L. Bergasova, Diffusion of Niobium with Some High-Melting Metals (in Russian), *Metalloved. Term. Obrab. Metal.*, 3: 44-46 (March 1967).
119. A. J. Mortlock, Near-Surface Diffusion Anomaly in Gold, USAEC Report ORNL-4141, Oak Ridge National Laboratory, July 1967.
120. E. Rudy and St. Windisch, Evidence for Zeta Fe_2N-Type Sublattice Order in W_2C at Intermediate Temperatures, *J. Amer. Ceram. Soc.*, 50: 272-273 (May 21, 1967).
121. V. M. Gropyanov and V. G. Sobolev, Investigation of Sintering and Properties of Solid Solutions of TiC and ZrC with NbC, *Porosh. Met., Akad. Nauk Ukr. SSSR*, 4, 30-33 (April 1967).
122. E. I. Gladyshevskii, V. S. Telegus, T. F. Fedorov, and Y. B. Kuzima, Ternary System W–Cr–C, *Izv. Akad. Nauk SSSR, Metal.*, 1: 190-193 (January–February 1967).
123. S. S. Ordan'yan, Structure of Alloys of the Zr–C–Nb System, Report NASA-TT-F-10493, December 1966.
124. E. N. Denbnovetskaya, Preparation of Solid Solutions of Some Complex Carbides of Transition Metals, *Porosh. Met., Akad. Nauk Ukr. SSR*, 3: 32-37 (March 1967).
125. U. S. Bureau of Mines, Albany Research Center, Quarterly Metallurgical Progress Report, April–June 30, 1967, USAEC Report USBM-RC-1302, pp. 4-11.
126. E. N. Denbnovetskaya, Physical Properties of Solid Solutions of the System NbC–MoC, *Porosh. Met., Akad. Nauk Ukr. SSR*, 4: 57-60 (April 1967).
127. O. I. Shulishova and I. A. Shcherbak, Investigation of Some Physical Properties of HfC–MoC and TaC–MoC Solid Solutions, *Izv. Akad. Nauk SSSR, Neorg. Mater.*, 2: 2145-50, December 1966.
128. A. Ya. Kuchma and G. V. Samsonov, Formation of Stable Electronic Configurations of Some Physical Properties of Transition Metal Carbides and Nitrides in the Range of Their Homogeneity, Report NASA-TT-F-10847, April 1967.
129. A. Kelly and D. J. Rowcliffe, Deformation of Polycrystalline Transition Metal Carbides, *J. Amer. Ceram. Soc.*, 50: 253-256 (May 21, 1967).
130. G. V. Samsonov and V. V. Stasovskaya, Relation Between Microhardness and Microbrittleness of Refractory Compounds with Their Electron Structure, Report NASA-TT-F-10935, May 1967.
131. H. Goretski, Neutron-Diffraction Studies on Titanium–Carbon and Zirconium–Carbon Alloys, *Phys. Status Solidi*, 20: 141-143 (Apr. 1, 1967).
132. I. D. Konozenko and Yu. T. Ryzhkov, Influence of Nu-

clear Irradiation on Properties of Refractory Compounds, *Fiz.-Khim. Mekh. Mater.*, 2: 607-615 (1966).
133. E. Rudy and C. E. Bruko, Lower-Temperature Modifications of Nb, C, and V_2C, *J. Amer. Ceram. Soc.*, 50: 265-268 (May 21, 1967).
134. K. V. Davidson, R. E. Riley, and J. M. Thub, Carbide–Graphite Composites, USAEC Report LA-3652, Los Alamos Scientific Laboratory, Sept. 26, 1966.
135. J. Rappeneau, M. E. Lagorio, J. Gilbert, and P. Piron, Irradiation Test of Concretes, *Bull. Inform. Sci. Tech. (Paris)*, No. 110: 31-48 (1966).
136. R. A. Tarnopolskaya and N. V. Gul'ko, The Structure of $SrO-ZrO_2$ System, *Dokl. Akad. Nauk SSSR*, 170: 1140-1142 (Oct. 11, 1966).
137. R. A. Tarnopolskaya and N. V. Gul'ko, Subsolidus Structure and Fusibility Diagram of the $SrO-Al_2O_3-ZrO_2$ System, *Dokl. Akad. Nauk SSSR*, 170: 1380-1387 (Oct. 21, 1966).
138. V. N. Pavlikov and S. G. Tresvyatskii, $Nb_2O_3-Cr_2O_3$ System, *Zh. Neorg. Khim.*, 11: 1422-1425 (1966).
139. M. O. Warman and D. W. Budworth, Effects of Residual Gas on the Sintering of Alumina to Theoretical Density in Vacuum, *Trans. Brit. Ceram. Soc.*, 66: 265-271 (June 1967).
140. D. P. H. Hasselman and R. M. Fulrath, Micromechanical Stress Concentrations in Two-Phase Brittle-Matrix Ceramic Composites, *J. Amer. Ceram. Soc.*, 50(8): 399-404 (August 1967).

Section

IV

Reactor Materials

Special Fabrication Techniques

Melting, Casting, and Working

Consumable-electrode arc-melting experiments on reactor-grade uranium were performed by National Lead Company of Ohio.[1] The electrodes for arc melting were produced by vacuum-induction melting uranium feedstock and casting into 5½-, 8-, and 9-in.-diameter molds. These electrodes were then arc melted in vacuum and prepared as 7-, 7⅜-, 10-, and 11-in.-diameter production-sized ingots. The phenomenon known as "glow discharge" occurred approximately halfway through each melting cycle. A glow discharge is an arc that moves up the electrode and crucible from its intended position at the electrode tip. This displaced arc does not melt the electrode but does heat the crucible wall rapidly. The periods of "glow" became more frequent and lasted longer as each melt progressed. Generally the arc remained hard and stable during melting except during the periods of glow and during hot topping.

Massive copper crucibles without external cooling were found adequate for the preparation of 7-, 7⅜-, and 10-in.-diameter ingots. For the 11-in.-diameter ingots, however, uranium attacked the copper severely, and ingot-crucible bonding occurred. All crucibles exhibited growth of the copper from thermal cycling, i.e., the inner diameter of the crucibles decreased with each succeeding melt. This growth made it necessary to rebore crucibles after every fifth melt.

On the basis of the results of the experiments, it was concluded that arc melting of uranium into production-sized ingots is feasible. The principal advantage of arc melting uranium appears to be that ingot structures containing extremely fine, uniformly dispersed carbide particles are produced. Contaminants are also better controlled in the arc-melting process, and, by eliminating the graphite ingot crucible, the source of erratic carbon contamination is avoided. Arc melting did not result in any significant chemical refinement or improvement in segregation over that of induction-melted electrodes, although the hydrogen content was lowered slightly. Some internal voids occurred in the prepared ingots.

Oak Ridge[2] has described an electron-beam-melting furnace designed to produce laboratory quantities of high-purity metals and a technique that permits molten charges of the high-purity metal to be drop cast into cylindrical or rectangular chill molds. It was observed that an improved cast structure and more desirable ingot shapes resulted in better fabricability and higher material yields. The drop-casting technique and melting equipment may be used to cast fabricable shapes of Ti, Zr, Nb, V, Ta, W, Mo, and their alloys.

The melting and fabrication of W–Tc alloys were investigated at Battelle–Northwest.[3] Alloys were prepared by electron-beam melting and were then encapsulated in molybdenum cans for forging at 1675 to 1700°C to 0.275 to 0.300-in. thicknesses. Tungsten alloys containing 50 and 60 at.% technetium fractured badly and penetrated the molybdenum-can surfaces. Small particles of the W–60 at.% Tc alloy were hard enough to become embedded in the anvil of the press forge. Technetium additions were observed to have a marked effect in reducing grain size of tungsten.

Electron-beam zone-melting techniques for the preparation of single crystals of tungsten and molybdenum were developed in France.[4] Application of these techniques was of particular interest in electronics and in research on emitters. Gaseous and solid impurities in materials prepared in this manner were greatly diminished, and the material's low-temperature mechanical and electrical properties were improved.

The French[5] have reduced the oxides of zirconium and hafnium to their corresponding metals in an electron-beam furnace at 2500 to 3500°K under vacuum of 10^{-6} to 10^{-4} torr. Reducing agents were carbon, silicon, and aluminum, all of high purity. It was determined by gas analysis that the oxygen was removed in the form of gaseous suboxides corresponding to the type of reductant used: CO, SiO, or Al_2O. The hafnium produced by this method had a purity of 99.7%.

General Electric[6] is conducting a program to develop chromium alloys for high-temperature applications. Approximately 40 chromium alloys were prepared by induction melting, cast as ingots of about 4 lb, and processed to small-diameter bar stock. An additional 150 compositions were arc melted as 40- to 100-g buttons and were selectively evaluated

with respect to critical properties. Several of the dilute dispersion-strengthened alloys exhibited ductility at subzero temperatures and tensile strengths over 35,000 psi at 1900°F (1038°C). An addition of 4 at.% molybdenum increased the tensile strength markedly but decreased the low-temperature ductility. Additions of tungsten were even more effective strengtheners but exhibited more detrimental effects on the workability than did molybdenum.

Reactive Metals[7] recommends an upset-forge method of fabrication to reduce costs in producing uranium billets for coextrusion into fuel elements for the N reactor at Hanford. The current process involves machining an oversize extrusion to the coextrusion billet dimensions. The upset-forge process for the production of finished size billets has been developed, and 52 billets have been produced and shipped to Hanford for inspection and testing. Experiments at Reactive Metals also indicated that precision extrusion can be used to prepare uranium in fuel-element sizes rather than in overstock sizes as is current practice. Precision extrusion can result in reduced fabrication costs by eliminating postextrusion machining.

The proposed design for a new reactor fuel element calls for a uranium tube with a very small inside diameter. It was found that uranium tubing could be extruded with an inside diameter as small as 0.150 in. It appeared that a fixed ballistics-type mandrel with a taper angle of 10° is optimum for this process and that fabrication of this type fuel element could be carried out as a production process with little difficulty.

National Lead Company of Ohio[8] has studied the forces produced during rolling of both uranium rods and tubes. Unalloyed uranium, an alloy containing approximately 150 ppm each of iron and silicon, and an alloy containing about 350 ppm iron, 350 ppm silicon, and 800 ppm aluminum have been examined. The change in wall thickness during the rolling of wrought feedstock was expressed by the equation $0.925-4.02\ (T/D) \times \%$ OD reduction, where T/D is the ratio of the initial wall thickness to the outside diameter. Wrought feedstock that had been beta heat-treated produced a nonlinear relation. The roll-separating forces when rolling both tubes and rods were proportional to their respective initial cross-sectional areas. The roll-pressure constant, K (separating force/contact area), for the unalloyed uranium tubes and rods was 26,000 psi. With the addition of 100 to 150 ppm iron and silicon, K was 29,500 psi; and with 350 ppm iron, 350 ppm silicon, and 800 ppm aluminum, K was 44,000 psi. When rods were not reheated between passes, the roll pressure increased with each additional pass as a result of strain hardening. The roll pressure was plotted against the logarithm of the estimated strain and produced a curve that was similar to high-strain-rate, true stress–strain curves produced for uranium by mechanical tests. Rods that were not reheated between passes had typical grain structures (a grain size of 0.033 mm and 50 to 100% recrystallization). However, billets that were reheated between passes fulfilled the conditions for critical grain growth and exhibited large grains. Reheating time between passes had the greatest effect on grain growth. The amount of work done (% reduction) also had some effect. Additions of iron and silicon retarded critical grain growth and recrystallization, with critical grain growth characterized by heavy twinning and the interspersion of both small and large grains.

Development and operation of a process to produce metal spheres each having a diameter of 10 mm have been described.[9] The process includes cold forging and results in estimated costs of $150 per kilogram of spheres. The feasibility of employing the lead-shot technique with a fused-salt bath for the preparation of spheres was established.

The British[10] are developing an Fe–Cr–Al–Y alloy with enhanced corrosion resistance and neutron economy for cladding Civil Advanced Gas Reactor fuel elements. They have assessed General Electric's development of similar alloys for operation in air up to 1200°C and are currently producing fuel cans of an Fe–15 wt.% Cr–4 wt.% Al–1 wt.% Y alloy and evaluating the mechanical and oxidation properties of this alloy under simulated reactor conditions. A series of torsion tests on bar specimens to assess the fabricability of the alloy at temperatures up to 600°C showed the material to be less ductile at room temperature than standard 18-8 stainless steels. Improved ductility occurred in the 200 to 400°C range, above which it markedly increased. The results indicated that the material could be tube drawn at 200°C using standard reductions and that drawing at room temperature was possible using smaller reductions.

Nuclear Metals[11] developed procedures for producing small-diameter thin-walled tubing from Ta–10 wt.% W and Nb–10.5 wt.% W–2.5 wt.% Zr (Cb-752) alloys. Tubing with outside diameters of ½, ¼, and ⅛ in. and wall thicknesses of 0.020, 0.015, and 0.010 in., respectively, was swaged from 3-in.-diameter billets that had been initially extruded to 1-in.-OD × 0.75-in.-ID tube rounds. The dimensions of the intermediate shapes were based on the maximum reductions the alloys would withstand in swaging. The limits on reduction were approximately 75 and 40% in area for Ta–10 wt.% W and Cb-752, respectively. Since these limits made it impractical to swage the 1-in. blanks to target dimensions, 2-in.-diameter billets, canned in steel and filled with various combinations of steel and graphite or calcium carbide, were extruded at 1830°F (1000°C) at reduction ratios varying from 2.1 to 1 to 28.5 to 1. The dimensions of the tube blanks follow.

OD × ID, in.	
Ta–10 W	Cb-752
0.613 × 0.501	0.544 × 0.466
0.324 × 0.234	0.292 × 0.266
0.185 × 0.125	0.161 × 0.113

The tube rounds were ground to remove approximately 0.005 to 0.013 in. from the outside diameter and were etched on the ID surface. The Cb-752 and Ta–10 wt.% W rounds were then vacuum annealed 1 hr at 2400° F (1316° C) or 1½ hr at 2675° F (1470° C), respectively.

The tube rounds were ironed to tubing with planetary ball swaging equipment. The device utilizes the force exerted by hardened-steel balls rolling in an outer race on the tubing which acts as the inner race. The conical outer race is rotated by an external power source. The tubing, held to prevent rotation, is drawn through the opening inside the track of the rotating balls. The reduction is controlled by the inside diameter of the outer race and the size and number of the hardened-steel balls. A hardened-steel mandrel free to move and rotate and only slightly smaller than the inside diameter of the tube was used for ironing reductions. In a typical operation the race driving the swaging balls was rotated at 450 rpm, and the tubing was drawn at 20 in./min.

All the tubes could be flared to a diameter 1.32 times the swaged diameter except the ⅛-in. Cb-752 material, which had the least tensile ductility in the cold-worked condition. All tubes passed helium leak tests, were within target specifications on dimensions, and had surface finishes smoother than 4 μin.

The application of ultrasonic vibration to wire and rod drawing is being investigated at the Naval Ordnance Test Station and at Aeroprojects, Inc.[12] At the Naval Ordnance Test Station, it was found that vibration lowered the force required to draw copper wire by 3 to 4%. With drawing forces up to 60 lb, the impedance of a horn-die assembly ranged from 84 to 115 ohms.

At Aeroprojects, experiments on rods were conducted with transducer-coupling systems operating in the longitudinal mode at 7, 15, and 28 kc/sec and in the radial mode at 15 and 38 kc/sec. The longitudinal mode resulted in four to five times the force reductions produced by the radial systems. The best results were obtained with the 7 kc/sec system vibrating the die in the direction of workpiece motion. The poorer results at higher frequencies were attributed to the smaller amplitudes of vibration caused by the higher drawing die-to-transducer mass ratios. Rods of 6061-0 aluminum, spheroidized 4340 steel, and annealed Ti–6 wt.% Al–4 wt.% V alloy were cold drawn, with reductions of 7 to 30% in area at speeds up to 200 ft/min. Copper and 4340 steel wires, 0.02 in. in diameter, were also drawn under various conditions.

It was concluded that the vibrating velocity of the die is the principal factor controlling the effect of ultrasonic energy on wire and rod drawing. The velocity is the product of the frequency and the amplitude of vibration, which depends on the power input, as illustrated by Fig. IV-1. The average velocity of the vibrating die varied from approximately 20 to 45 in./sec in most experiments. In rod drawing the greatest velocities were produced by the 7 kc/sec transducer. The average acoustic power measured at the die ranged from 12 to 30% of the power input to the transducers and increased with die velocity. Measurements indicated that ultrasonic activation raised the die temperatures about 20° F when drawing aluminum and 125° F when drawing steel or titanium. These temperature increases appear to be too small to affect flow strengths but could influence lubrication.

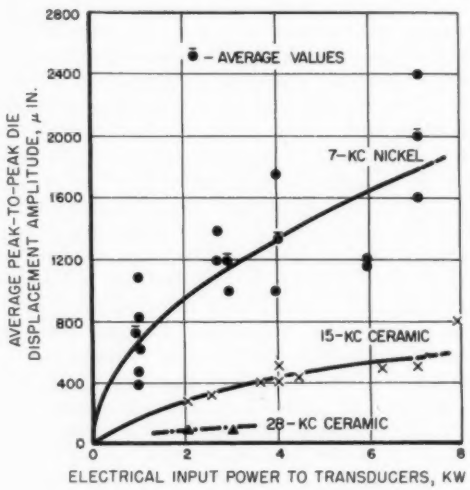

Fig. IV-1 Average vibratory displacement amplitude of the die during drawing as a function of input power to the transducers.[12]

Table IV-1 shows some of the data obtained in drawing aluminum and steel rods at a low speed with and without the superimposition of vibrational energy. The reductions in force for drawing aluminum ranged from 9 to 35%, with corresponding efficiency increases of 1.7 and 5.8%. The power contribution of vibrational energy was better in the experiments on steel, suggesting a better impedance match. The reductions in drawing force ranged from approximately 10 to 20%. From a practical standpoint the values for minimum reductions in drawing loads are most pertinent to production operations. Force reductions averaged about 8% for the titanium alloy, and stick-slip frictional conditions were avoided by ultrasonic drawing.

Table IV-1 SUMMARY OF DATA AND POWER COMPUTATIONS FOR DRAWING* WITH AND WITHOUT ULTRASONIC VIBRATIONAL ENERGY[12]

	6061-0 aluminum	Spheroidized 4340 steel
Drawing forces,† lb		
Nonultrasonic	2200	14,000
Ultrasonic		
Minimum effect	2000	12,700
Maximum effect	1440	11,400
Average effect	1720	12,050
Power, computed from drawing forces,‡ kw		
Nonultrasonic	1.00	6.32
Ultrasonic		
Minimum effect	0.90	5.65
Maximum effect	0.65	5.03
Average effect	0.78	5.34
Differences in mechanical power requirements, kw		
Nonultrasonic		
Ultrasonic		
Minimum effect	0.10	0.67
Maximum effect	0.35	1.29
Average effect	0.22	0.98

*Drawing speed, 20 ft/min; reduction in area, 15% on $^{11}/_{16}$-in. rods; ultrasonic power to transducers, 6 kw.
†Drawing forces measured by load cells.
‡Draw bench power for drawing is equal to force times drawing speed and can be expressed in horsepower, watts, or other units of power.

A hydrostatic extrusion device has been developed in England[13] which surmounts previous size limitations in that the workpiece is cyclically fed through a ratchet-action clamp into the pressurized system from outside the device. The workpiece is in the form of a straight bar and therefore can be of large diameter, of indefinite length, and, if necessary, of a brittle material. The principle involved is that of augmented hydrostatic extrusion, already used in a U. K. Atomic Energy Authority (UKAEA) 1600-ton hydrostatic extrusion machine. One of the most satisfactory features of the system is the absence of the high energy release at the completion of simple hydrostatic extrusion. Figure IV-2 is a schematic drawing of a typical hydrostatic extrusion assembly, and Fig. IV-3 is a schematic drawing of an augmented hydrostatic extrusion setup. In operation the augmented assembly is closed by vessel *a* being pushed toward vessel *b* in a hydraulic press. This generates a pressure in the liquid that is present in all cavities in both vessels, which are interconnected by the small drilled hole through the punch. The pressure is therefore the same on each end of the punch, and this results in an out-of-balance load that moves the punch against the rear face of the billet. This out-of-balance force augments that already being applied by the liquid pressure and makes a direct contribution to the extrusion pressure. In the new design the augmented hydrostatic extrusion setup is modified further to allow the continuous extrusion of bar.

(S. G. Nelson)

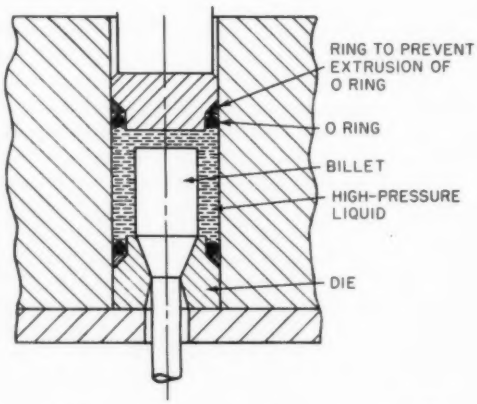

Fig. IV-2 Hydrostatic extrusion assembly.[13]

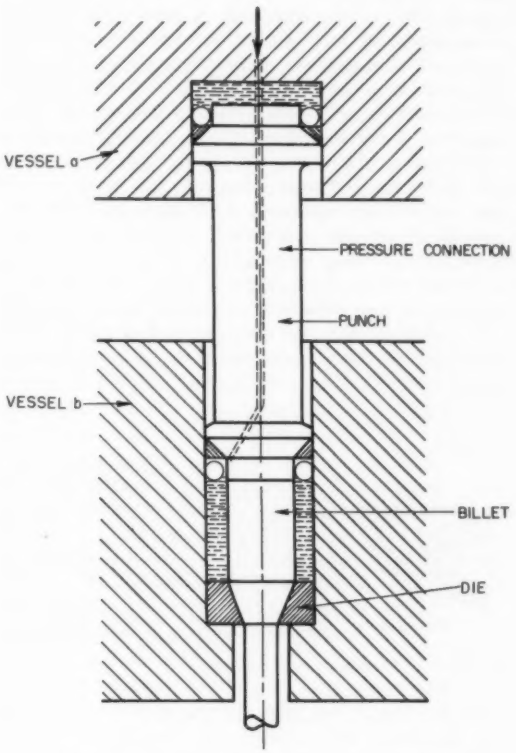

Fig. IV-3 Augmented hydrostatic extrusion.[13]

Powder Metallurgy Materials

The Russians[14] have studied the influence of ultrasonic vibrations on sintering and high-temperature

pressing of products from the powders of metals and their compounds. Laboratory equipment and experimental techniques were described, although specific results with powder materials were not cited.

A literature survey[15] concerned with the packing of particles has been compiled by Gilman. References on compaction of spherical particles as produced by sol-gel, plasma, and other techniques are included. This information has application in the fields where particulate fuels are employed.

The fabrication of small-diameter thin-wall refractory-alloy tubing has shown steady progress through the development of improved processing techniques. In a continuation of earlier work, Argonne[16] investigators have produced high-quality tubing of both W–30 wt.% Re–30 wt.% Mo and W–25 wt.% Re from single extruded tube blanks by a sequence of primary ductile-core drawing and secondary mandrel drawing. The final tube size had a 0.250-in. outside diameter and a 0.018- to 0.023-in. wall. Both outer and inner tube surfaces were extremely smooth and free of all extrusion striations, as well as of other scratches or irregularities. On the basis of preliminary results, mandrel drawing appeared to be a feasible technique for processing either alloy to smaller diameters. The tooling arrangement for the mandrel drawing operation is shown in Fig. IV-4.

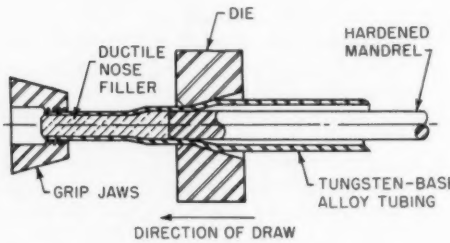

Fig. IV-4 Mandrel drawing with a ductile nose filler.[16]

Using procedures developed for tungsten-base alloys, General Electric[17] has fabricated Mo–35 wt.% Re alloy tubing. The usual procedure of drawing commercially prepared Mo–35 wt.% Re failed to yield a full-density product, and extrusion as a subsequent operation was required. The technique involved a process in which sintered alloy cores were coextruded in a molybdenum billet. A major difficulty was encountered in extracting the alloy from the molybdenum extrusion billet by pickling, since Mo–35 wt.% Re is subject to nitric acid attack at about the same rate as is molybdenum. The separation problem was overcome by wrapping both the bore and outer peripheral surface of the sintered core with a 0.002-cm-thick sheath of tungsten foil before extruding. Following processing it was possible to leach the extruded molybdenum container down to the tungsten sheath and thus prevent acid penetration into the Mo–35 wt.% Re alloy. Using the tungsten-sheathing technique, four extrusions were successfully processed into bar and tubing blanks. The procedure appears to be well suited for use on other alloys such as Mo–5 wt.% W, which, without sheathing, would be almost impossible to separate from the extrusion container.

The effect of purification treatments on the weldability of unalloyed molybdenum was investigated at General Electric.[17] It was found that the control of carbon impurities in unalloyed molybdenum was mandatory for the development of a high degree of ductility. These impurities were reduced to less than 10 ppm in fabricated sheet by treating the initial molybdenum powder in a hydrogen–water vapor atmosphere (5°C dew point) for 6 weeks at 1000°C. Carbon and other trace elements in finished sheet prepared from such purified powders were found to be in the low-ppm range in contrast to commercially produced unalloyed molybdenum sheet, which usually contains 30 to 150 ppm carbon.

In a study conducted at NASA–Lewis,[18] powder-metallurgy tungsten with and without $\frac{1}{4}$-in.-thick molybdenum cladding was reduced from 12 to 1 by extrusion in the temperature range 2400 to 4000°F (1316 to 2205°C). With cladding, extrusion was possible with preheat temperatures as low as 2400°F, but unclad billets could not be extruded with preheat temperatures less than 2800°F (1538°C). Extrusion temperature and technique (clad or unclad) affected the as-extruded hardness, grain size, and room-temperature tensile strength. Tensile strengths at 3000 and 3500°F (1649 and 1930°C) were not influenced by extrusion temperature or technique. There was no correlation between the elevated-temperature ductility and the posttest hardness or grain size.

Battelle[19] has prepared a report on the state of the art of making shapes of stainless steel by casting and powder-metallurgy methods. It was noted that the use of stainless-steel powders to make parts is increasing rapidly.

Several papers from the 12th Sagamore Army Materials Research Conference described dispersion-strengthened materials. Grant[20a] discussed the effects of structure on the ductility of oxide dispersion-strengthened alloys. Trends toward alloyed matrices rather than the pure metals, with emphasis on the oxidation-resistant alloys, were cited. Problems of oxide contamination, oxide stability at high temperatures, and oxide particle growth were reviewed. In another paper, Bufferd[20b] reviewed methods and processes for the preparation of metal-oxide dispersion composites that have been utilized either commercially or in research and development. These procedures included surface oxidation of powders,

internal oxidation, coprecipitation, electrodeposition, and salt decomposition. The methods were described in terms of their advantages and limitations, with examples of various metal and alloy systems.

(C. A. MacMillan)

Pressure Bonding

Transition joints of SAP-895 and 347 stainless steel approximating the size required for Heavy Water Organic-Cooled Reactor pressure tubes were prepared by hot-press diffusion bonding and evaluated in thermal cycling tests.[21] The tubular components were bonded by applying a 50-ton load for 5 min at 1025° F (552° C). Details of joint designs, procedure, and tensile properties were also reviewed and have been described previously.[22] The joints were alternately heated and cooled by lowering into a heated Santowax R bath and raising into a cooled argon cover gas. After 1100 complete thermal cycles between 550 and 750° F (288 and 399° C), a transition joint of this type remained helium leaktight with no apparent loss in tensile strength. Similar results were obtained with a joint cycled 10,000 times between 650 and 750° F (343 and 399° C).

The densification of submicron tungsten powders using both belt and piston cylinder high-pressure apparatus has been examined at the Lawrence Radiation Laboratory.[23] Samples were consolidated at pressures of 0.4 to 35 kbars, at temperatures of 600 to 1400° C, with times ranging from 10 sec to 20 min. Tungsten pressed at 23 kbars and 1170° C for 10 min yielded a density of greater than 99.6% of theoretical. A study of the effects of varying pressure at 1080° C and 10 min showed a marked change in densification at about 1 kbar, but little difference was observed in the range of 1.4 to 30 kbars. A density maximum noted in material consolidated near 1100° C was related to the onset of grain growth under pressure. Over the particle-size range of 0.25 to 7.0 μ, the gas content of the compact appeared to be the primary determinant of end-point density, and the densification observed in these tests was adequately described by a plastic-flow mechanism. Self-diffusion and activation-energy data calculated for compacts consolidated at 23 kbars agreed closely with data obtained from pressureless sintering.

A patent has been granted which describes the use of hot isostatic pressing in the fabrication of stainless-steel–UO_2 tubular fuel elements.[24] The fuel core tube is first formed by extrusion of a mixture containing stainless-steel-coated spherical UO_2 particles, stainless-steel matrix powder, and a binder. The binder is then removed, and a stainless-steel cladding is bonded to the tubular fuel component by hot isostatic pressing.

(S. W. Porembka)

Plating

Nonelectrolytic Chemical Plating

A survey of technology and research in the field of "vapometallurgy" (chemical vapor deposition of metals) has been published by staff members at Oak Ridge.[25] The review covers important work at a number of locations which has mainly concerned coating and cladding processes.

Martin workers have conducted a feasibility study of intermolecular bonding of various metals and alloys by chemical vapor deposition at temperatures below their respective recrystallization temperatures.[26] The materials studied were aluminum alloy 2219-T87 and 321 stainless steel. For aluminum-alloy joining, aluminum was deposited in the joint by decomposition of triisobutyl aluminum. Actual weldments were not obtained, but the chemical and metallurgical quality of the aluminum deposit was sufficiently high to warrant further development. Successful joining of stainless steel was achieved by codeposition of iron, nickel, and carbon from iron and nickel carbonyls. Joint strengths of 40,000 psi were attained. The tendency for microcracks in the parent material to propagate through the deposited weldment was the major problem encountered.

General Atomic has determined the effects of intentional additions of nonmetallics to vapor-deposited tungsten.[27] The addition of carbon (24 to 320 ppm), nitrogen (15 to 101 ppm), and oxygen (4 to 66 ppm) increased the low-temperature yield strengths without increasing the ductile-to-brittle transition temperature above 200° C. Yield strengths at 1800° C were higher for tungsten specimens containing the intentional additions. Creep behavior of these materials at 1760° C was also determined.

The Conference on Chemical Vapor Deposition of Refractory Metals, Alloys, and Compounds, sponsored jointly by the American Nuclear Society and the American Institute of Mining, Metallurgical, and Petroleum Engineers, was held at Gatlinburg, Tenn., in September 1967. The proceedings of that conference are now available.[28] The subject matter of the conference was divided into three parts: theory of deposition, methods of deposition, and applications and evaluation. Some of the papers are reviewed briefly below.

Oak Ridge workers[28a] have performed creep-rupture tests on chemically vapor-deposited (CVD) tungsten at 1650 and 2200° C and compared the results with similar tests on powder-metallurgy (PM) tungsten. At 1650° C the CVD product exhibited low fracture strains and a lower minimum creep rate. At high stresses the rupture life of the CVD material was shorter than that of the PM material, but at low stresses the rupture lives were about equal. At 2200° C the minimum creep rate was higher and the

rupture life lower for the CVD product. This mechanical behavior was correlated with the formation and growth of voids and the columnar nature of the grains in the CVD material. The voids appeared to be caused by the presence of an impurity having a high vapor pressure; however, a correlation between the fluorine content and the volume of voids formed under stress was not shown.

CVD techniques for the production of tungsten tubing were reviewed.[28b] Typical process variables were presented as follows:

ID of tube	0.200 in.
Temperature	650°C
WF_6 flow rate	100 cm^3/min
H_2 flow rate	2100 cm^3/min
Pressure	10 torrs
Deposition rate	0.0055 in./hr
Efficiency	>90%

Tubing sizes were routinely produced in the range 0.020 in. to larger than 1 in. with various wall thicknesses. For tubes to be used in the as-deposited condition, the deposition is carried out on a resistance-heated thin-wall stainless-steel tube. Resistance heating enhanced the uniformity of the deposit since the low-tungsten areas became hotter, and thus the deposition rate was increased at those areas. The tungsten tube was readily removed from the mandrel after cooling. Heavy-wall tube shells can also be produced by CVD; the tube shells can then be extruded and hot plug drawn to achieve the desired final wrought structure as well as the required final size. In the as-deposited form, CVD tungsten tubing is less costly than tubing produced by more conventional means.

Neutron and X-ray diffraction measurements were used to examine the structure of chemically vapor-deposited W–Re alloys.[28c] An A15-type phase in the composition range near W_3Re was identified. In the temperature range of the study, 1000 to 1500°C, the phase occurred with and without the beta or sigma phases. The A15 phase was about four times harder than the beta phase and much more brittle. The new phase was metastable, being transformed to either beta or beta-plus-sigma during long-time anneals at deposition temperatures.

Workers at Lawrence Radiation Laboratory[28d] have described the process development for CVD tungsten and W–Re alloys. The process makes use of premixed liquid fluorides that are accurately fed to a flash vaporizer and also employs mechanical rubbing of the surface during the deposition to obtain a finer grain structure and higher tensile strength. The observed effects of several deposition variables and heat-treatments on the room-temperature mechanical properties of CVD tungsten and W–Re alloy tubing were also discussed.[28d] Tensile strengths as high as 150,000 psi were obtained with unalloyed tungsten deposits. Stress-relief annealing of fine-grain deposits at 1000°C led to measurable ductility. Codeposited W–Re alloys exhibited ultimate tensile strengths in excess of 200,000 psi and uniform elongations as high as 2%. The results indicate that deposits with mechanical properties approaching those of wrought material can be produced by CVD.

Studies at Los Alamos of the deposition of coatings consisting of ternary alloys of tungsten, molybdenum, and rhenium have been reported.[28e] The deposition process employed the hydrogen reduction of the mixed vapors of the metal fluorides. Experimental conditions were:

Temperature	550–800°C
Pressure	10–200 torrs
H_2/total fluoride	10/1

Alloy compositions studied were in the range 60 to 85 wt.% W, 15 to 40 wt.% Mo, and 1 to 25 wt.% Re. The composition and uniformity of the deposits were analyzed by chemical and electron-microprobe techniques and metallographic examination. Impurity levels were not determined and physical-property measurements were not made. (E. H. Hall)

Electroplating

Sandia described details of a reliable procedure for electroplating nickel on uranium which did not require heat-treating or outgassing after plating.[29] Exposure for 90 hr to water-saturated air at 200°F (93°C) caused no blistering. The undercutting at an exposed face was restricted to $\frac{3}{16}$ in., or less, in comparison with undercutting of $>\frac{1}{4}$ in. with other plated specimens. The process included degassing, pickling in 8*M* nitric acid to remove oxides, treating in a heated solution of stannous chloride and nitric acid, immersing again in 8*M* nitric acid, and plating in a nickel bath containing a leveling agent. An improved treating solution[30] removed less uranium metal and produced a smoother finish (60 to 80 μin.). It contained 1800 g of hydrated nickel chloride, 1200 ml of nitric acid, and 1400 ml of water, and was heated to about 40°C. Immersion in an ultrasonically agitated solution of sodium silicate and sodium phosphate both before and after treating was recommended.

Liquid-propellant rocket-motor injectors electroformed in nickel at Camin Laboratories contained accurately dimensioned manifolds and connecting orifices difficult to produce by machining and impractical to produce without burrs that distort hydraulic flow.[31] Injectors were formed on nickel master mandrels passivated with potassium dichromate solution. Segments of 0.020- and 0.030-in.-diameter glass tubing were inserted in holes drilled into the face of the mandrel. After >0.12 in. of nickel was electrodeposited on the mandrel and removed mechanically, manifolding was introduced by machining, the glass tubing was removed by chemical dissolution in hydrofluoric acid solution, and the mani-

folds were filled with wax. After wax surfaces were covered with a silver paste to make them conductive, another layer of nickel (approximately 0.125 in.) was deposited on the assembly. After the final outer surface machining, inlet and outlet holes were drilled into the manifolds, and the wax was removed by melting and solvent degreasing. Jet impingement characteristics were satisfactory for each of three prototype injectors. The nickel was electroformed with a solution and conditions that produced metal with a yield strength exceeding 100,000 psi and an elongation of 20%. The development demonstrated the capability of electroforming high-strength metal for fabricating shapes with accurately dimensioned internal passages.

Techniques for electrolyzing glass and ceramics are being studied at the Bureau of Standards.[32] Glow discharge in a vacuum is used to transmit current from the electrical leads to the electrolyte. A potential of 1000 to 1500 volts impressed on the cell caused glass to become opaque on the surface. Experimental evidence indicated that sodium metal was produced on a disk of sodium chloride.

(W. H. Safranek)

Brazing and Welding

Joining for High-Temperature Applications

The feasibility of preparing surfaces to be brazed with a plasma spray has been demonstrated at Aerojet-General.[33] A tube designed to carry liquid coolant from a reactor was first plasma sprayed with an alumina coating. The tube was then plasma sprayed with molybdenum or niobium that served as a surface to be brazed to a molybdenum block for transfer of heat to a thermionic device. The brazes were made in a vacuum with pure nickel or 60 wt.% Ni–35 wt.% Mo–5 wt.% Fe as the filler metal.

NASA–Lewis has been studying brazing alloys for tungsten that will permit service in hydrogen at 4530°F (2500°C).[34] The 15 alloys below, which were made by arc-melting pellets or powder, homogenizing, and then crushing to a coarse powder, were evaluated for flow characteristics, strength, and metallurgical reactions with the tungsten.

Composition wt.%	Observed melting range, °F
Unalloyed molybdenum	4720
Mo–3 Cr	4720–4885
Mo–7 Cr	4530–4585
Mo–5 Os	4700–?
Mo–1 Pd	4763–?
Mo–3 V	4720–?
Unalloyed osmium	4885
W–15 Cr	Not determined
W–35 Cb	5325–?
W–50 Mo–3 Re	5170–?
W–53 Mo	5305–?
W–25 Os	5385–?
W–44 Os	4845–?
W–10 Ru	5530–?
W–23 V	5335–5480

Tests on butt-brazed joints in 0.02-in.-thick commercially pure tungsten made using a gas tungsten arc as the heat source showed three of the alloys to be promising. The results of tensile tests at 3990°F (2200°C) on joints made with these alloys are given in Table IV-2.

Table IV-2 RESULTS OF 2200°C TENSILE TESTS ON BRAZED TUNGSTEN JOINTS[34]

Braze-alloy composition, wt.%	Condition*	Engineering stress at fracture, psi: Base metal	Engineering stress at fracture, psi: Braze metal	Location of fracture†
W–25 Os	AB	3060	2620	Base metal, 1/8 in. from braze metal
W–25 Os	HT	2810	2610	Base metal, 1/8 in. from braze metal
W–50 Mo–3 Re	AB	2930	2610	Base metal, 3/32 in. from braze metal
W–50 Mo–3 Re	HT	3110	2820	Partly base and partly braze metal
Mo–5 Os	AB	2770	2330	Braze metal
Mo–5 Os	HT	2960	2630	Base metal, 3/8 in. from braze metal

*AB, as brazed; HT heat-treated at 2500°C for 10 hr in hydrogen.

†Distances from braze metal at face of joint.

Westinghouse has assembled Inconel 718 fuel-assembly grids by brazing either in a vacuum or in hydrogen with a Ni–14 wt.% Cr–10 wt.% P filler metal.[35] The base metal was first nickel plated and then brazed in a relatively long brazing cycle to improve joint strength. The strengths obtained at a testing temperature of 600°F (316°C) were as follows:

Time of brazing temperature, min	Shear strength, psi: Vacuum	Shear strength, psi: Hydrogen
20	12,600	12,400
40	13,100	12,800
60	25,800	26,000
120	25,400	26,200

Reactor fuel tube spacers of Hastelloy X and Incoloy 800 have been successfully brazed with the alloy used by Westinghouse and also with a Ni–19 wt.% Cr–10 wt.% Si brazing alloy.[36] The latter alloy seemed to yield better joints but was attacked during corrosion tests in flowing steam. No loss of tubing strength or ductility resulted from the brazing operation.

Patents issued on brazing filler metals for refractory metals and their alloys are U. S. patents 3,312,539, 3,317,288, and 3,309,180 and British patent 1,063,274 (Refs. 37 to 40).

Gilliland has investigated methods of joining tungsten and has shown a number of processes to be useful.[41] Experimental Ta–V–Nb and Ta–V–Ti brazing alloys wet tungsten readily and produce excellent-quality joints. The production of good joints by thermochemical deposition was hampered by joint design and cracking problems. Excellent results were obtained by gas tungsten-arc welding. Of greatest interest were the beneficial effects shown when gas tungsten-arc welds in thermochemically deposited tungsten were given a postwelding heat-treatment. Stress relieving of these welds in powder-metallurgy tungsten in vacuum for 1 hr at 3270°F (1800°C) reduces the ductile-to-brittle transition temperature about 210°F (117°C). Identically stress-relieved welds in the thermochemically deposited tungsten showed greater improvement. The results are summarized in Table IV-3.

Table IV-3 DUCTILE-TO-BRITTLE TRANSITION TEMPERATURES OF TUNGSTEN JOINTS[41]

Joining technique	Type of tungsten	Joint condition	Approximate ductile-to-brittle transition temperature, °F
Gas tungsten-arc weld	Powder metallurgy, parallel	As welded	840
	Powder metallurgy, transverse	As welded	885
	Powder metallurgy, parallel	Stress relieved, 3270°F	<660
		Stress relieved, 5070°F	>930
	Thermochemically deposited	As welded	1040
	Thermochemically deposited	Stress relieved, 1830°F	660
Electron beam	Arc cast	As welded	795
Thermochemically deposited	Powder metallurgy, parallel	Stress relieved, 1830°F	~455
	Thermochemically deposited	Stress relieved, 1830°F	~390

A Westinghouse study of refractory-metal welding indicates only nominal weldability for 0.035-in. sheet of arc-cast unalloyed tungsten and the W–25 wt.% Re alloy, even when using a 550°F (288°C) preheat.[42] The powder-metallurgy alloy W–0.5 wt.% Hf–0.02 wt.% C (Sylvania A) was considered nonweldable. The successful welding of tungsten and W–25 wt.% Re was limited to 15 in./min or less. Above this speed, severe cracking occurred. Small, low-heat-input welds exhibited better ductility. A 2550°F (1400°C) postweld stress-relief treatment was considered to be ineffective in improving the ductility of welds. Low-heat-input electron-beam welds in the same alloys gave essentially the same results.

A program to investigate methods that eliminate or at least minimize electrode sticking when resistance spot welding refractory metals has been completed.[43] The alloys included in the study were Cb-752 niobium, D-43 niobium, Ta–10 W, T-222 tantalum, and TZM molybdenum alloys. In general, electrode sticking was found to be caused by a combination of brazing, solid-state welding, and mechanical bonding, depending on the temperatures reached during welding. Class 1 copper electrodes were found to be less susceptible to sticking than other standard electrodes or pure molybdenum electrodes. The thickness of the material being welded made little difference in the electrode sticking encountered. Material- and electrode-surface finish had little influence. Electrode-contour variations also showed little effect.

Cryogenic electrode cooling, solid-state welding, and projection welding were the techniques found most useful for relieving electrode sticking. Projection welding, utilizing a solid-state bond, showed more promise than other techniques because of the better mechanical properties obtainable.

Process Developments

Diffusion-bonded joints in beryllium and titanium alloys are being successfully produced on modified resistance-welding equipment at North American.[44] Joints were made in Be–2 wt.% BeO sheet that sustain stresses greater than the yield strength of the base material. Uniformity of the results was good, and cracking during bonding was not a problem. Promising results also were obtained on Ti–6 wt.% Al–4 wt.% V and on Ti–8 wt.% Al–1 wt.% Mo–1 wt.% V alloys.

The relatively new commercial plasma-arc welding process (Linde Needle Arc) has been evaluated on a comparative basis with gas tungsten-arc welding on several sheet alloys (0.010 to 0.030 in.) by Allison.[45] It was concluded that the plasma-arc welds were equivalent to the gas tungsten-arc welds. These advantages were cited for the plasma arc: simpli-

fied prepositioning for starting, insensitivity to arc length during manual welding, and excellent low-amperage arc stability. (R. M. Evans)

Nondestructive Testing

Ultrasonic Techniques

At the American Nuclear Society Symposium on Quality Assurance in the Civilian Nuclear Industry held at Pittsburgh, Pa., Worlton[46] discussed factors restricting full endorsement of nondestructive testing (NDT) as a source of valid quality assurance data. All nondestructive tests, especially the newer electronic techniques, contain inherent measurement errors; that is, their response to a given defect or condition is not exactly constant. Raw NDT data do not distinguish between measurement errors and condition of the part, regardless of whether the source is in the instrumentation or elsewhere in the system. A fundamental principle in the development of reliable NDT data was given as: "a quantitative handle on the kinds and magnitudes of these errors must be established before valid quality assurance data can be determined." Usually, in attempts to assure product quality by nondestructive testing, the need to determine and compensate for the measurement error is not fully considered. The validity of the results obtained would be substantially improved if this were taken into consideration.

The use of computers in applications involving thousands of measurements was cited as a worthwhile means of processing the raw NDT data. In this way, measurement performance and, therefore, true product quality were automatically determined. The acoustic emission technique for determining approaching failure of a part under static test was also discussed. As the part approaches failure, sonic disturbances are generated. Signal character is a function of material brittleness, i.e., loss of ductility in the sample may conceivably be predicted by the analysis of the signals. The method has been used to predict imminent failure.

Regarding the use of acoustic emission at Battelle–Northwest, Hutton[47,48] has described its use in the detection of the growth of flaws in pressure piping at temperatures of 600 to 650°F (316 to 343°C). Surprisingly few problems were encountered with isolating the acoustic emission signals from background noise and with interpreting the signals after they had been identified. As expected, the acoustic energy propagated at shear-wave velocity. A theoretical analysis of the phenomenon may lead to a better understanding of the mechanism of the source of the sonic energy.

The development of ultrasonic-thickness measuring devices in the Soviet Union appears to parallel that in the United States. Nechaev and Ermolov[49] reviewed the development of a portable pulse-type ultrasonic-thickness gauge that uses double-transceiver types of transducers similar to those in common use in this country. The range of usefulness cited was from 3 to 25 mm (approximately 0.118 to 1 in.). Little difficulty has been experienced in the United States in measuring thicknesses of 0.025 in. with the same technique, and there is no reason to believe that the Soviets have not been able to do the same since publication of their results. (D. Ensminger)

NDT Methods Other Than Ultrasonic

A joint feasibility study by Atomics International and Combustion Engineering[50] has demonstrated that the Hall effect is suitable for measuring nickel-layer thicknesses on 347 stainless steel. Thicknesses varying from 70 to 210 μin. of electroplated nickel were examined with a Hall detector, and the results were compared with those obtained by metallographic measurements. With the Hall detector it was possible to distinguish small differences in nickel thickness in this range, but an analysis of accuracy was not presented. The equipment appeared to be a commercially available gauss meter.

In connection with the continued development of the closed-circuit neutron television system at Argonne,[51] two amplifier units have been under study. A video amplifier constructed at Argonne will provide gain values up to 100, with the Vidicon camera, assuming there are no electrical noise limitations. Actual television tests are planned to evaluate the performance. Further tests with the contrast-expander amplifier for use with the neutron television system show that the contrast for low-attenuation types of objects can be enhanced considerably. However, the contrast is normally not enhanced for higher attenuation objects in the black regions of the image.

An investigation of proposed means to detect stress corrosion and fatigue damage has been reported by Benson and Associates.[52] It was found that, as surface damage inflicted by a corrosive bath on a half-wave linear resonator was increased, the bandwidth of the aluminum resonator increased in an apparently linear relation with hours of exposure. The test frequency was 1 gHz, and the bandwidth was determined with the aid of a small amount of frequency modulation obtained by the use of a Varactor diode. Measurements of mechanically fatigued specimens by the same technique were not fully conclusive. When data were taken at lower frequencies by means of inductive coupling to localized areas of the fatigued specimens, the location of damaged areas could be readily observed. (A. F. Leatherman)

References

1. R. L. Schardt, Consumable-Electrode Arc Melting of Uranium, USAEC Report NLCO-916, National Lead Company of Ohio, March 1967.

2. C. W. Dean, R. E. McDonald, and C. F. Leitten, Jr., High-Purity Shape Casting with an Electron-Beam Furnace, USAEC Report ORNL-P-3133 (CONF-660456-1).
3. R. S. Kemper and D. P. O'Keefe, A Study of Tungsten–Technetium Alloys, Quarterly Progress Report, April 1–October 1, 1966, USAEC Report BNWL-414, Battelle–Northwest, April 1967.
4. A. M. Shroff and C. Borromee, Application of Electron Beam Furnace to Tungsten and Molybdenum Zone Melting, *Rev. Int. Hautes Temp. Refract.*, 3: 385-393 (October–December 1966).
5. G. Gosse, P. Lehr, and P. Albert, Application of Electron-Beam Furnace to Metallurgical Elaboration Problems, *Rev. Int. Hautes Temp. Refract.*, 3: 371-384 (October–December 1966).
6. J. W. Clark and C. S. Wukusick, Development of High-Temperature Chromium Alloys, Semiannual Report, Report NASA-CR-80657 (N67-13536), General Electric Company, Materials Development Laboratory, Apr. 22, 1966.
7. Reactive Metals, Inc., Annual Progress Summary (on Uranium Fabrication), 1966, USAEC Report RMI-8, Apr. 20, 1967.
8. H. W. Hesselbrock, Rolling Studies of Uranium Rods and Tubes, USAEC Report NLCO-990, National Lead Company of Ohio, April 1967.
9. J. C. Geertsma et al., A Discussion of the Programme of the Extractive Metallurgy Division, December 1–3, 1965, South African Report PEL-121 (Vol. 3).
10. U. K. Atomic Energy Authority, Atomic Energy Research Establishment Ceramics Division, unpublished.
11. R. F. Huber, R. N. Randall, and H. F. Sawyer, Development of Advanced Techniques for the Fabrication of Refractory Metal Tubing, Report AFML-TR-65-341, Nuclear Metals Division of Textron Inc., October 1965.
12. F. C. Holden and F. W. Boulger, Seventh Status Report of the U. S. Government Metalworking Processes and Equipment Program, Report DMIC-237, Battelle Memorial Institute, Defense Metals Information Center, June 1, 1967.
13. H. K. Slater and D. Green, U. K. Atomic Energy Authority, unpublished, 1966.
14. V. R. Poksyshev and V. I. Marchenko, Method of Obtaining Compaction Products from Refractory Metallides Using Ultrasonic Activation, Report NASA-TT-F-10774 (N67-25012), National Aeronautics and Space Administration, Lewis Research Center, February 1967.
15. W. S. Gilman, Packing of Particles, USAEC Report MLM-1424, Mound Laboratory, Dec. 29, 1966.
16. Argonne National Laboratory, Reactor Development Program Progress Report, May 1967, USAEC Report ANL-7342, pp. 92-94.
17. General Electric Company, Nuclear Materials and Propulsion Operation, AEC Fuels and Materials Development Program Progress Report No. 67, USAEC Report GEMP-67, pp. 65-67, June 30, 1967.
18. T. P. Herbill, C. A. Hoffman, and J. W. Weeton, Effect of Cladding on Extrudability and Properties of Powder-Metallurgy Tungsten, Report NASA-TN-D-3941, National Aeronautics and Space Administration, Lewis Research Center, May 1967.
19. J. G. Kura, V. D. Barth, E. T. Hall, W. H. Safranek, and H. O. McIntire, Making of Stainless Steel Shapes by Casting and Powder Metallurgy, Report NASA-TM-X-53577, Battelle Memorial Institute, Feb. 16, 1967.
20. J. J. Burke, N. L. Reed, and V. Weiss (Eds.), *Strengthening Mechanisms, Metal and Ceramics*, Syracuse University Press, 1966.
    a. N. J. Grant, Dispersion Strengthening, pp. 63-82.
    b. A. S. Bufferd, Preparation of Metal-Oxide Dispersion Composites, pp. 531-548.
21. E. C. Supan, Development of SAP-Steel Pressure Tube Transition Joints for the HWOCR, USAEC Report AI-CE-46, Atomics International and Combustion Engineering Inc., Aug. 15, 1967.
22. S. W. Porembka, Pressure Bonding, *Reactor Mater.*, 10(4): 260 (Winter 1967–1968).
23. G. E. Zima and J. F. Lakner, High-Pressure Consolidation of Submicron Tungsten, USAEC Report UCRL-50172, University of California Lawrence Radiation Laboratory, Dec. 28, 1966.
24. D. E. Goslee and L. Frank, Method of Producing Nuclear Fuel Elements of Stainless Steel Coated UO_2 Particles, U. S. Patent 3,318,695, to USAEC, May 9, 1967.
25. S. H. Smiley and J. R. Merriman, Vapometallurgy: Present Technology and Some Future Aspects, USAEC Report K-L-6130-2, Union Carbide Corp., Nuclear Division, 1967.
26. R. Wilson, Intermolecular Bonding of Various Metals and Alloys by Thermochemical Vapor Deposition, Report NASA-CR-80721 (N67-13671), Martin Co., November 1966.
27. J. Chin, A. F. Weinberg, and J. R. Lindgren, Effects of Additions of Nonmetallics on the Properties of Vapor Deposited Tungsten, Report NASA-CR-85906 (N67-31223), General Atomic Division, General Dynamics Corp., November 1966.
28. Proceedings of the Conference on Chemical Vapor Deposition of Refractory Metals, Alloys, and Compounds, held at Gatlinburg, Tenn., September 1967, American Nuclear Society, Inc., Hinsdale, Ill.
    a. H. E. McCoy and J. O. Stiegler, Mechanical Behavior of CVD Tungsten at Elevated Temperatures, p. 391.
    b. W. R. Martin, R. L. Heestand, R. E. McDonald, and G. A. Reimann, Application of Chemical Vapor Deposition to the Production of Tungsten Tubing, p. 303.
    c. J. I. Federer and J. E. Spruiell, Formation and Characterization of the A15-Type Structure in Chemically Vapor Deposited Tungsten–Rhenium Alloys, p. 443.
    d. W. R. Holman and F. J. Huegel, CVD Tungsten and Tungsten–Rhenium Alloys for Structural Applications: Part I, Process Development, p. 127; Part II, Evaluation, p. 427.
    e. C. I. Fairchild, Chemical Vapor Deposition of Tungsten–Molybdenum–Rhenium Ternary Alloy, p. 149.
29. R. D. Anderson and P. R. Coronado, Electroplating Uranium with Nickel, USAEC Report SCL-DR-67-43, Sandia Corp., July 1967.
30. J. W. Dini and P. R. Coronado, Electroplating Uranium with Nickel, USAEC Report SCL-DR-67-44, Sandia Corp., July 1967.
31. S. S. Hammer, Development of Electroforming Techniques for the Fabrication of Injectors, Camin Laboratories, May 15, 1967.
32. A. Brenner and J. L. Sligh, Electroless Electrolysis of Solid Electrolytes, Report for Period of December 1966–June 1967, National Bureau of Standards, June 1967.
33. R. M. Baciarelli, Refractory Metals Brazed for Operation at 2200°F, *Metal Progr.*, 91(4): 189-192 (April 1967).
34. T. J. Moore, J. E. Japka, and E. Gordeon, Brazing Tungsten for High-Temperature Nuclear Service in Hydrogen, Report NASA-TN-D-3944, National Aeronautics and Space Administration, Lewis Research Center, and United Nuclear Corp., May 1967.
35. L. Marti-Balaguer and M. E. Rinker, Furnace Brazing Inconel 718 for Nuclear Reactors, *Metal Progr.*, 91(5): 113 (May 1967).
36. S. R. Vandenberg, Two Ways to Join Wire Spacers to Reactor Fuel Tubes, *Metal Progr.*, 91(6): 67-69 (June 1967).
37. J. C. Marshall and H. G. Smith, Brazing Alloys for Tungsten and Molybdenum, U. S. Patent 3,312,539, to USAEC, Apr. 4, 1967.
38. J. C. Marshall and R. H. Mueller, Niobium–Silicon

Brazing Alloy for Refractory Metals, U. S. Patent 3,317,288, to USAEC, May 2, 1967.
39. J. C. Marshall, Brazing Alloys for Tantalum, U. S. Patent 3,309,180, to USAEC, Mar. 14, 1967.
40. Brazing Alloys for Tungsten, Molybdenum, and Alloys Thereof, British Patent 1,063,274, Mar. 30, 1967.
41. R. G. Gilliland, Joining of Tungsten, USAEC Report ORNL-TM-1606, Oak Ridge National Laboratory, October 1966.
42. G. G. Lessmann and D. R. Stover, Determination of the Weldability and Elevated-Temperature Stability of Refractory Metal Alloys, Report NASA-CR-72073, Westinghouse Electric Corporation, Astronuclear Laboratory, Mar. 20, 1966.
43. J. V. Peck, Resistance Welding of Refractory Metals, Report AFML-TR-67-130, Thompson Ramo Wooldridge Inc., June 1967.
44. J. P. King, Jr., R. P. Robelotto, and A. C. Dillingham, Jr., Diffusion Bonding of Titanium and Beryllium, Interim Engineering Progress Report, February 16–May 15, 1967, Report IR-8-318(VII) (NA-65-850-6), North American Aviation, Inc.
45. P. T. MacAbee, J. R. Dyar, and N. F. Bratkovich, Plasma Arc Welding of Thin Materials, Report AFML-TR-67-177, Allison Division, General Motors Corp., June 1967.
46. D. C. Worlton, Nondestructive Testing: A Key to Quality Assurance, USAEC Report BNWL-SA-901, Battelle–Northwest, Oct. 3, 1966.
47. P. H. Hutton, Detection of Flaw Growth in Pressure Piping by Sensing Acoustic Emission, USAEC Report BNWL-SA-1076, Battelle–Northwest.
48. Battelle–Northwest, unpublished, July 1967.
49. Yu. A. Nechaev and I. N. Ermolov, Portable Ultrasonic Pulse-Type Semiconductor Thickness Gauge, *Defectoscopy–Soviet J. Nondestructive Testing*, No. 6: 449-453 (November–December 1966).
50. Atomics International and Combustion Engineering Inc., Heavy Water Cooled Reactor, Quarterly Technical Progress Report, October–December 1966, USAEC Report AI-CE-56, pp. 127-131, Aug. 15, 1967.
51. Argonne National Laboratory, Reactor Development Program Progress Report, June 1967, USAEC Report ANL-7349, pp. 102-103, July 31, 1967.
52. R. W. Benson, Development of Nondestructive Methods for Determining Residual Stress and Fatigue Damage in Metals, Report NASA-CR-79304 (N67-12227), Robert W. Benson and Associates, Inc., June 30, 1966.

LEGAL NOTICE

This journal was prepared under the sponsorship of the U. S. Atomic Energy Commission. Neither the United States, nor the Commission, nor any person acting on behalf of the Commission:

A. Makes any warranty or representation, expressed or implied, with respect to the accuracy, completeness, or usefulness of the information contained in this journal, or that the use of any information, apparatus, method, or process disclosed in this journal may not infringe privately owned rights; or

B. Assumes any liabilities with respect to the use of, or for damages resulting from the use of any information, apparatus, method, or process disclosed in this journal.

As used in the above, "person acting on behalf of the Commission" includes any employee or contractor of the Commission, or employee of such contractor, to the extent that such employee or contractor of the Commission, or employee of such contractor prepares, disseminates, or provides access to, any information pursuant to his employment or contract with the Commission, or his employment with such contractor.

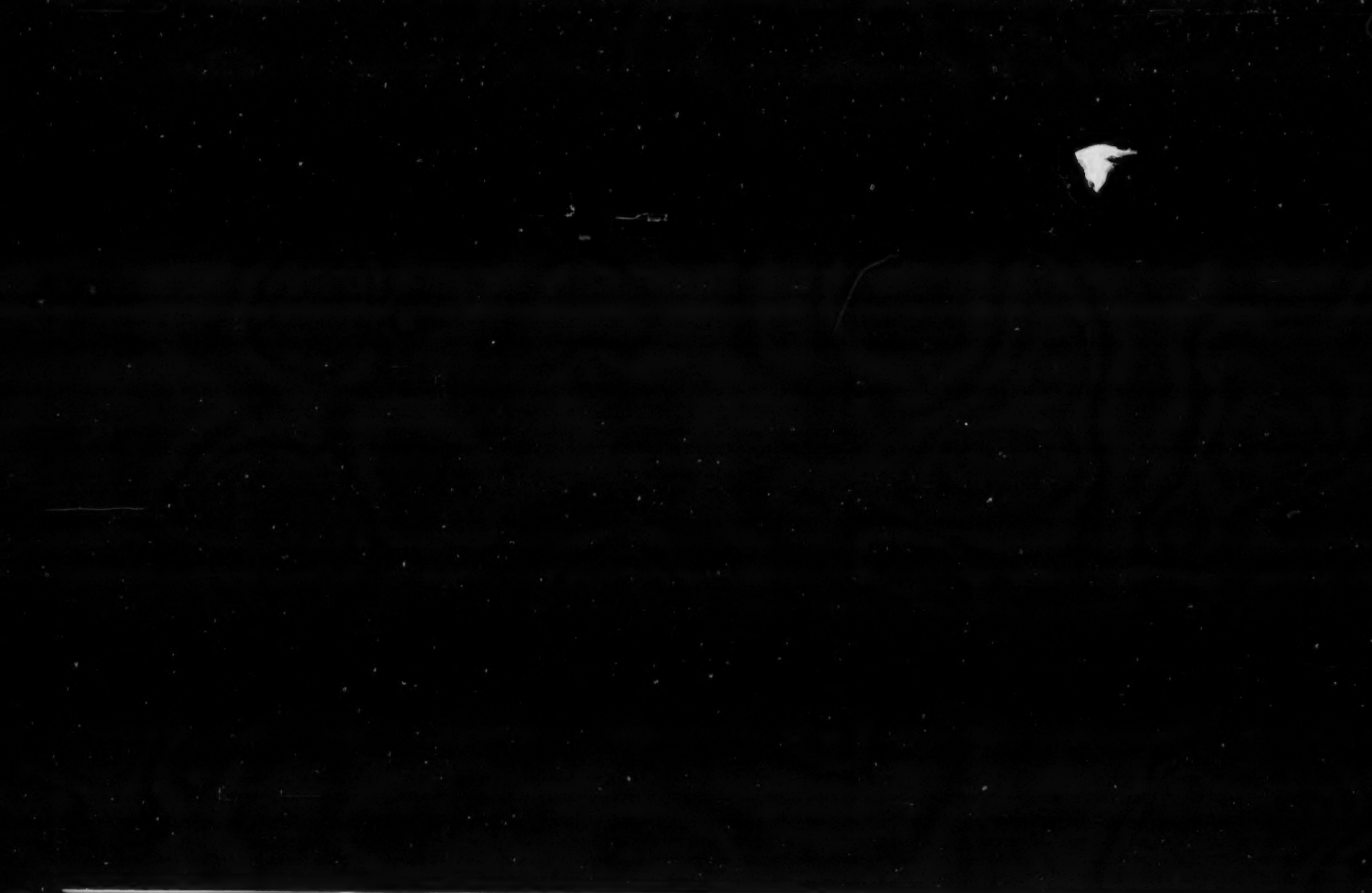

NUCLEAR SCIENCE ABSTRACTS

The U. S. Atomic Energy Commission, Division of Technical Information, publishes *Nuclear Science Abstracts* (*NSA*), a semimonthly journal containing abstracts of the literature of nuclear science and engineering.

NSA covers (1) research reports of the U. S. Atomic Energy Commission and its contractors; (2) research reports of government agencies, universities, and industrial research organizations on a worldwide basis; and (3) translations, patents, books, and articles appearing in technical and scientific journals.

Complete indexes covering subject, author, source, and report number are included in each issue. These are cumulated quarterly, semiannually, and annually providing a detailed and convenient key to the literature.

Availability of *NSA*

SALE *NSA* is available on subscription from the Superintendent of Documents, U. S. Government Printing Office, Washington, D. C., 20402, at $30.00 per year for the semimonthly abstract issues and $22.00 per year for the four cumulated-index issues. Subscriptions are postpaid within the United States, Canada, Mexico, and all Central and South American countries, except Argentina, Brazil, Guyana, French Guiana, Surinam, and British Honduras. Subscribers in these Central and South American countries, and in all other countries throughout the world, should remit $37.00 per year for subscriptions to semimonthly abstract issues and $25.00 per year for the four cumulated-index issues.

EXCHANGE *NSA* is also available on an exchange basis to universities, research institutions, industrial firms, and publishers of scientific information. Inquiries should be directed to the Division of Technical Information Extension, U. S. Atomic Energy Commission, P. O. Box 62, Oak Ridge, Tennessee, 37830.

DOCUMENTS
MAY 17 1968
MICHIGAN STATE UNIVERSITY
LIBRARIES

TECHNICAL PROGRESS REVIEWS may be purchased from Superintendent of Documents, U. S. Government Printing Office, Washington, D. C., 20402. *Nuclear Safety* at $3.50 per year (six issues) for each subscription or $0.60 per issue; each of the other journals at $2.50 per year (four issues) or $0.70 per issue. The use of the coupon below will facilitate the handling of your order.

POSTAGE AND REMITTANCE: Postpaid within the United States, Canada, Mexico, and all Central and South American countries except Argentina, Brazil, Guyana, French Guiana, Surinam, and British Honduras. For these Central and South American countries and all other countries: add, for each annual subscription, $1.00 for *Nuclear Safety* and $0.75 for each of the other journals; for single issues, add one-fourth of the single-issue price. Payment should be by check, money order, or document coupons, and MUST accompany order. Remittances from foreign countries should be made by international money order or draft on an American bank payable to the Superintendent of Documents or by UNESCO book coupons.

order form

SUPERINTENDENT OF DOCUMENTS
U. S. GOVERNMENT PRINTING OFFICE
WASHINGTON, D. C., 20402

Enclosed:

document coupons ☐ check ☐ money order ☐

Charge to Superintendent of Documents No. _____

Please send a one-year subscription to

☐ ISOTOPES AND RADIATION TECHNOLOGY
☐ NUCLEAR SAFETY
☐ REACTOR AND FUEL-PROCESSING TECHNOLOGY
☐ REACTOR MATERIALS

SUPERINTENDENT OF DOCUMENTS
U. S. GOVERNMENT PRINTING OFFICE
WASHINGTON, D. C., 20402

(Print clearly)

_____
Name

_____
Street

_____
City, State, ZIP Code